Report on
EQC Project 77/U539 - Improving the identification of volcanic deformation in GPS arrays

A. Peltier

GNS Science Consultancy Report 2009/85
April 2009

The data presented in this Report are available to GNS Science for other use from April 2009

BIBLIOGRAPHIC REFERENCE

A. W. Hurst 2009. Improving the identification of volcanic deformation, *GNS Science Consultancy Report* 2009/85. 49 p.

CONTENTS

APPENDICES

FIGURES

EXECUTIVE SUMMARY

The aim of this post-doctoral fellowship, financed 50% by the Earthquake Commission of New Zealand (EQC) and 50% by the European Commission, 6th Framework Project-'VOLUME' (VOLcanoes: Understanding subsurface Mass movEment), was to improve the analysis of ground deformation recorded during the last decades on New Zealand's active volcanoes in order to better understand their functioning. Three main projects have been developed:

(1.) Improving the identification of volcanic deformation in GPS arrays, with the example of the Tongariro National Park network

(2.) Modelling the eruptive system of Taupo using lake leveling data recorded between 1979 and 2007.

(3.) Modelling the eruptive system of White Island using leveling data recorded since 1967.

SUMMARY REPORT

1.0 IMPROVING THE IDENTIFICATION OF VOLCANIC GPS DEFORMATION RECORDED ON THE TONGARIRO NATIONAL PARK (APPENDIX 1)

In the last decade, Global Positioning System (GPS) geodesy has became a well-known tool to measure ground deformation with a precision reaching a few mm, and it is widely used in studies of geodynamics. Around the Tongariro National Park, one of the limitations of precise GPS measurements (especially vertical measurements) lies in the difficulty of estimating tropospheric delay in a region of strongly varying topography. The tropospheric delay is caused by signal refraction as the 19-24 cm wavelength GPS signals pass through the troposphere, an electrically neutral atmospheric layer. The main variability in tropospheric delay is due to water vapour in the lower levels of the troposphere. In standard GPS processing, the tropospheric delay is estimated with high accuracy from the GPS data itself, but this estimation relies on the assumption that the atmosphere is horizontally stratified. In regions like the Tongariro National Park, the height of the volcanoes (e.g., Ruapehu 2797m) can cause that assumption to break down, especially when weather fronts are moving across the region. This leads to inaccuracies in the tropospheric delay estimates that are reflected as inaccuracies in site position. The weather-related variations in apparent position, mainly at periods of up to a day, can reach 10 cm. Such variations can be confused with deformation precursors of an eruption; it is thus important to identify and subtract any long- and short-term weather signature in the GPS position time series before attempting interpretation of the volcano deformation.

The most effective way to solve this problem is likely to be a modification of the GPS processing strategy to take into account variations in tropospheric delay along satellite-receiver paths based on the actual state of the atmosphere. This is likely to require detailed models of the atmospheric state in the region, with ray tracing through the models. For real time analysis of volcanic ground deformation signals, weather model predictions would need to be used. There are groups around the world working on this type of strategy, but it is a difficult problem and requires detailed weather models in near real time. Rather than follow this type of physical modelling, we decided to investigate a much simpler heuristic approach to see if it could provide any benefit over standard GPS processing.

We used neural network techniques to try to find a relationship between the evolution of the atmospheric parameters (including pressure, temperature, humidity and wind) and the GPS signal variations during a quiet period without eruptive activity. For most of this work, we used hourly-averaged position time series from RTD, a near real time GPS processing system that produces an independent solution every epoch (30 s). This is because we are interested in the application of the method to near real time analysis of volcanic deformation signals. We also have available daily post-processed solutions using Bernese v5.0 software.

We find that estimating a residual tropospheric delay parameter using weather parameters embedded in a neural network improves the reliability of the processing especially for the long-term variations. Our results reveal that the long-term seasonal variations and the intermediate-term (i.e. 5-10 days) have been clearly reduced. But although the short-term daily variations have been attenuated, they remain at a level of about 5 cm (instead of 10 cm when the data were not corrected). One reason may be that some of the apparent variations are due to snow and ice build-up on the station GPS antennae. This is most likely during winter storms.

2.0 MODELLING THE ERUPTIVE SYSTEM OF TAUPO (APPENDIX 2 & 4)

The Taupo Volcanic Zone (TVZ) is a region characterized by regional rifting, geothermal fields and fault motions, which can strongly affect the ground deformation and must be distinguished from any magmatic deformation. The aim of this work was to constrain the sources and the structures involved in the current vertical deformation at Lake Taupo in order to provide useful information with regard to prediction of possible future volcanic activity in this area. In the TVZ, repeated lake levelling measurements have been conducted since 1979 in the lake filling the caldera of the Taupo dormant volcano. Data covering the period 1979-2003 reveal a long-term subsidence in the northern part of the lake occasionally disturbed by short-term uplifts in localized areas. Interpretation of the deformation data through numerical modelling provides information on the structures involved in the relative vertical crustal movement throughout the southern end of the TVZ. The best-defined feature is a long term global subsidence of the northern part of the lake ($7 mm.y^{-1}$) due to the cumulative effect of the crust stretching and a deep deflation source. This long term subsidence is occasionally disturbed by strong short-term uplifts linked with overpressure sources located below the northern part of the lake, near the Horomatangi Reef, an active geothermal field. Episodes of uplift can be attributed to various combinations of the following two processes taking place beneath the geothermal field (1) Movement or formation of rhyolitic magma (deepest sources) (2) Pressurization of the shallow hydrothermal fluid reservoir that traps volatiles exsolved from a crystallizing rhyolitic magma (shallowest sources). The pressurization of the shallow hydrothermal system gives rise to tensional stresses in the upper crust, resulting in seismic and aseismic fault ruptures. Slow slip motion of the Kaiapo fault causes short-term decoupling of the ground deformation pattern on both sides of the fault.

In the future, the recognition of periods of significant uplift may allow us to forecast the shallow seismic swarms along the Kaiapo fault and below the Horomatangi Reefs as observed between March and August 2008.

3.0 MODELLING THE ERUPTIVE SYSTEM OF WHITE ISLAND (APPENDIX 3)

Compilation of a large database of 40 years measurements allows us to make a precise analysis of the long-term ground deformation pattern at White Island. The aim of this work was to constrain the sources of ground deformation at White Island between 1967 and 2008 through numerical modelling inversions in order to understand the relationship between ground deformation, eruptive activity and hydrothermal circulation. Indeed, White Island is characterized by strong hydrothermal and magmatic activity, and ground deformation induced by these two activities must be distinguished from each other in order to better forecast eruptions in the future. Interpretation of the deformation data using numerical modelling reveals that shallow pressure sources (200-500m deep) extending almost up to the groundsurface dominated the long-term deformation pattern consisting of inflation/deflation cycles. Evolution of height changes, magnetic changes, fumarole temperature and chemistry reveal that surface changes were caused by increasing temperature below the main crater, reflecting the presence of magma at shallow depth. Uplift preceding each eruption is interpreted as due to a hydrothermal response to heat flow and thermal expansion rather than directly by magma emplacement itself, whereas the subsidence during and following an eruption could be linked with removal of material at depth and changes to the hydrothermal system.

4.0 OUTCOMES

✓ **2 papers** published in international journals (In Press at Journal of Volcanology and Geothermal research) (Appendix 2 & 3)
  - Peltier, A., T. Hurst, B. Scott, V. Cayol, 2009, Structures involved in the vertical deformation at Lake Taupo (New Zealand) between 1979 and 2007: New insights from numerical modelling.
  - Peltier, A., B. Scott, T. Hurst, 2009, Ground deformation patterns at White Island volcano (New Zealand) between 1967 and 2008 deduced from levelling data.

✓ **2 conference presentations** (Appendix 4)
  - IAVCEI, international conference in Volcanology, Reykjavik (Iceland) August 2008
  - New Zealand Geosciences Conference, Wellington, November 2008

APPENDICES

APPENDIX 1 GNS INTERNAL REPORT – IMPROVING THE IDENTIFICATION OF VOLCANIC DEFORMATION IN GPS ARRAYS – THE CASE OF THE TONGARIRO NATIONAL PARK NETWORK

1.1 Project

GNS Science is currently operating about 20 continuous GPS stations within the Taupo Volcanic Zone (TVZ). Eleven stations are on and around the andesite volcanoes Ruapehu, Ngauruhoe and Tongariro in the Tongariro National Park.

The GPS stations in the Tongariro National Park are affected by tectonic plate movements. The GPS stations in the TVZ mainly show the continuous deformation as the north-west part of New Zealand moves with the Australian Plate, and the region east of the TVZ rotates clockwise in association with the TVZ back-arc rifting (e.g., Wallace et al., 2004). The back-arc rifting, averaged over a moderate time, induces northwest-southeast extension of about 15 mm/year across the northern part of the TVZ, near the Bay of Plenty coast, decreasing to about half this at the southern end near Ruapehu.

Examining the GPS position time series, no significant long-term variation is seen in the apparent baseline differences between GPS stations of the Tongariro National Park network. However it is noticeable that there are large short-period variations that may be weather-related. These variations, often taking place over about a day, can reach up to 10 cm and are thought to be related to atmospheric changes, as influenced by Mt Ruapehu (2797m), locally affecting the tropospheric GPS corrections.

Such variations can be confused with deformation precursors of an eruption; we therefore need to investigate ways of correcting for them. The most effective way to solve this problem is likely to be a modification of the GPS processing strategy to take into account azimuthal variations in tropospheric delay based on the actual state of the atmosphere. This is likely to require detailed models of the atmospheric state in the region, with ray tracing through the models. For real time analysis of volcanic ground deformation signals, weather model predictions would need to be used. There are groups around the world (e.g. Pany et al, 2001) working on this type of strategy, but it is a difficult problem and requires detailed weather models in near real time. Rather than follow this type of physical modelling, we decided to investigate a much simpler heuristic approach to see if it could provide any benefit over standard GPS processing.

Our proposal was to use neural network techniques to see whether a relationship can be found between the atmospheric parameters (pressure, temperature, humidity, wind) and their rates of change, and the apparent position changes from GPS, that would enable these apparent baseline changes to be partly corrected, so that any remaining deformation can be taken as representing real ground movement.

1.2 GPS Network

In the last decade, Global Positioning System (GPS) geodesy has became a well-known tool to measure ground deformation with a precision reaching a few mm, and it is widely used in studies of geodynamics. In mountainous and volcanic areas, the main limitation of precise

GPS measurements (especially vertical measurements) lies in the estimation of the tropospheric delay. The standard tropospheric delay estimate relies on an assumption that the atmosphere is horizontally stratified. In areas of high topographic variation, such as the Tongariro National Park, the assumption of a horizontally stratified atmosphere breaks down during evolving and variable weather conditions (such as a front moving across a volcano). So in mountainous and volcanic areas, the tropospheric delay estimate may be erroneous under these conditions. The vertical error can reach up to 10 cm. It is thus important to estimate and subtract any long and short-term weather signature in the GPS signal before attempting interpretation of the volcano deformation. We used neural network techniques to attempt to find a relationship between the evolution of the atmospheric parameters (including pressure, temperature, humidity and wind) and the apparent position changes from GPS during a quiet period without eruptive activity. The validated neural network will allow us to partly correct the apparent baseline changes due to the influence of atmospheric parameters, so that any remaining deformation can be taken as representing real ground movement.

1.2.1 GPS Network around the Tongariro National Park

Around the Tongariro National Park, ground deformation has been monitored by continuous GPS measurements since 2004. The network now includes eleven stations (nine on and around Ruapehu volcano and two on Tongariro volcano, Figure 1).. Data are acquired every 30 s, and are downloaded hourly. Two data processing systems are operated.

(1) A daily solution running about 20 hours after the end of each UT day using the Bernese software (v5.0). This is a full network solution using double differencing and with a piecewise continuous estimate of zenith tropospheric delay at each station every hour giving us a daily New Zealand-wide solution. IGS rapid or final satellite orbits are used.

(2) A solution running every hour using Geodetics Inc.'s RTD software. This provides hourly solutions by averaging the independent 30-sec "epoch-by-epoch" solutions. Two sets of RTD solutions are done for the Ruapehu stations, one uses VGOB as the reference station and the other uses VGMT as the reference station. Tropospheric delay estimates are made at each station during the RTD solution, with the tropospheric zenith delay at the base station being fixed at the value given by the a priori model. There is also an option to let the base-station zenith delay vary with a specified standard deviation; adopting this option with a 50 cm standard deviation led to insignificant differences in the position solutions. IGS predicted orbits are used for the RTD solutions.

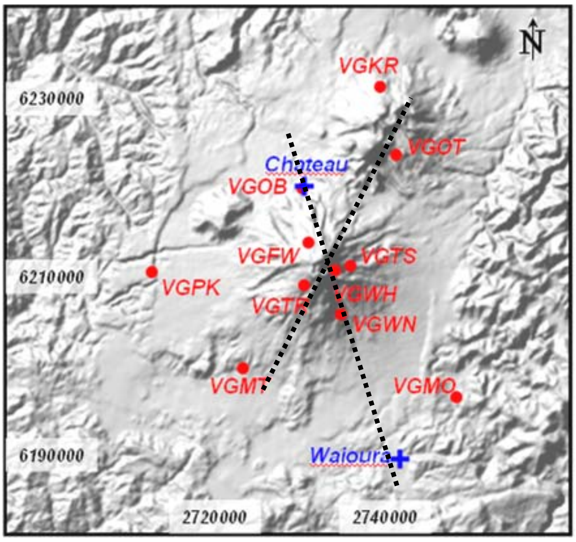

Figure 1 In red: location of the permanent GPS stations around the Tongariro National Park. In blue: meteorological stations used in this study. The dotted lines represent the cross-sections used in Figure 4.

Figure 2 shows the ground displacement rates relative to the Australian plate recorded by the stations located around the Tongariro National Park. The relative displacements to the Australian plate are not significantly different from one station to the other and from other regional sites (Wallace et al., 2004) and reveal motions toward the southeast at rates of about 3 mm.y^{-1}. So, the major component of the site velocities is not of magmatic origin but instead is generated by the effect of regional tectonic stresses due to plate movements.

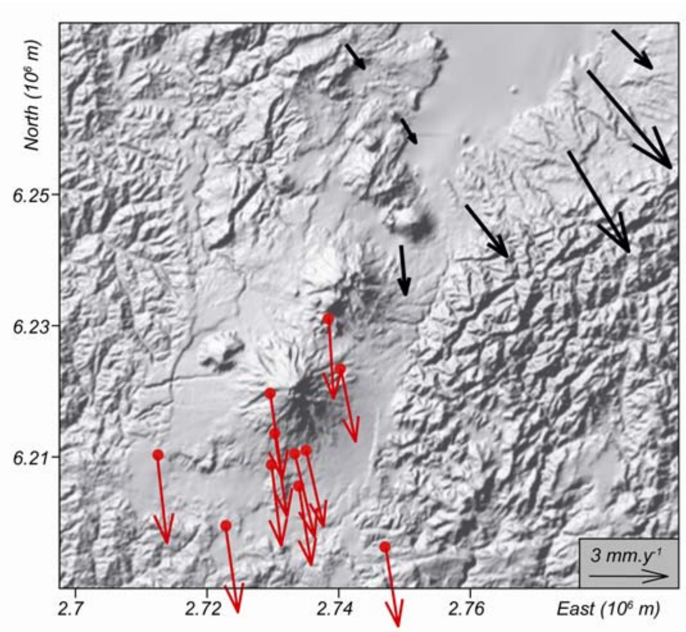

Figure 2 GPS displacement rates (mm.y^{-1}) relative to the Australian plate around the Tongariro National Park. In red: permanent GPS stations of the Tongariro National Park. In black: the closest sites periodically measured (Laura Wallace, GNS, personal communication).

Baseline solution analysis between the stations of the Tongariro National Park network is a more efficient tool for detecting deformation events of magmatic origin because the regional tectonic signal is cancelled. Because in the case of volcano crisis management we need to have near real-time data, we looked mainly at the hourly RTD data. The time series of displacements relative to the VGOB station shows no significant deformation over the entire observing period for each station (hourly values, Figure 3). But it is noticeable that there are large short-term variations in the apparent baselines, often taking place over about a day, that are probably weather-related (Figure 3).

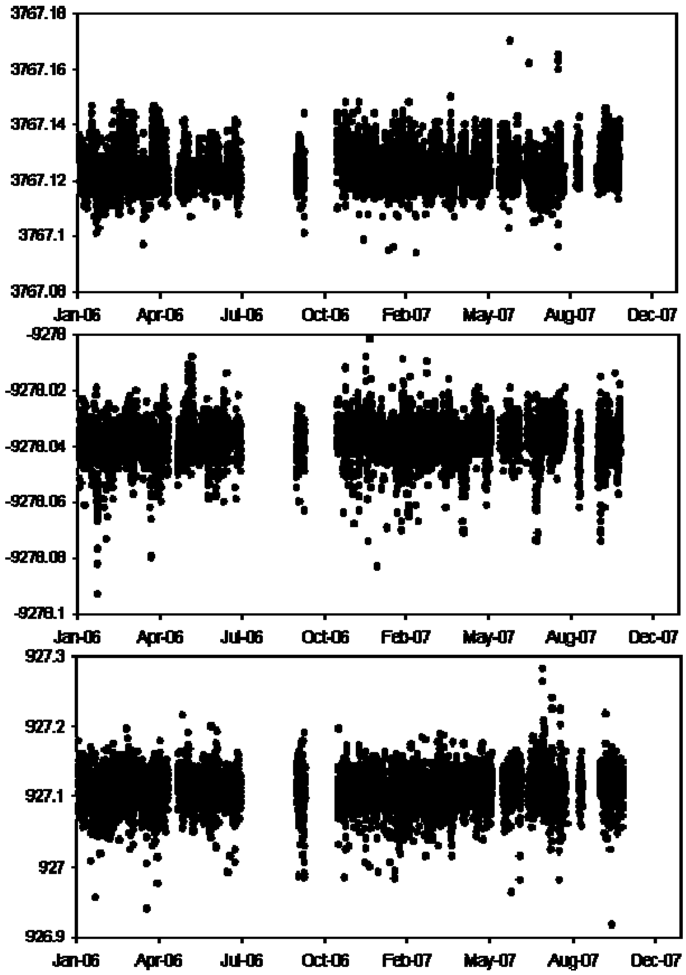

Figure 3 Evolution of the displacements (m) recorded in 2006-2007 on the VGWH GPS station relative to VGOB on the east (top), north (middle) and vertical (bottom) components. (RTD hourly averages).

The daily variations of up to 5 and 10 cm on the horizontal and vertical components, respectively, are thought to be related to atmospheric changes, influenced by the topography around Ruapehu (2797m) which affects the tropospheric GPS corrections (Figure 4). The height difference in the baselines related to the VGOB reference station are 50 m for (VGOB-VGPK) and 991 m for (VGOB- VGWH); and related to the VGMT station are between -48 m for (VGMT - VGPK) and 1252 m for (VGMT - VGWH).

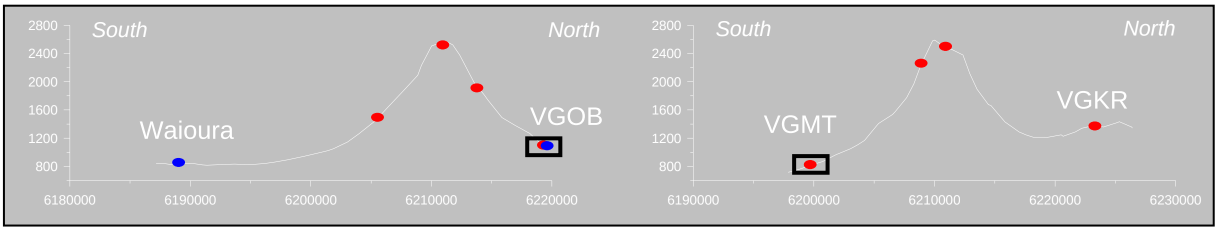

Figure 4 Elevation of the permanent GPS stations on the Ruapehu volcano (red: GPS stations, blue: meteorological stations) represented on two south-north cross sections (see Figure 1 for location of the cross-sections) (units are metres).

For example in June 2008, a blizzard crossed the central volcanic plateau (22-25 June), generating very bad weather conditions with snow showers in the Tongariro National Park (Figure 5).

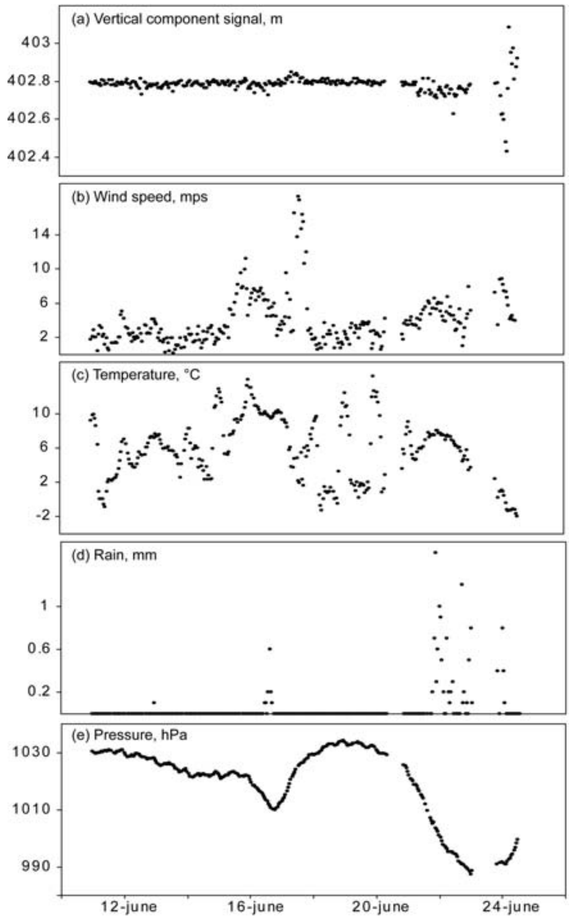

Figure 5 Comparison between the evolution of (a) the estimated vertical displacement of the VGWN - VGOB baseline (RTD hourly values), (b) the wind speed, (c) the temperature and (d) the rain recorded on the "Chateau" meteorological station and (e) the pressure recorded on the "Waiouru" meteorological station in June 2008.

The influence of the bad weather on the GPS recordings is especially clear on the VGWN-VGOB baseline, with high perturbations on 22, 23, 24, 25 June (days 174, 175, 176 and 177 on Figure 6) (Figures 5, 6); the two stations are located on opposite flanks of the Ruapehu volcano and are influenced by distinct weather conditions. These strong signal perturbations reveal the failure of the RTD GPS processing during bad weather conditions on the volcano. There are at least two possible reasons for the failure. One is that the assumption of horizontal stratification of the atmosphere is invalid. Another is that snow or ice has collected on one of the antennas (J. Beavan, personal communication); this can strongly affect the antenna phase pattern and therefore cause trade offs between the highly-correlated parameters of station height, zenith delay and antenna phase pattern. The VGWN-VGMT baseline was less disturbed because both stations are located on the same side of the volcano and by consequence were influenced by more or less the same weather conditions (Figure 7).

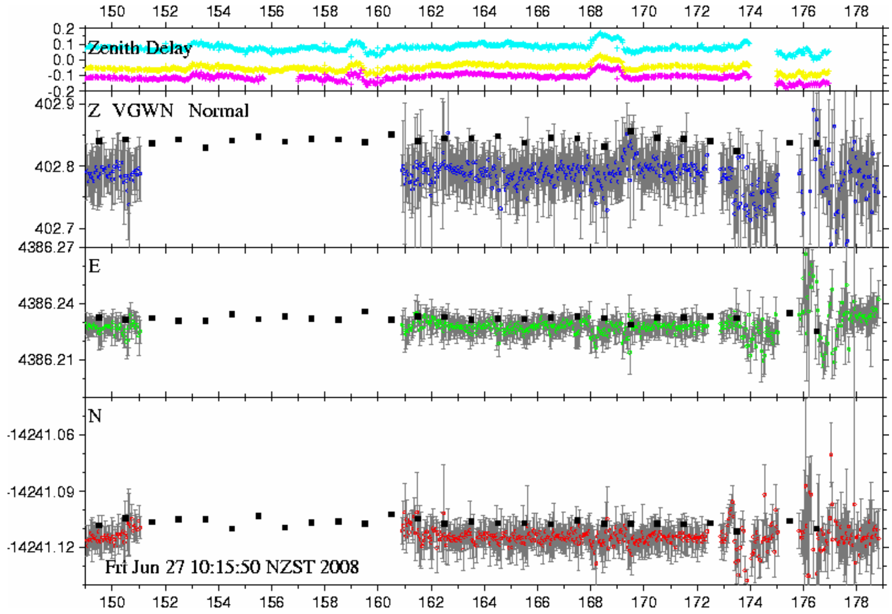

Figure 6 Evolution of the VGWN-VGOB baseline (m) in June 2008. (RTD hourly values, for comparison the squares represent the daily Bernese values). The daily zenith delays are from the Bernese processing.

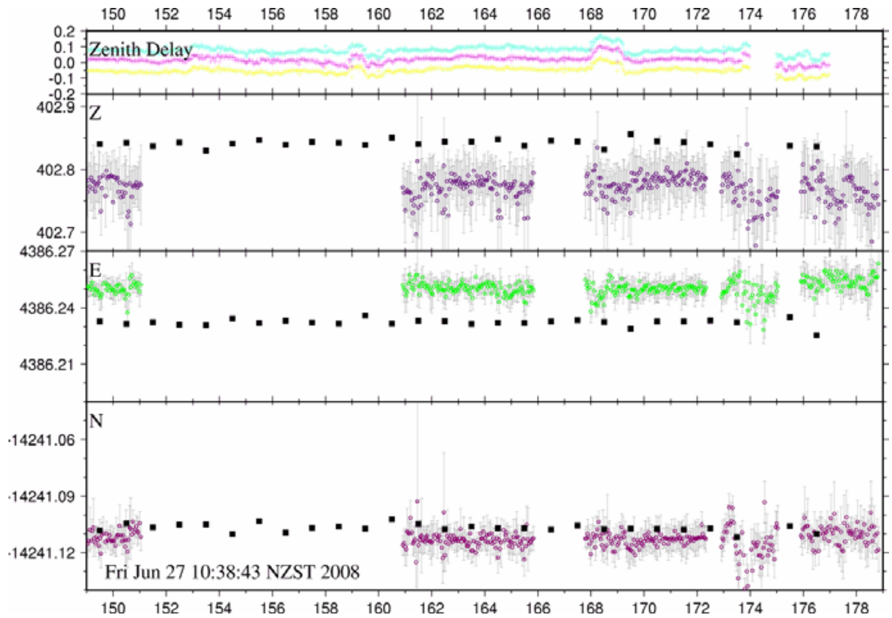

Figure 7 Evolution of the VGWN-VGMT baseline (m) in June 2008. (RTD hourly values, for comparison the squares represent the daily Bernese values). The daily zenith delays are from the Bernese processing.

In the same way, Figure 8 compares the evolution of vertical displacement of the VGWN-VGOB baseline recorded in June 2008 with the differential temperature recorded close to the VGWN summit station (FWVZ seismic station) and the “Chateau” station located close to the VGOB station (at about 1200m). The perturbation of the GPS signal corresponded to a period during which the weather conditions and notably the temperature were particularly variable between Ruapehu summit (VGWN) and the base of the volcano (VGOB) (Figure 8). Note that the FWVZ temperature (close to the VGWN GPS station) is recorded inside the instrument box, but typically follows the outside temperature pattern, although the inside temperature is higher, and rapid changes are delayed and attenuated. The time correlation between the temperature changes and the noisy GPS data highlights the relationship between these signals, and suggests the possibility of a causal connection.

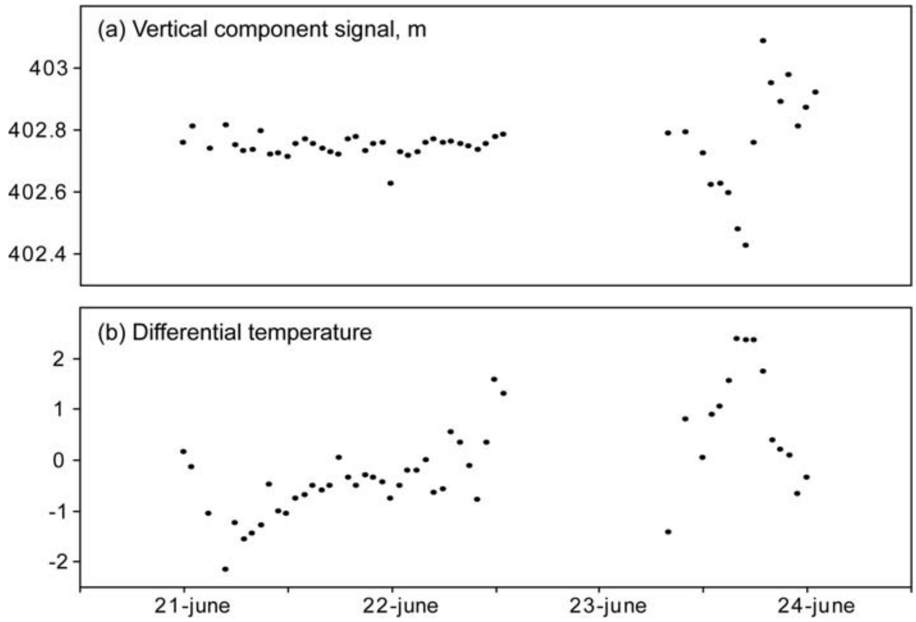

Figure 8 (a) Vertical displacement of the VGWN - VGOB baseline (RTD hourly values), and (b) temperature difference between the “Chateau” meteorological station (near VGOB) and the “FWVZ” seismic station (near VGWN) in June 2008.

Superimposed on these daily variations, slight long-term annual (seasonal) variations are found over all the GPS positions of the network with amplitudes of around 2 cm. These annual perturbations are shown on Figure 9 with an example of the vertical displacement recorded at the VGWH station relative to VGOB. There is a correlation between the long-term variations of the GPS signal, and the seasonal changes in temperature, pressure and humidity can be noted for (Figure 9).

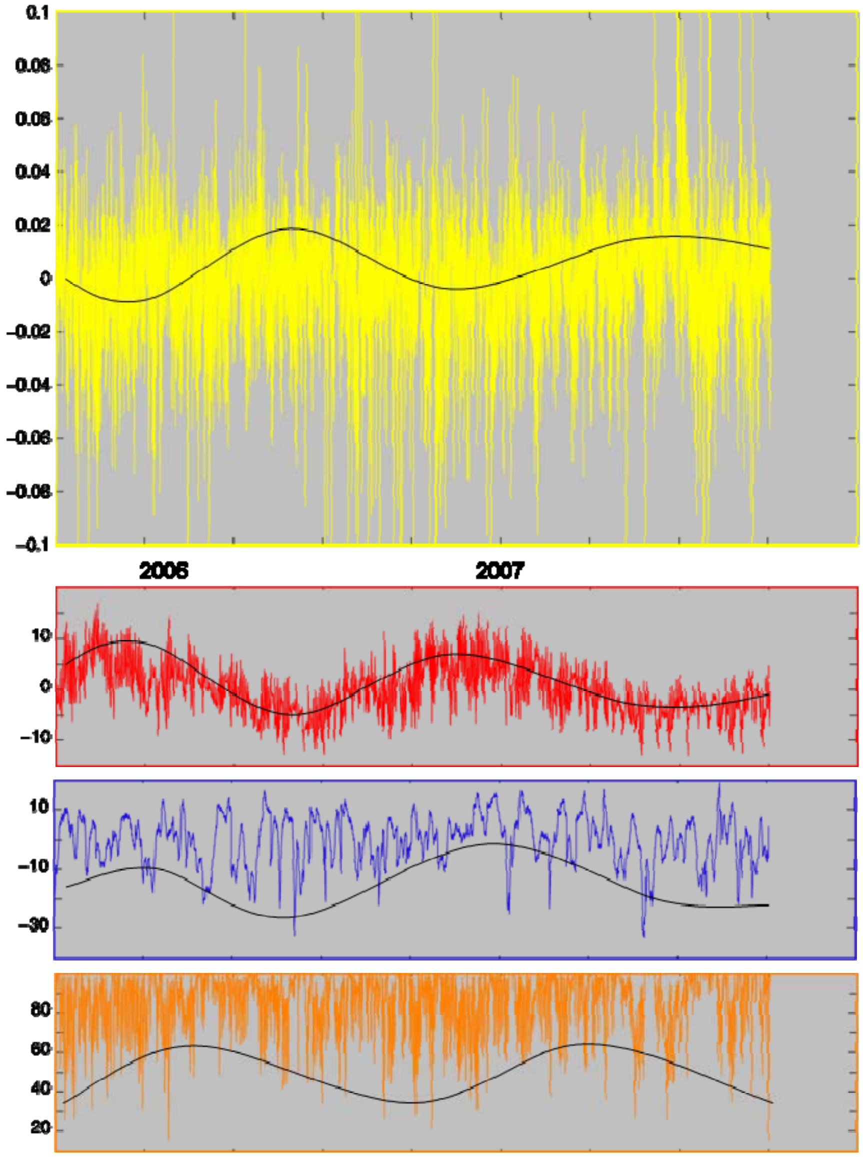

Figure 9 Comparison between the evolution of the vertical displacement of the VGWH - VGOB baseline (m, yellow; RTD hourly values), the temperature (°C, red) and humidity (%, orange) at the Chateau meteorological station, and the pressure recorded at the Waiouru meteorological station (hPa, blue) in 2006 and 2007. Black curves show a quasi-annual component obtained by smoothing each dataset.

Figure 10 compares the evolution of the apparent baseline difference between the VGWN and VGOB stations and the calculated daily zenith delay. The strong correlation (north component) and anti-correlation (east component) suggests that the main variations and thus a main part of the GPS background noise signals are linked to the tropospheric GPS corrections and are weather-related.

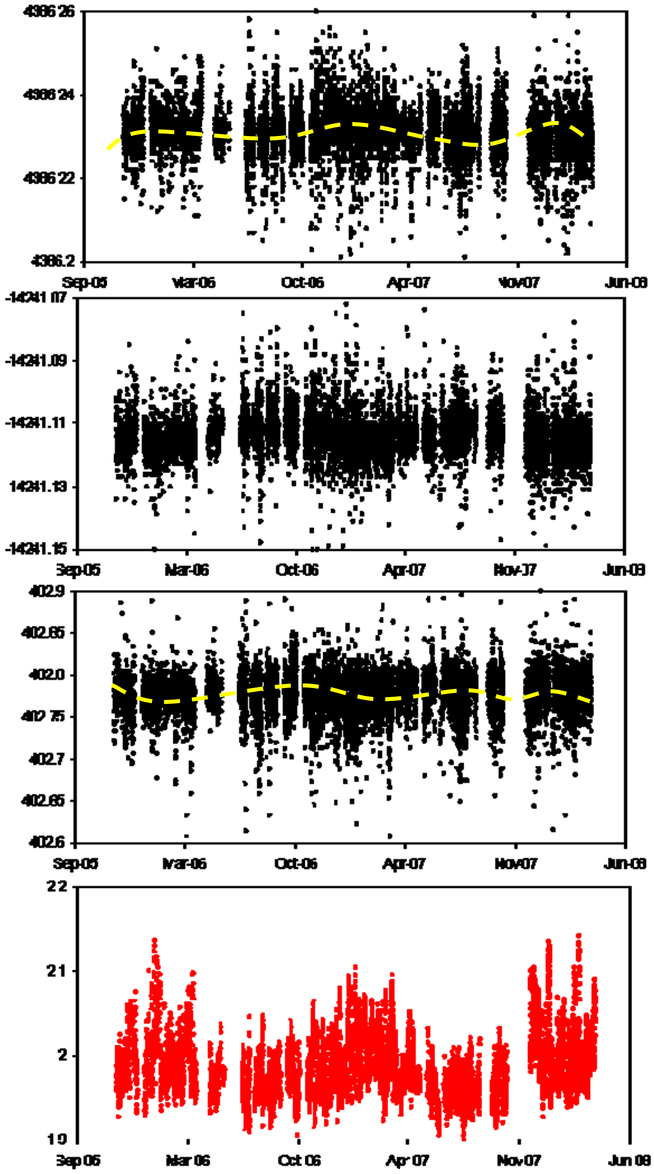

Figure 10 Evolution of the displacements (m) recorded in 2006-2007 on the VGWN station relative to VGOB on the east (top panel), north (2nd panel) and vertical (3rd panel) components (RTD hourly values). In red: the daily zenith delays calculated by the Bernese software. Dashed yellow and black lines: smoothed data.

Such daily and seasonal variations can easily be confused with deformation precursors of an eruption. Moreover pre-eruptive deformation expected on such andesitic volcanoes can be very weak (< 5 cm) and may thus be hidden by this high background noise. It is thus important to subtract any long and short-term weather signature before attempting any interpretation of the volcano deformation. We have tried to develop a method to correct for weather so as to better detect volcano deformation that might be a precursor of an eruption. For that, we looked at combining meteorological parameters used as inputs and GPS signal (which we assume is free of volcano deformation) used as output in a neural network, in order to calculate that part of the GPS signal linked with atmospheric parameters variations, and thus to correct the GPS readings.

1.3 Methods

We used neural network techniques to find a relationship between the atmospheric parameters (pressure, temperature, humidity, wind), and the apparent position changes of GPS recordings (background noise).

A multilayer neural network is regarded as a nonlinear mathematical function, which maps a set of input variables into a set of output variables. The process of determining the values of the parameters (weights assigned to interconnections between neurons) is called learning and training (Bishop, 1994; Rojas, 1996; White, 1990). The neural network is capable of learning and extracting complex relationships. Under a certain mathematical condition, a multilayer neural network can approximate any function with arbitrary accuracy by training it appropriately (Funahashi, 1989; White, 1990). As the network training process contains smoothing and interpolating functions, the network can produce a smooth inverse transformation of data. Those features make multilayer neural networks extremely useful and interesting for modelling complicated nonlinear relationships.

The commonest type of artificial neural network consists of three layers (input, hidden and output layers). The layer of "input" units is connected to the layer of "hidden" units, which is connected to the layer of "output" units (Figure 11).

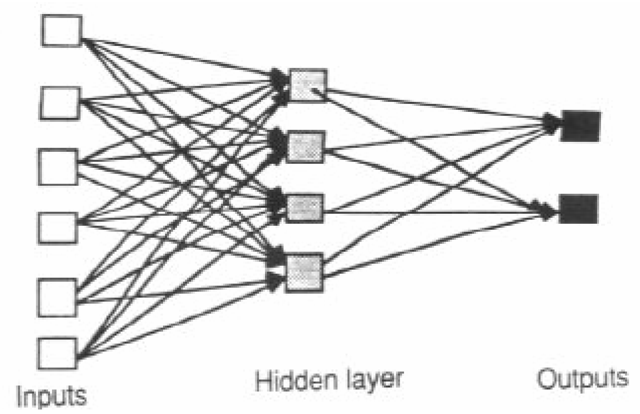

Figure 11 Neural network layout

The activity of the input units represents the raw information that is fed into the network. The activity of each hidden unit is derived by summing the activities of the input units, but with each activity being multiplied by the weight on the connection between that input unit and the hidden unit. Similarly, the behaviour of the output units depends on the activity of the hidden units and the weights between the hidden and output units. Both sets of weights are derived from the training process, in which we the network is tested with data for which the output is known.

In our case, we have five input units corresponding to the atmospheric parameters (temperature, humidity, pressure, rain, wind speed) and one output unit corresponding to the GPS background noise (bgn) signal (Figures 12, 13). We have also made further investigations that include the daily zenith delay in the input layers. For the output we use the RTD hourly-averaged data and consider each component of each baseline separately (i.e. a separate neural network has been calculated for each component of each baseline).

The atmospheric parameters are from the National Climate Database of NIWA (National Institute of Water and Atmospheric Research Ltd). We took the atmospheric data recorded on stations close to the GPS network, the “Chateau-Mt Ruapehu” land station (near the VGOB reference station, west of the network, Figure 1 for location) for the rainfall, temperature, solar radiation, humidity and wind speed, and the “Waiouru” land station (south-east of the network, Figure 1 for location) for the atmospheric pressure which is not recorded at “Chateau-Mt Ruapehu”. We made also further investigations with the temperature and the pressure recorded on the FWVZ seismic station located close to the VGFW GPS station at the summit of Ruapehu. But, as previously mentioned, the temperature and the pressure of the FWVZ seismic station are recorded inside the instrument box.

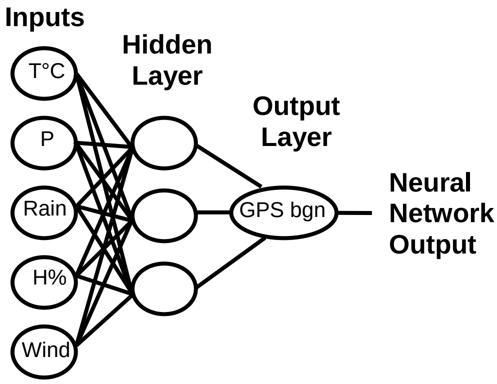

Figure 12 Neural network layouts used for our study

We used in our numerical program the “newff” non-linear function of the “neural network” toolbox of Matlab which creates a feed-forward backpropagation network.

We took the complete set of GPS data available for each station recorded between 2005 and 2008 (more than 10000 values), which seems not to be affected by volcano deformation. The first step was to divide the data up into training, validation and test subsets. One quarter of the data was taken as the validation set, another quarter as the test set and half as the training set. Then the inputs and targets of the training set were normalized so that they had zero mean and unity standard deviation.

During the learning/training stage, the neural network searches the relationship between the inputs and the output layer and generates an output result corresponding to a model of the background noise; i.e. the part of the GPS signal induced by the atmospheric parameter variations.

The neural network is then validated with new data, previously unknown to the neural network.

The validated neural network can be then used to apply a correction on the whole set of data and in the future on new data. The neural network output result is used as a filter to correct the GPS recording from background noise linked with the atmospheric parameter variations:

Output Layer (bgn) - Neural Network Output = No weather-dependent signal

The remnant signal could be thus attributed to real ground movement or other sources not weather-related.

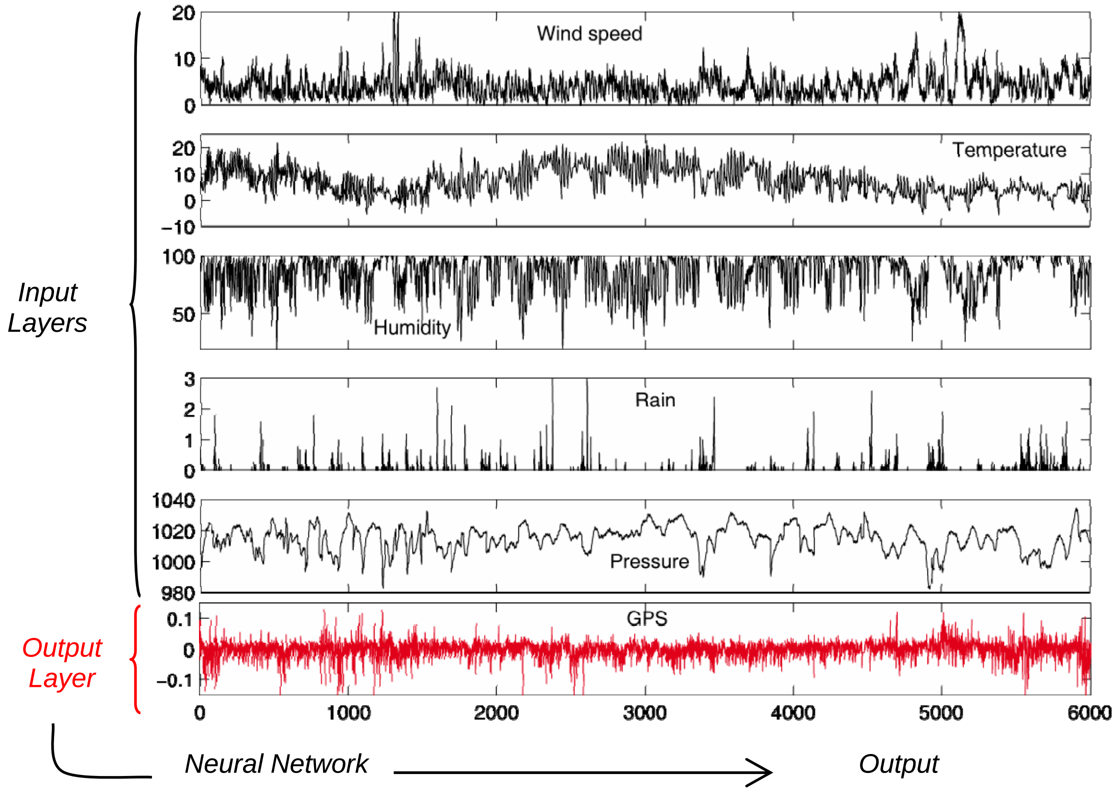

Figure 13 Data used in the neural network layers. Wind speed km/hr, temperature °C, humidity %, rain cm and pressure hPa.

1.4 Results

To correct the signal recorded for each GPS station, we have used the neural network which displayed the best results after the learning/training and the validation stages applied on time periods not disturbed by volcanic activity; note that valid neural network is different for each component of each baseline. The valid neural network allows us to draw the background noise generated only by the variations of atmospheric parameters. The output of the neural network has then been used as a filter to correct the GPS recordings and delete (or at least minimize) the perturbations due to the atmospheric parameter variations (Figure 14, 15).

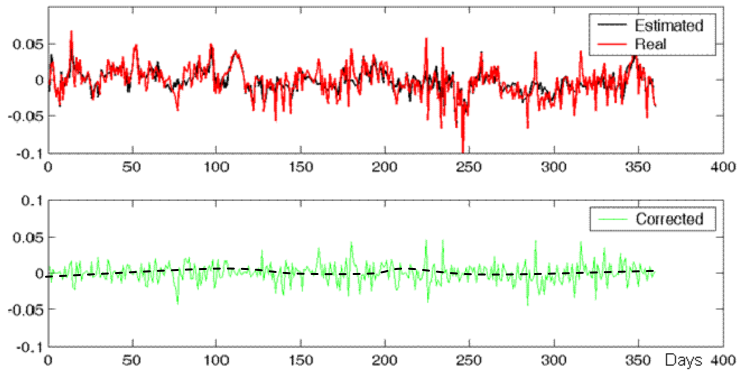

Figure 14 Red: uncorrected signal (RTD hourly values), i.e. the evolution of the vertical displacements of the VGWH-VGOB baseline in 2006; Black: background noise linked with the variation of atmospheric parameters estimated by neural network; Green: corrected signal. Dashed black lines: smoothed data.

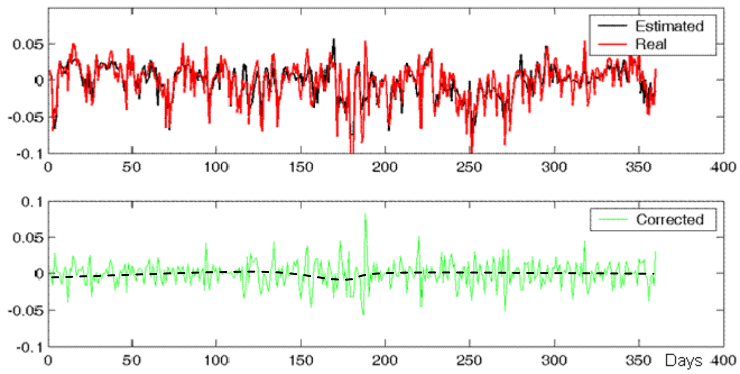

Figure 15 Red: uncorrected signal (RTD hourly values), i.e. the evolution of the vertical displacements of the VGWH-VGMT baseline in 2006; Black: background noise linked with the variation of atmospheric parameters estimated by neural network; Green: corrected signal. Dashed black lines: smoothed data.

Our results reveal that the long-term seasonal variations, previously described, and the intermediate-term variations (i.e. 5-10 days) have been clearly reduced. But although the short-term daily variations have been attenuated, they remain at a level of about 50 mm (instead of 100 mm when the data were not corrected) (Figures 14, 15).

The long-term seasonal variations can be easily corrected with a neural network integrating only the atmospheric parameters recorded on the "Chateau" meteorological station as inputs. Indeed, during one year (one season) the amplitude variation of the weather parameters can be supposed similar at each GPS station (averaged over a long period). Note that the best results are obtained for the VGOB baselines, probably because the weather conditions affecting the VGOB GPS station are the same as the ones recorded on the "Chateau" meteorological station, located only 300m away.

1.5 Discussion

The neural network corrections have only partially reduced the short-period variations. This may be because of the lack of records of atmospheric parameters at each GPS station. These trials were done on the RTD results, as they had the time resolution to see whether the short-period variations were corrected. In fact, the improvement in the longer-period resulted in the RTD long-period noise level dropping to be comparable with the Bernese results. Use of the neural network on the Bernese results did not produce any significant improvement. In other words, the neural network has allowed us to improve the RTD solutions, but only to about the standard of Bernese solutions.

Because of the high elevation of the Ruapehu volcano and the long baselines between each station, the weather parameters and their changes during the same day can be very different on opposite flanks of Ruapehu volcano and at the base and the summit of the volcano. Figure 8 showed that the distinct weather conditions on the two stations of a baseline could be relatted to the short-term perturbations on GPS recordings. For instance, in January 2008, the absolute temperature and its daily amplitude variation was normally somewhat greater at the "Chateau" meteorological station (1097m altitude) than at the FWVZ seismic station (2043m altitude, and recorded inside the box), but around the 22nd January the FWVZ temperature decreased some time before the Chateau station was affected (Figure 16). This coincided with substantial variations in the VGWH-VGOB baseline (FWVZ was not operating) shown in Fig 17. Note that in January, significant snow or ice deposition is unlikely, even at high altitudes.

The remnant daily errors are thus due to the long baselines and the high differential elevation between stations, which imply different conditions at different places in the lower level of the troposphere, in other words, the troposphere is not horizontally stratified. In order to remove the daily variations that produce a background noise of several cm, further investigations will be necessary, notably by taking into account the weather parameters recorded at the two stations of a baseline.

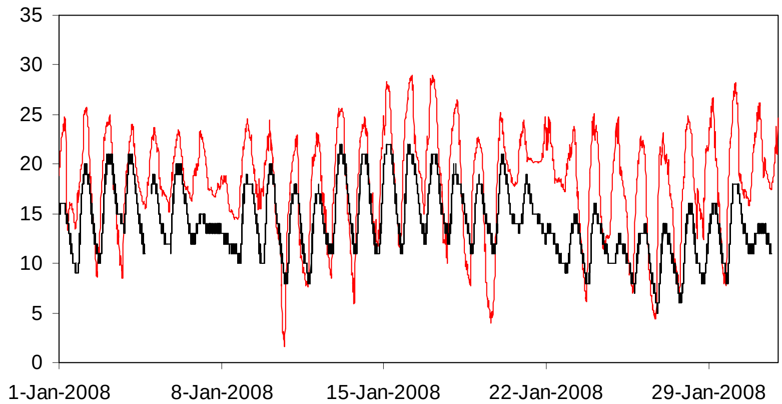

Figure 16 Temperature fluctuations recorded on the "Chateau" meteorological station located at 1097 m of elevation (°C, red) and on the FWVZ seismic station (°C, black) located at 2043 m of elevation in January 2008.

The strong correlation shown on Figure 8 between atmosphere parameters and GPS variations is not always so evident, even if we take into consideration the temperature data recorded close to the GPS station on the volcano. During the two week period shown in Figure 5 a time series analysis indicated no direct correlation between the resultant height component and the corresponding temperature, pressure and humidity measures Further investigations will be thus necessary.

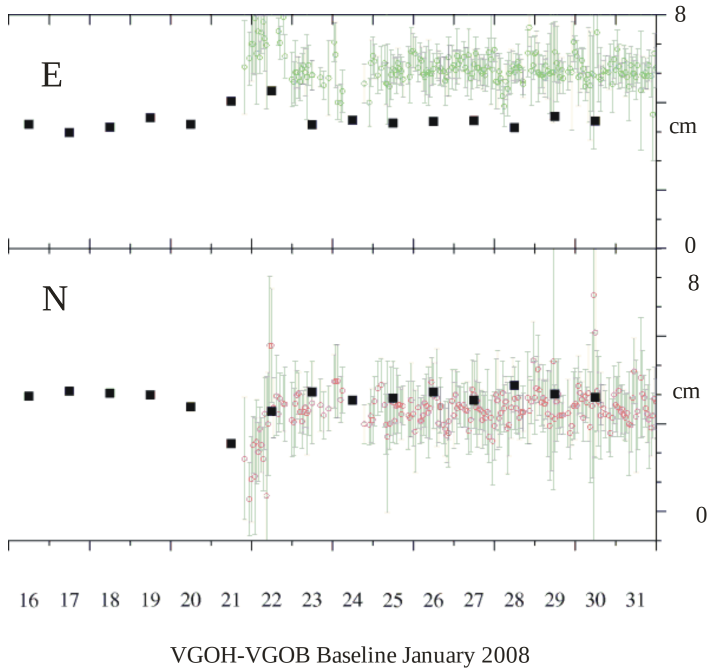

Figure 17 VGWH-VGOB baseline lengths during January 2008. Black squares are Bernese daily values, coloured symbols show hourly RTD values (with inter-quartile range).

The Bernese solutions, which are normally done for 24 hours of data, include a tropospheric tilt term to account for first order changes in the troposphere with position. John Beavan (pers. comm.) tried more frequent analysis of the tropospheric terms for 22-26 January 2008, and found that some improvement was obtained. This suggests that the way forward may be to use an improved atmospheric model within the GPS processing system, rather than trying to use a heuristic method such as a neural network to correct GPS data processed with an inadequate tropospheric model

Another way to improve the accuracy of the GPS positions may be to relate each station high on a volcano to a nearby base station off the volcano, rather than try and have a single base station. The shorter baseline should give smaller errors between the high and low stations, while we may be able to get accurate relative positions of the low stations because they are far enough from the volcano that the horizontally stratified assumption for the troposphere may be valid. It would be worth investigating whether such a technique can improve the consistency of the calculated positions.

1.6 Conclusion

For a GPS network implemented in the mountainous Tongariro area, RTD processing produces background noise in the site position time series, which is worse when severe weather systems are passing across the region.. Estimating a correction to the GPS baseline values using weather parameters embedded in a neural network provided some improvement to the consistency of the RTD processed results, especially for the long-term variations. Further investigations will be necessary to make any greater reduction in the noise level of the GPS processing from the volcano network and better understand its origin.

1.7 References

Bishop, B.M., 1994. Neural networks and their applications. Rev. Sci. Instrum., 65: 1803-1832.

Elgered, G., 1993. Tropospheric radio-path delay from ground-based microwave radiometry. In: J.W.a.S. Inc (Editor), Atmospheric Remote Sending by Microwave Radiometry, pp. 215-258.

Funahashi, K., 1989. On the approximative realization of continuous mappings by neural networks. Neural Networks, 2: 183-192.

Rojas, R., 1996. Neural networks: A systematic Introduction. Springer, New-York.

Pany, T., Pesec, P. and Stangl, G., 2001. Atmospheric GPS slant path delays and ray tracing through numerical weather models, a comparison. Physics and Chemistry of the Earth, Part A: Solid Earth and Geodesy. 26: 183-188.

Wallace, L., Beavan, J., McCaffrey, R. and Darby, D.J., 2004. Subduction zone coupling and tectonic block rotations in the North Island, New Zealand. Journal of Geophysical Research, 109(BI12406): doi:10.1029/2004JB003241.

White, H., 1990. Connectionist nonparametric regression: Multilayer feedforward networks can learn arbitrary mappings. Neural Networks, 3: 535-549.

Journal of Volcanology and Geothermal Research xxx (2009) xxx–xxx

Contents lists available at ScienceDirect

Journal of Volcanology and Geothermal Research

journal homepage: www.elsevier.com/locate/jvolgeores

Structures involved in the vertical deformation at Lake Taupo (New Zealand) between 1979 and 2007: New insights from numerical modelling

Aline Peltier [a,*], Tony Hurst [a], Bradley Scott [b], Valérie Cayol [c]

[a] ~~GNS Science, Lower Hutt, New Zealand~~
[b] ~~GNS Science, Taupo, New Zealand~~
[c] ~~Laboratoire Magmas et Volcans, Clermont-Ferrand, France~~

A R T I C L E   I N F O

Article history:
Received 16 May 2008
Accepted 9 January 2009
Available online xxxx

Keywords:
Lake Taupo
Taupo Volcanic Zone
lake levelling
numerical modelling
vertical deformation
rifting
hydrothermal circulation

A B S T R A C T

Since 1979, repeat levelling measurements have been conducted on the lake filling the caldera of the dormant Taupo rhyolitic volcano in the North Island of New Zealand. Interpretation of these data through numerical modelling provides information on the structures involved in the relative vertical crustal movement throughout the southern end of the Taupo Volcanic Zone (TVZ), an area of active back-arc extension. The best-defined feature is a long term global subsidence of the northern part of the lake (7 mm yr^{-1}) due to the cumulative effect of the crust stretching and a deep deflation source. This long term subsidence is occasionally disturbed by strong short-term uplifts linked with overpressure sources located below the northern part of the lake, near active geothermal fields. Episodes of uplift can be attributed to various combinations of the following two processes taking place beneath the geothermal field (1) Movement or formation of rhyolitic magma (deepest sources) (2) Pressurization of the shallow hydrothermal fluid reservoir that traps volatiles exsolved from a crystallizing rhyolitic magma (shallowest sources). The pressurization of the shallow hydrothermal system gives rise to tensional stresses in the upper crust, resulting in seismic and aseismic fault ruptures. Slow slip motion of the Kaiapo fault decouples on a short-term scale the ground deformation pattern on both sides of the fault. Our results, discriminating what parts of the deformation are due to the regional setting, the hydrothermal circulations and the seismic activity, reveal that each seismic swarm is preceded by 1 to 3 years of inflation of the eastern part of the lake. This systematic behaviour may allow us in the future to better predict the occurrence of the seismic swarms below the lake.

1. Introduction

Since the 20th century, lake levelling measurements have been used as natural tiltmeters to constrain ground deformation by evaluating the relative water height changes measured at different sites on a lake (Wilson and Wood, 1980; Hamilton, 1987; Hudnut and Beavan, 1989; Otway and Sherburn, 1994). In the Taupo Volcanic Zone (TVZ) of New Zealand, repeated lake levelling measurements have been conducted since 1979 in the lake filling the caldera of the Taupo dormant volcano. Data covering the period 1979–1999 has been already well described by Otway (1986, 1987, 1989), Otway et al. (2002), Otway and Sherburn (1994) and Smith et al. (2007) and reveal a long-term subsidence in the northern part of the lake occasionally disturbed by short-term uplifts in localized areas. Except for Smith et al. (2007) who have modelled the subsidence observed between 1986 and 1999 by a Mogi point dilatation at 8 km depth, the cause of the vertical deformation evolution through time has not been well constrained. Thus the location and the shape of pressure sources and the mechanisms at the origin of vertical deformation fluctuations at Lake Taupo between 1979 and 2007 remain poorly known. Regional rifting, geothermal fields and fault motions, which all characterize the Taupo area, can strongly affect the ground deformation and must be distinguished from any magmatic deformation. Ellis et al. (2007) investigate the effect of a hypothetical magmatic inflation event in the subsurface magmatic system of Taupo. The models demonstrate that surface displacements associated with magma body inflation up to 10 km^3 in volume at 15 km depth beneath Lake Taupo may be almost entirely hidden. It is thus important to understand the origin of the current deformation recorded at Lake Taupo and to discriminate the part of the deformation linked with regional rifting, geothermal fields and fault motions. The aim of this paper is to constrain the location and the origin of the sources and the structures involved in the vertical deformation at Lake Taupo between 1979 and 2007. We present an overview of the levelling data recorded between 1979 and 2007 and their interpretation through 3D numerical modelling using both finite element method (FEM), taking into account the regional

* Corresponding author. Present address: Institut de Physique du Globe de Paris, CNRS, UMR 7154-Géologie des Systèmes Volcaniques, 4 place jussieu, Paris, France. Tel.: +33 1 44 27 25 06; fax: +33 1 44 27 73 85.
E-mail addresses: peltier@ipgp.jussieu.fr (A. Peltier), t.hurst@gns.cri.nz (T. Hurst), b.scott@gns.cri.nz (B. Scott), V.Cayol@opgc.univ-bpclermont.fr (V. Cayol).

0377-0273/$ – see front matter © 2009 Elsevier B.V. All rights reserved.
doi:10.1016/j.jvolgeores.2009.01.017

setting (rifting) and the local structures of the TVZ, and boundary element method inversion (BEM).

2. Geological setting

The Taupo volcano is located in the southern part of the rifting continental crust of the TVZ (Fig. 1A, B). The TVZ is about 50 km wide and 200 km long and lies above the oblique subduction of the Pacific plate beneath the North Island of New Zealand and the Australian plate. This zone of crustal thinning and extension is characterized by exceptionally high fracturing expressed by the Taupo Fault Belt, with dominantly normal faults oriented in a northeast direction, high heat flows with numerous geothermal fields, and intense volcanic activity.

The Taupo caldera formed during the voluminous Oruanui eruption about 22,600 years before present (BP) and is now filled by Lake Taupo. Most of the past activity was characterized by rhyolitic eruptions occurring down the eastern side of the Lake Taupo along a NNE–SSW trend (Fig. 1C; Wilson et al., 1995; Sutton et al., 2000; Wilson, 2001). The most recent major eruption took place about 1800 years BP from at least three vents along a NE–SW-trending fissure centred on the Horomatangi Reefs, corresponding to a prominent low-resistivity zone (Fig. 1C; Caldwell and Bibby, 1992; Whiteford et al., 1994).

3. Seismic activity

Seismic activity in the TVZ zone is particularly well marked (Fig. 2A) and is characterized by numerous shallow earthquakes of M_L 2–4 located at depths less than 8 km (Bryan et al., 1999). During the 1979–2007 period, the shallow seismicity (mostly around 5±2 km depth) recorded below Lake Taupo was focused in localized areas beneath the central, eastern and southern parts of the lake (Fig. 2B). The Taupo Fault Belt, north of the lake, was also seismically very active, whereas the northern half of the lake corresponding to the caldera was aseismic. Thus, four main seismic restricted zones can be distinguished (Sherburn, 1992; Bryan et al., 1999): (1) the area east of Scenic Bay (SB in Fig. 1C) extending along the Waihi Fault, (2) the Horomatangi Reefs area, (3) the area near Motuoapa (MA in Fig. 1C) and extending outside of the southern part of the lake and (4) the Taupo Fault Belt, north of the lake.

Fig. 2A represents the cumulative number of shallow earthquakes recorded in the Taupo Lake area between 1979 and 2007. The seismicity distribution is not uniform over time. At irregular intervals, seismic swarms occurred. Such shallow seismic swarms (≤5 km depth) were recorded in February 1983, June–July 1983, March 1984, March 1987, July 1997–December 1998, and December 2000–June 2001 (Fig. 2A, C).

- The first seismic swarm of the study period occurred in February 1983 in the western part of the Taupo Fault Belt, around 10 km northwest of Kinloch (KH in Fig. 1C) (Fig. 2C).
- On 16 June 1983, another seismic swarm began and was followed by 5 weeks of local seismicity (64 events with magnitudes of 3 or more, Webb et al., 1986). Two clusters can be distinguished, one in the Taupo Fault Belt in the northern part of the lake between Kinloch (KH in Fig. 1C) and Acacia Bay (AB in Fig. 1C) and one near the Horomatangi Reefs (1–2 July 1983, Webb et al., 1986). One week after the beginning of the seismic swarm, a 50 mm normal fault offset was recorded on the Kaiapo fault with ground rupture over a distance of 1.2 km (Grindley and Hull, 1984; Otway, 1986). The Kaiapo fault motion, located east of the first seismic swarm and north of the second one, was not obviously linked directly with the swarms and may reveal a slow slip fault motion.
- The two small seismic swarms recorded in March 1984 and March 1987 occurred below the south-western and middle-western part of the lake, respectively.
- After about ten years of low seismic activity, a new seismic swarm occurred below the lake from July 1997 to December 1998. The epicentres were located near the Horomatangi Reefs and along the southern rim of the caldera (Fig. 2C).
- From December 2000 to June 2001, a strong increase of the seismicity was recorded (Fig. 2A). During this period, two main clusters can be distinguished: one in the area of Scenic Bay occurring in December 2000 followed by one north of the lake along the northern end of the Kaiapo fault occurring between January and June 2001 (Fig. 2C).

Between 2001 and 2007, seismicity has been more or less constant over time without any significant peak of strong activity and is distributed uniformly between each of the seismic zones described above (Fig. 2A and C).

4. Lake levelling data

4.1. Survey method

Since April 1979, periodic (3–4 times per year) lake levelling surveys have been conducted to monitor relative vertical deformation at Lake Taupo. The network consisted of only 7 sites in 1979–83 but following the June 1983 seismic swarm, the network was improved and now consists of 22 sites around the shoreline and on islands (Fig. 1C; Otway et al., 2002). Data are collected with a portable water level gauge that samples the

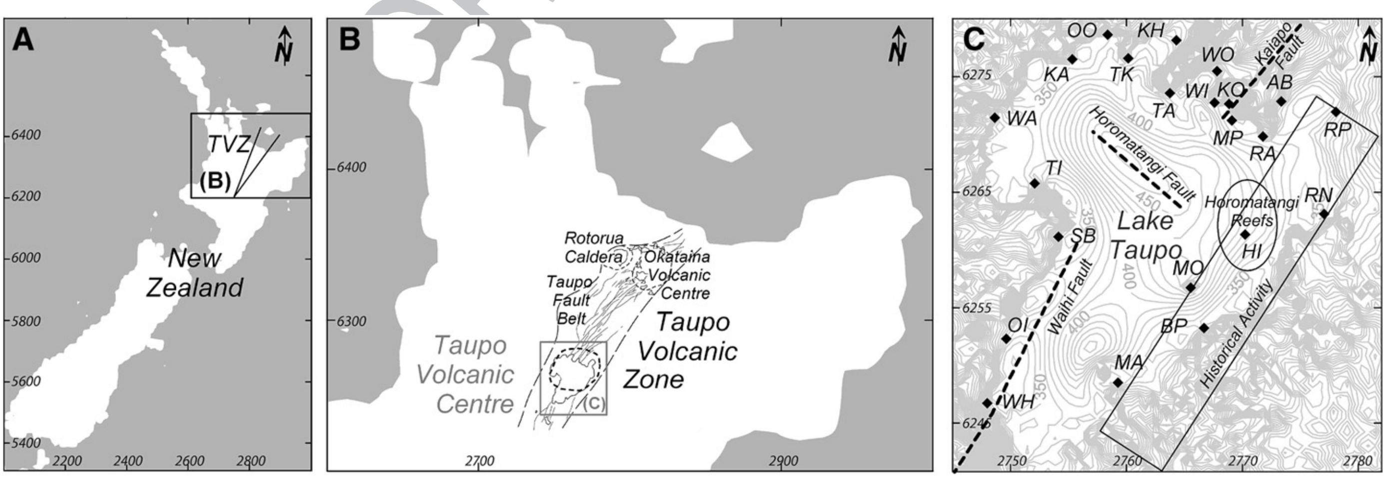

Fig. 1. (A) Location of the Taupo Volcanic Zone (TVZ). (B) Location of the main structures of the TVZ (the main calderas are underlined by dotted circles). (C) Location of lake levelling sites (diamonds), Waihi, Horomatangi and Kaiapo fault traces (dotted lines) and historical activity (NNE–SSW rectangle, after Wilson et al., 1984). Coordinates are in New Zealand Map Grid Projection (km).

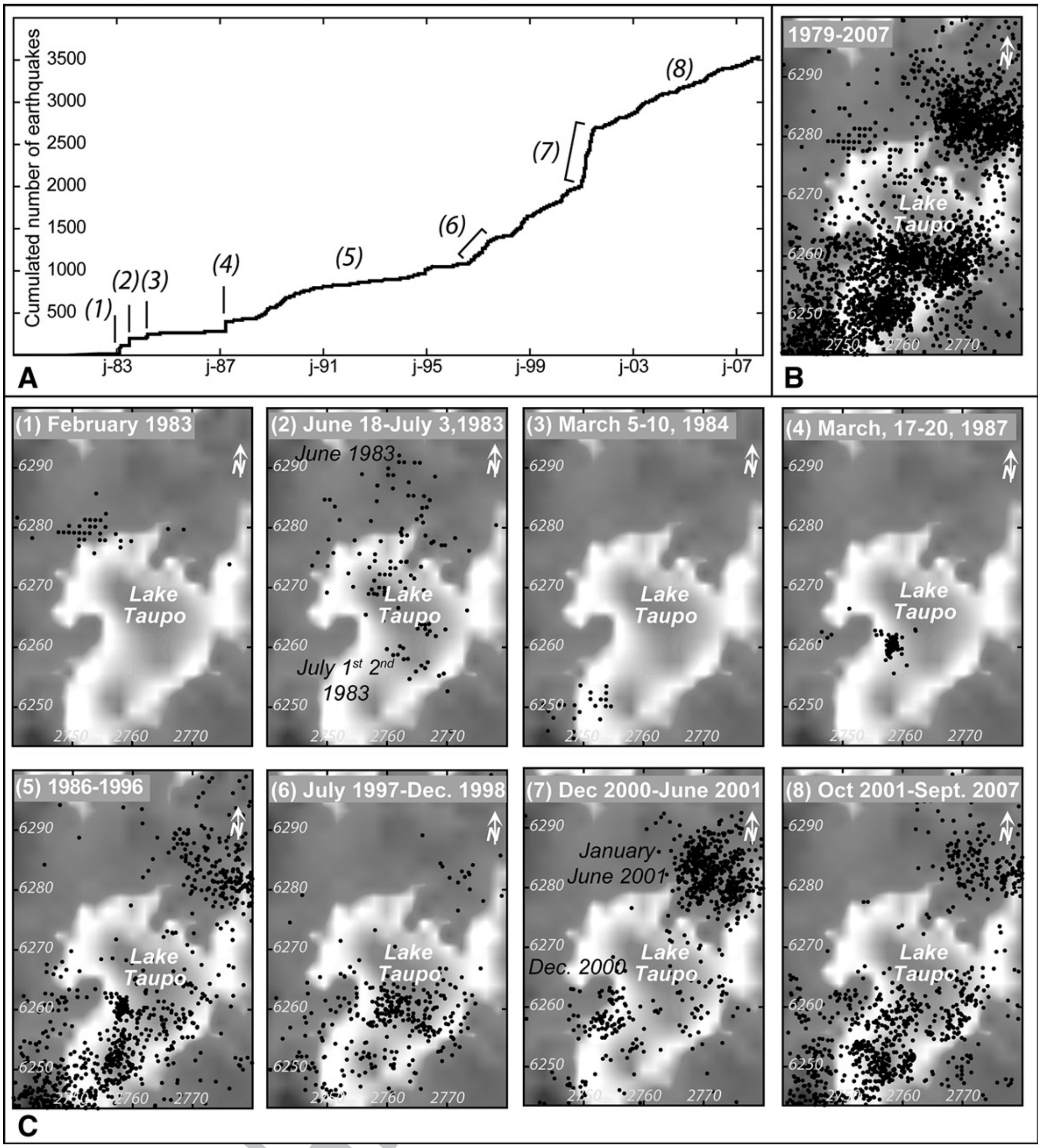

Fig. 2. (A) Cumulative number of shallow earthquakes (<6 km depth) recorded between January 1979 and December 2007, (B) Location of the shallow seismicity epicentres recorded between January 1979 and December 2007 in the Lake Taupo area, and (C) recorded during specific time periods: (1) February 1983, (2) 18 June to 3 July 1983, (3) 5 to 10 March 1984, (4) 17 to 20 March 1987, (5) 1986–1996, (6) July 1997 to December 1998, (7) December 2000 to June 2001, (8) October 2001 to September 2007. Data are from http://magma.geonet.org.nz/resources/quakesearch and from Webb et al. (1986) for the 1983 seismic swarms. Coordinates are in New Zealand Map Grid Projection (km).

water level every 15 s and records for about 30 min to cover the period of typical seiches in the lake and obtain a mean value. Otway et al. (2002) estimated that the standard error for each site could be represented by: SE (mm) = 1.2 + 0.1*D* where *D* is map distance in kilometres from the origin, RP. For a typical survey the standard deviation ranges from 2 to 5 mm (Otway, 1987; Otway et al., 2002).

4.2. Vertical deformation evolution between 1979 and 2007

Lake levelling data recorded at each site between 1979 and 2007 are plotted in Fig. 3 in the form of apparent height changes relative to the origin, RP.

Regarding the evolution of the vertical motion trend of the whole network, eight main periods can be distinguished: (1) October 1982–June 1983, (2) June 1983–January 1984, (3) January 1984–March 1996, (4) March 1996–December 1999, (5) December 1999–June 2001, (6) June 2001–June 2002, (7) June 2002–June 2003 and (8) December 2004–September 2007. For the 1979–1982 period, vertical deformation was weak and no clear trend can be highlighted.

To visualize the pattern and the wavelength of vertical deformation for the eight selected periods, rates of vertical displacements relative to the origin, RP, are reported in Fig. 4.

(1) October 1982–June 1983

From October 1982, the rate of height change relative to the origin RP increased with a strong rise recorded until June 1983 at five of the six sites (HI, KH, RA, RN, SB) already in place (0.01 to 0.07 m yr^{-1}), whereas the MA site located in the south-eastern part of the lake recorded a subsidence of 0.02 m yr^{-1} relative to RP. The greatest change was recorded at the RA site, far away from the February 1983 seismic swarm (Figs. 2C and 4).

(2) June 1983–January 1984

Please cite this article as: Peltier, A., et al., Structures involved in the vertical deformation at Lake Taupo (New Zealand) between 1979 and 2007: New insights from numerical modelling, Journal of Volcanology and Geothermal Research (2009), doi:10.1016/j.jvolgeores.2009.01.017

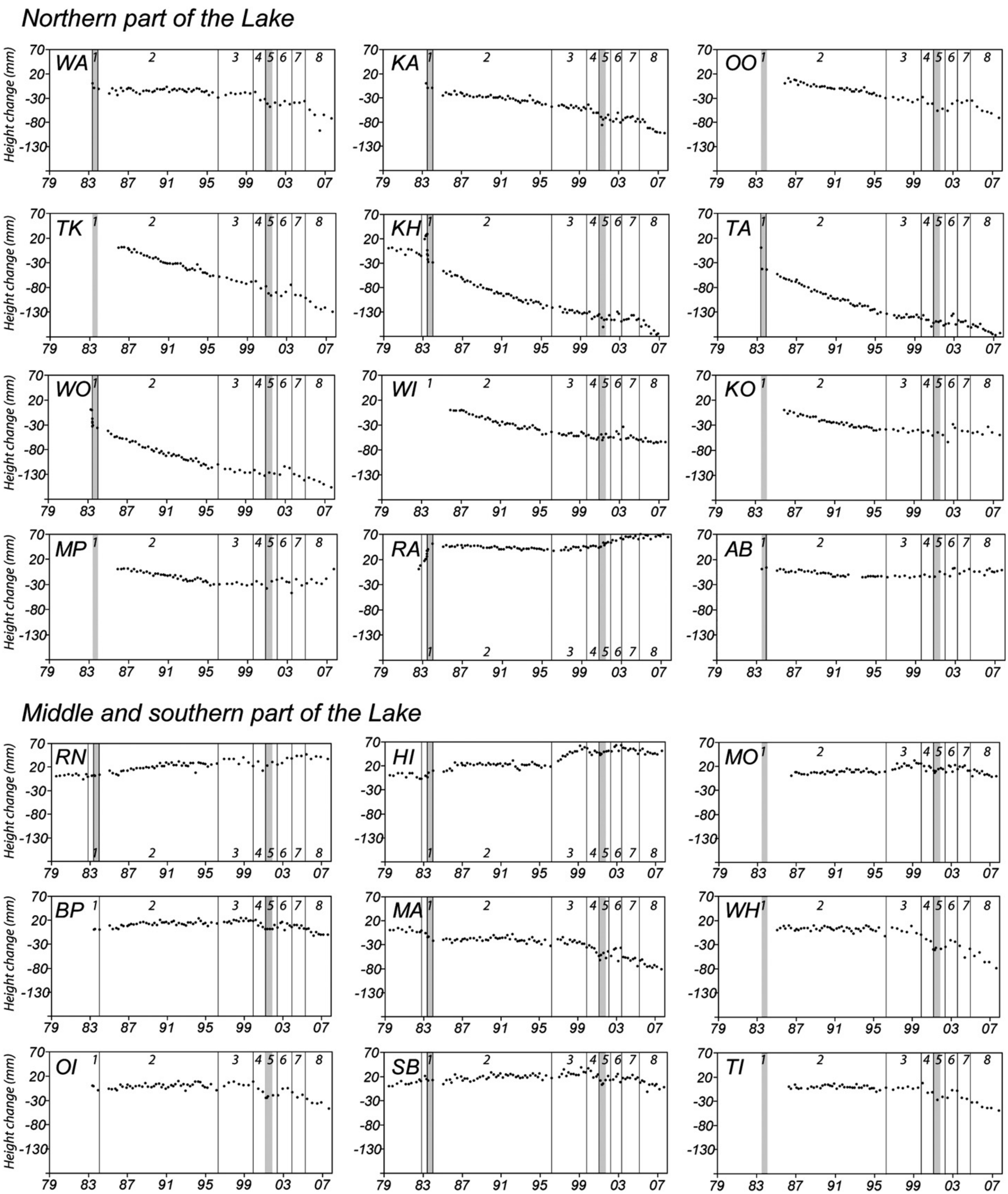

Fig. 3. Height changes relative to RP (mm) recorded between April 1979 and September 2007 at Lake Taupo. The lines highlight changes in the global deformation trend and numbers refer to the distinct deformation periods described in the text. Grey areas represent periods of strong seismic activity below the lake.

The global uplift recorded on the northern part of the lake since October 1982 was disrupted in June 1983. On 20 June 1983, an abrupt inversion of the signal at the KH site occurred with a total subsidence of 0.03 m relative to RP recorded between June 13th and July 19th 1983. This change in the lake tilt behaviour happened at the same time as the increase of the seismicity below the lake area (June–July 1983 seismic crisis, Fig. 2C) and the 50 mm offset on the Kaiapo fault, located north-east of the lake (Grindley and Hull,

Please cite this article as: Peltier, A., et al., Structures involved in the vertical deformation at Lake Taupo (New Zealand) between 1979 and 2007: New insights from numerical modelling, Journal of Volcanology and Geothermal Research (2009), doi:10.1016/j.jvolgeores.2009.01.017

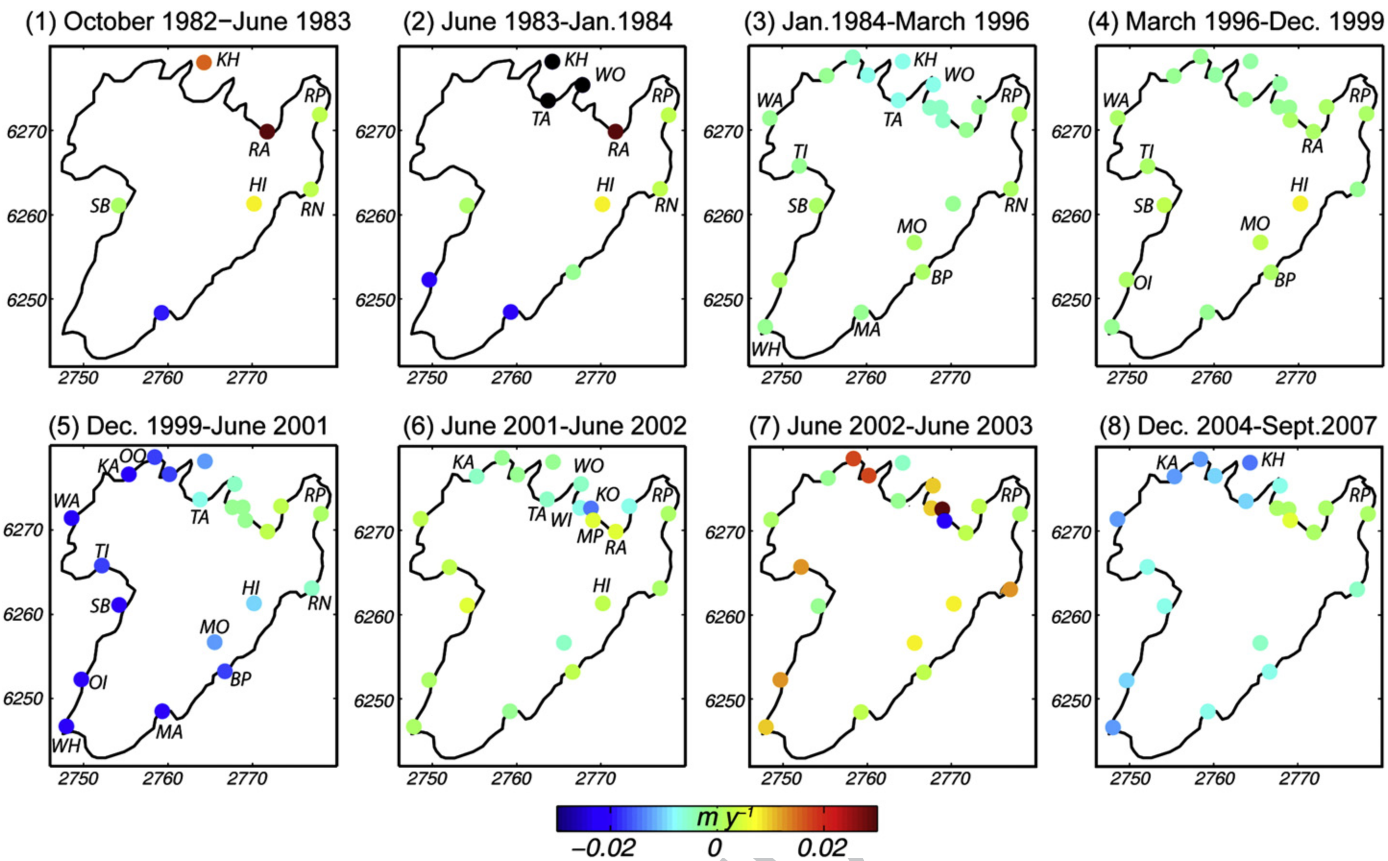

Fig. 4. Vertical deformation rates relative to RP (in m yr^{-1}) for the eight separate periods: (1) October 1982 to June 1983, (2) June 1983 to January 1984, (3) January 1984 to March 1996, (4) March 1996 to December 1999, (5) December 1999 to June 2001, (6) June 2001 to June 2002, (7) June 2002 to June 2003, and (8) December 2004 to September 2007. The labels refer to the sites mentioned on the text. Coordinates are in New Zealand Map Grid Projection (km).

1984). Within the monitored area both uplift and subsidence were recorded until January 1984. During this period, all sites located east of the Kaiapo fault (RA, HI, RN) recorded a rapid uplift relative to the origin (0.002 to 0.03 m yr^{-1}), whereas the sites (KH, TA, WO) located west of the fault recorded a subsidence relative to the origin (0.03 to 0.06 m yr^{-1}) (Figs. 3 and 4).

(3) January 1984–June 1996

From 1984 to 1996, vertical deformation rates were lower, with a global subsidence of the lake centred on KH, TA and WO sites, north of the lake. The highest subsidence was recorded at the KH site with a mean rate of 7 mm yr^{-1} relative to RP. The sites located in the middle and southern part of the lake reveal a lower rate of subsidence (MA, WH, TI, WA < 0.001 m yr^{-1}) or a slight uplift (RN: 0.002 m yr^{-1}, and SB, MO, BP < 0.0005 m yr^{-1}). Note that during this period, only minor rises and falls in the global height change trend were observed on a few sites during local small seismic swarms (Otway, 1989; Otway and Sherburn, 1994).

(4) March 1996–December 1999

From March 1996, the previous long term trend was disturbed by an abrupt change with a rise recorded at the sites located in the eastern part of the lake. The highest uplift rates relative to RP were recorded at the HI (Horomatangi Reefs), MO, BP and RA sites (0.01 m yr^{-1}, 0.004 m yr^{-1}, 0.002 m yr^{-1}, 0.002 m yr^{-1}, respectively). An uplift relative to RP was also recorded at a lower rate at the WA, TI, SB and OI sites (<0.004 m yr^{-1}) in the western part of the lake. This temporal change in the vertical deformation of the lake exhibits a strong time and space correlation with the seismicity recorded between July 1997 and December 1998 (Fig. 2C).

(5) December 1999–June 2001

At the end of 1999, the WH, OI and TI sites located in the south-western part of the lake, which did not record any significant deformation since 1979, began to record a subsidence relative to RP (0.02 m yr^{-1}) (Fig. 3). An increase of the subsidence rate relative to RP was also observed at the MA, MP, KA, OO, TA sites (0.005–0.02 m yr^{-1}). At the same time the signal recorded at the BP, SB, HI, RN, MO, WA sites reversed, revealing a subsidence relative to RP. The global behaviour during this period was thus a global tilt of the lake to the west south-west. This period finished with a strong seismic swarm occurring along the northern end of the Kaiapo fault between January and June 2001 (Fig. 2C).

(6) June 2001–June 2002

After 1.5 years of lake tilting to the west and six months of strong seismic activity, the signals recorded at the sites north of the lake, especially near the Kaiapo fault, were strongly disturbed until December 2004 (Figs. 3 and 4). Although the seismic swarm occurred along the northern end of the Kaiapo fault, distinct vertical deformation was recorded at the sites located on both sides of the southern end of the fault. Sites MP, RA and HI located east of the Kaiapo fault recorded an uplift relative to the origin (around 0.005 m yr^{-1}), whereas sites KA, WI, WO, TA and KO located west of the fault recorded a subsidence relative to RP (up to 0.02 m yr^{-1}). At the same time, the signal recorded at the sites located in the southern and western part of the lake began to reverse, revealing a slight uplift relative to RP (0.002 to 0.006 m yr^{-1}) and thus on a larger scale a global tilt to the north north-east.

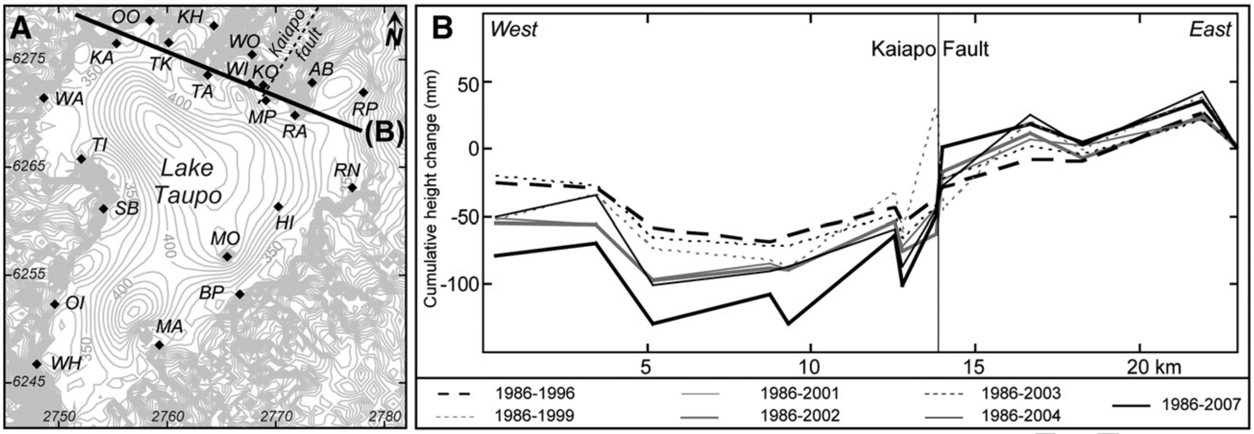

Fig. 5. (A) Location of the cross section for the plot (B), (B) Cumulative height change (in mm) along a west-east cross-section in the northern part of the lake recorded between 1986 and 1996.

(7) June 2002–June 2003
Compared to June 2001–June 2002, an inversion of the signals recorded at the sites north of the lake was observed. The sites located east of the Kaiapo fault recorded a subsidence relative to RP whereas the sites located west of the Kaiapo fault recorded an uplift relative to RP (Fig. 3). This reversal of the deformation behaviour on both side of the Kaiapo fault was not linked to any significant seismic swarm. The global tilt to the north north-east recorded by the sites located west of the lake since June 2001 remained.

(8) December 2004–September 2007
As for the December 1999–June 2001 period, a global trend with a tilt of the lake to the west has been recorded since December 2004, with an increase of the subsidence rate relative to RP at the KA and KH sites (0.01–0.02 m yr^{-1}) (Figs. 3 and 4).

To summarize, during the whole 1979–2007 monitored period, Lake Taupo has been affected by three types of deformation with the greatest signals recorded at the northern sites:

(1) long-term subsidence across the northern part of the lake visible during the quiet seismic period of 1984–1996;
(2) short-term uplifts east of the lake (or tilt to the west) preceding and/or accompanying seismic activity and fault ruptures (October 1982–June 1983, March 1996–December 1999, December 1999–June 2001, December 2004–September 2007);
(3) short-term disturbed vertical deformation accompanying and/or following seismic activity displaying distinct relative displacements on the two sides of the Kaiapo fault (June 1983–January 1984, June 2001–June 2002, June 2002–June 2003).

All these observations reveal the close relation between the most significant changes in the deformation behaviour at Lake Taupo and the occurrence of fault ruptures sometimes accompanied by seismic swarms. Profiles of apparent cumulative height change from west to east across the northern part of the lake since 1986 (all the sites available) are shown in Fig. 5. The global trend is a general tilt from east to west with a maximum subsidence of more than 100 mm recorded between 1986 and 2007 at the KH site. The rapid change in the deformation behaviour occurring near the Kaiapo fault reveals a strong structural control.

4.3. Comparison with GPS and InSAR data

GPS campaigns have been carried out between 2005 and 2007 around Lake Taupo and allow us to constrain the regional deformation outside of the lake (Wallace et al., 2004). Because of the larger error on the vertical component, only horizontal displacements can be interpreted. Horizontal GPS displacement velocities recorded between the 2005 and 2007 campaigns are plotted together with levelling data in Fig. 6. To compare the two sets of data we have recalculated GPS displacements and lake levelling with the BP (lake levelling) and B4LG (GPS) sites as references. The GPS data, away from the lake, reveals a global extension along the TVZ at a rate of about 8 mm yr^{-1} in the Lake Taupo area (Wallace et al., 2004). The GPS displacements were highly disturbed near the Kaiapo fault where a strong vertical height change was recorded by lake levelling. The 2012 and 2406 sites recorded only slight horizontal displacements toward the west whereas the 2011 site recorded a disturbed displacement toward the NNW. Note that the 2353 and 2013 sites, east of the Kaiapo fault, are known to be affected by Wairakei geothermal subsidence (Fig. 6; Darby et al., 2000).

Envisat ASAR data, available from 2003 to 2006, reveal a subsidence relative to Taupo town (near the RP site) of the points

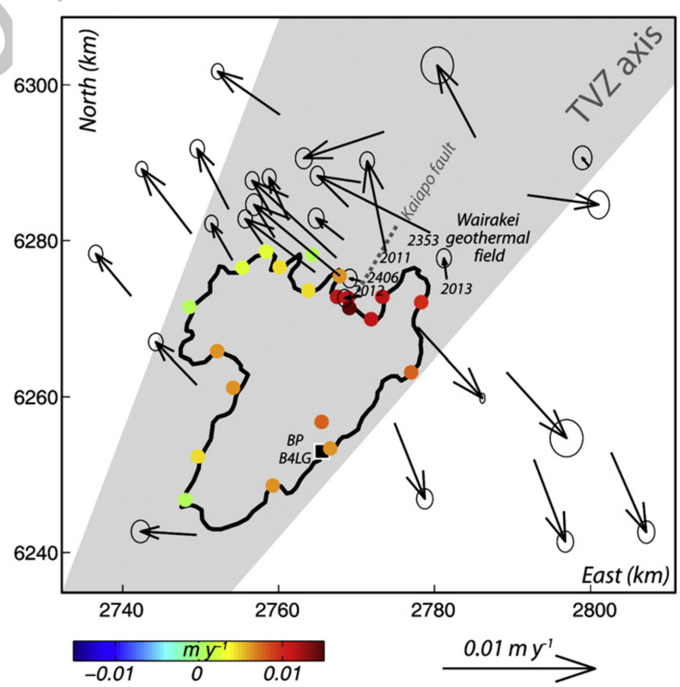

Fig. 6. Comparison between vertical displacements (coloured circles) recorded by levelling data (relative to BP) and horizontal displacements (arrows) recorded by GPS (relative to B4LG) between February 2005 and February 2007. Coordinates are in New Zealand Map Grid Projection (km). (For interpretation of the references to colour in this figure legend, the reader is referred to the web version of this article.)

Please cite this article as: Peltier, A., et al., Structures involved in the vertical deformation at Lake Taupo (New Zealand) between 1979 and 2007: New insights from numerical modelling, Journal of Volcanology and Geothermal Research (2009), doi:10.1016/j.jvolgeores.2009.01.017

located west of the TVZ and north of the KH site (10.9 mm yr^{-1}) and an uplift of the points located near the AB site (Hole et al., 2007). No more data are available to the east and west of Taupo town to constrain the wavelength of more distant deformation.

Regarding the seismicity distribution and the highly disturbed deformation pattern north of the lake (levelling data, GPS, InSAR), we favour an inflation of the north-eastern part of the lake, rather than a deflation of the south-western part, to explain the lake tilting to the west in December 1999–June 2001 and in December 2004–September 2007. The north-eastern part of the lake corresponds to the location of the historical volcanic activity and to highly active geothermal fields often disturbed by seismic activity; whereas no significant seismic activity or old volcanic activity has occurred west of the lake. Over the whole period studied, it is evident that less deformation was recorded by the sites located south of the lake (Fig. 3), so to model the tilt to the west and highlight the inflation of the north-eastern area in December 1999–June

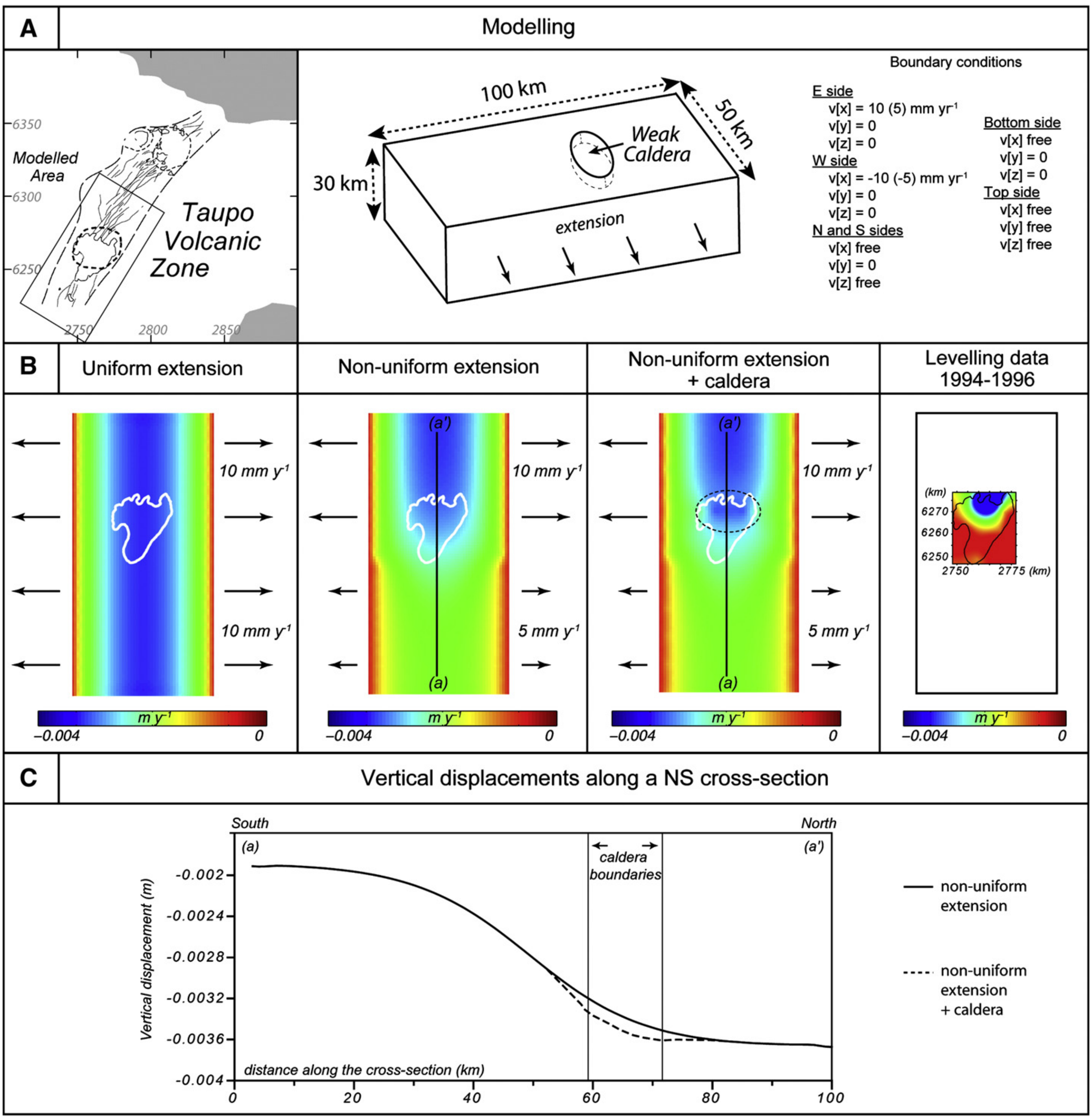

Fig. 7. Effect of the rifting and the weak caldera infill on the ground vertical displacements. (A) Framework of the modelling. (B) Predicted ground vertical displacement for an uniform extension rate of 10 mm yr^{-1}, for a non-uniform extension rate of 5 mm yr^{-1} to the south and 10 mm yr^{-1} to the north, and for non-uniform extension rate including the effect of a weak caldera. And comparison with the interpolated levelling data observed between 1984 and 1996 (C) Comparison between predicted vertical displacements on a north–south cross section (see B for location) across Lake Taupo.

2001 and in December 2004–September 2007 we have recalculated for these two periods the height level change relative to WH.

5. Numerical modelling

5.1. Influence of the rifting and the caldera structure

The regional rifting which characterizes the Taupo Fault Belt, generates ground deformation and must be distinguished from any deformation generated by deep pressure sources. Moreover, the medium-scale heterogeneity characterizing the TVZ, with the presence of numerous faults and weak elastic layers near the surface, can also affect the distribution of ground deformation (Gudmundsson and Brenner, 2004; Letourneur et al., 2008). As suggested by Manville and Wilson (2003), faulting and deformation may be concentrated around the caldera because the caldera structure and associated magmatic system form weak zones in the crust. Ellis et al. (2007) demonstrated that the elliptical region of Taupo caldera, filled to a depth of 3–4 km by weak volcanic rubble from the Oruanui eruption and more recent events (Davy and Caldwell, 1998), can locally amplify the ground deformation.

To evaluate the influence of the rifting and the caldera structure on the vertical ground deformation pattern at Lake Taupo, we have made investigations using the finite element engineering Abaqus software (Abaqus, 2004). Abaqus allowed us to model the static effects of the regional stresses and the effects of different stiffness for the rocks within the edifice. For this purpose, we modelled a 100 × 50 km block, which corresponds to the width of the rifting zone and to a length sufficiently long to keep the boundaries of the modelled region far enough away in order to avoid edge effects. The topography was taken into consideration and we used an elastic medium, with a density of 2700 kg m^{-3}, a Young modulus of 30 GPa and a Poisson's ratio of 0.25 (Ellis et al., 2007). The caldera was modelled as a structure with elliptical cross section (16 × 10 km) and vertical sides 4 km deep. The material density and Young modulus of the caldera were assumed to be 2200 kg m^{-3} and 5 GPa, respectively (Ellis et al., 2007). We applied extensional boundary conditions on the east and west sides to model the extension due to the rifting, and the boundary condition at the base was free horizontal slip (Fig. 7A). We meshed the structures with triangular cells; we used a propagation of cell size with depth and at the edges to decrease the computation time. At the surface the mesh was fine enough to capture the response to stress.

5.1.1. Influence of regional rifting stresses

GPS surveys reveal an extension rate across the Lake Taupo area of 8–10 mm yr^{-1} (Fig. 6; Darby et al., 2000; Wallace et al., 2004). According to Villamor and Berryman (2006), the extension rate is not constant along the axis of the Taupo rift and decreases to the south with an abrupt change of extension rate in the southern part of Lake Taupo (accommodation zone). To quantify the vertical ground deformation due only to the stretching of the crust generated by the rifting, we have run two models: one with a constant extension rate of 10 mm yr^{-1} and one with distinct extension rates of 10 mm yr^{-1} and 5 mm yr^{-1} for the northern and the southern part of Lake Taupo area, respectively (Fig. 7B).

Our models reveal that a uniform crustal extension of 10 mm yr^{-1} generates a maximum subsidence in one year equal to 3.7 mm yr^{-1} in the middle part of the TVZ (Fig. 7B). Considering the model with an abrupt change in extension rate to the south of the lake (Villamor and Berryman, 2006), the modelled ground deformation are in agreement with the long-term subsidence distribution observed from 1984 to 1996 with a highest signal recorded north of the lake (3.7 mm yr^{-1}) and less significant signal to the south (2 mm yr^{-1}; Fig. 7B). However, assuming that the modelled extension rates are correct (Darby et al., 2000; Wallace et al., 2004), a second source needs to be involved to explain the magnitude of the subsidence, up to 7 mm yr^{-1}, recorded in the northern part of the lake relative to the reference, RP, between 1984 and 1996 (Fig. 4).

5.1.2. Influence of local weak structures

To test the influence of the weak caldera infill on the ground deformation recorded at the northern sites, we added to the previous modelling (stretching) the collapse structure located north of the lake (Fig. 7A). As already highlighted by Ellis et al. (2007) for an inflating magma body the presence of the weak caldera infill increases the ground deformation (Fig. 7C). In our model, the weak caldera infill increases the subsidence linked to the crust stretching by around 5% in the caldera area compared to the model with a uniformly elastic crust (Fig. 7C).

The presence of a weak caldera structure and the higher stretching rate to the north contributes partially to the distinct long-term subsidence behaviour recorded at the northern and southern sites between 1984 and 1996. Nevertheless a deep under-pressurized source must also be involved to explain the whole subsidence recorded during the 1984–1996 period. In order to constrain the shape and the location of the under-pressurized source involved in the 1984–1996 deformation pattern but also the sources which can account for the main deformation pattern recorded during the successive periods previously defined, we have made further investigation using a mixed boundary element method modelling combined with a near-neighbourhood inversion (Fukushima et al., 2005).

5.2. Sources of pressure

5.2.1. Methods

To correct the influence of the regional stresses on the levelling data, we first de-trended the data for tectonic extension (up to 3.7 mm yr^{-1} of vertical subsidence in some areas, Fig. 7B, C). Corrected lake levelling data were used as an input in a 3D elastic model based on a mixed boundary element method (Mc3f, Cayol and Cornet, 1997), which runs faster than the finite element method, allowing to combine the models with inversions. The models were combined with Sambridge's near neighbourhood inversion method (Sambridge, 1999; Fukushima et al., 2005). The misfit function we use is the chi-square given by:

$$\chi^2 = \sum_{i=1}^{N} \left(\frac{u_0^i - u_m^i}{\sigma^i}\right)^2$$

where u_0^i and u_m^i are the observed and modelled levelling displacements at the ith measurement point, respectively, σ^i is the standard error of ith measurements and N is the number of measurement points.

The Mc3f code can not take into consideration any heterogeneity of the medium. But our finite element models revealed that the effect of the weak caldera on the ground deformation distribution is very small and can so be disregarded for the inversion modelling. The medium was assumed to be elastic, homogeneous and isotropic, with a Young's modulus of 30 GPa, and a Poisson's ratio of 0.25 (Ellis et al., 2007). The shape of the structures (topography and pressure sources) was modelled using a mesh consisting of triangular elements. Boundary conditions were stresses, which can be pressure changes (ΔP) for reservoirs or hydraulic fractures or shear stress drop (ΔS) for faults. Sources of deformation extending uniformly in space were modelled by over/under-pressurized ellipsoids at depth. Ellipsoids were defined by 7 parameters: the 3D coordinates of its centre, the dimensions of its three half axes and ΔP (Peltier et al., 2007). Sources of the decoupled deformation on the two sides of the Kaiapo fault in the northern part of the lake were modelled by a fault. Because of the lack of data to constrain the extent of the fault toward the north, we constrained the surface fault geometry using geological data observed outside the lake (Villamor and Berryman, 2001). The modelled fault was connected to the topography along the pre-existing Kaiapo fault which comes to the

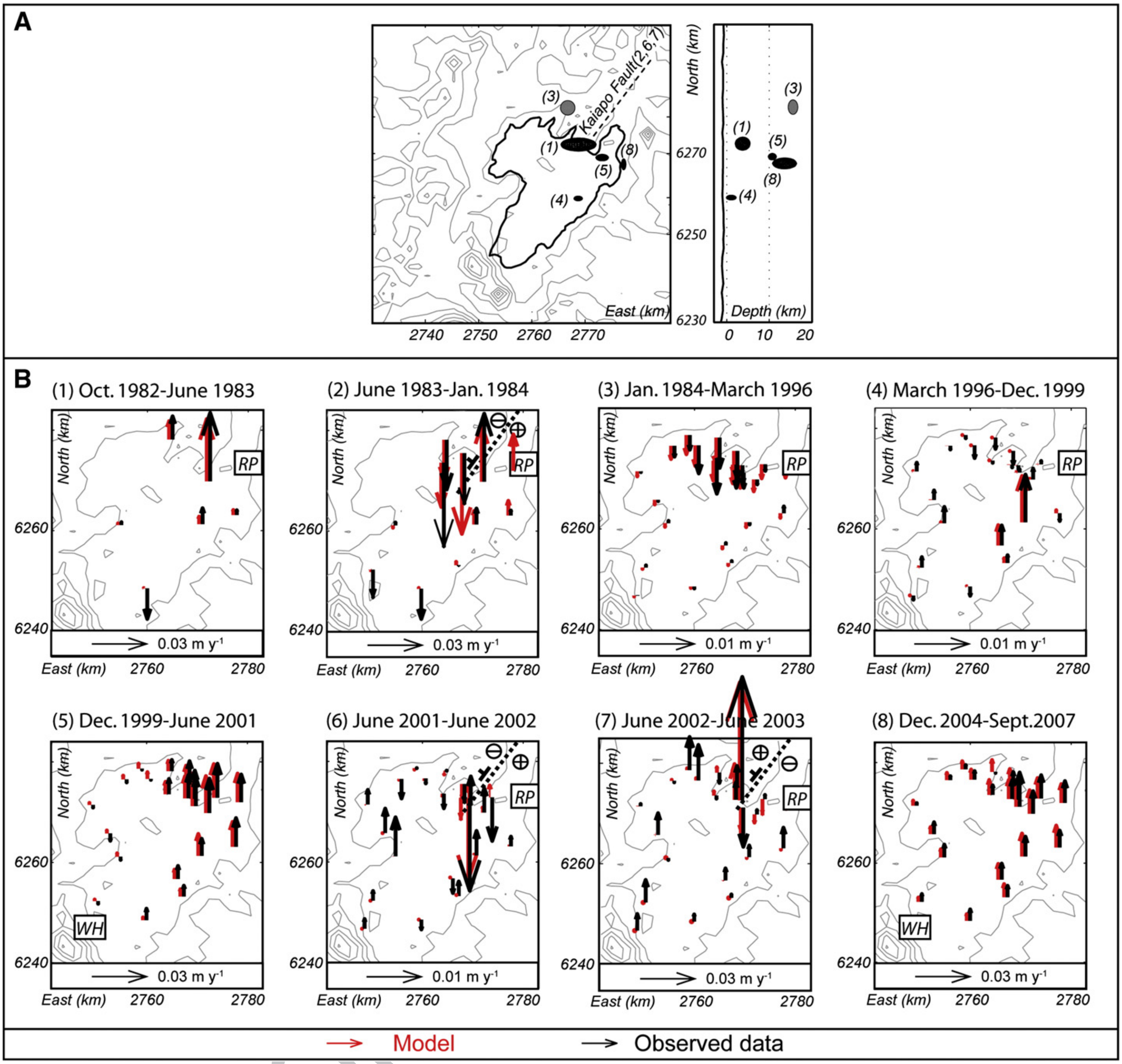

Fig. 8. (A) Location and geometry of the pressure sources modelled for the eight periods (in black: overpressurized source, in grey: underpressurized source) : (1) October 1982 to June 1983, (2) June 1983 to January 1984, (3) January 1984 to March 1996, (4) March 1996 to December 1999, (5) December 1999 to June 2001, (6) June 2001 to June 2002, (7) June 2002 to June 2003, and (8) December 2004 to September 2007. (B) Comparison between observed (black) and calculated (red) height changes relative to the origin represented as vectors. The dotted line represents the Kaipo fault. RP and WH represent the location of the origin. Coordinates are in New Zealand Map Grid Projection (km). (For interpretation of the references to colour in this figure legend, the reader is referred to the web version of this article.)

surface. In the inversions, three parameters were searched: a dip, a bottom depth and ΔS, a constant shear stress drop applied along the fault dip (shear stress drop along the fault strike was supposed to be negligible regarding the geological setting).

5.2.2. Results

Fig. 8A shows the location and the shape of the pressure sources that best explain the vertical deformation of Lake Taupo associated with the eight periods previously defined. For the considered periods, three types of pressure sources can be highlighted: inflating pressure sources (1982–1983, 1996–1999, 1999–2001, 2004–2007), deep deflating pressure sources (1984–1996) and superficial fault motions (1983–1984, 2001–2002, 2002–2003).

5.2.2.1. Inflating pressure sources. The 1982–1983 and 1996–1999 uplifts can be modelled by shallow over-pressurized sources. 82% of the 1982–1983 uplift of the whole northern part of the lake can be fitted by a pressure source (ΔP=0.2±0.1 MPa yr^{-1}) located at 3.7±0.9 km depth beneath the northern part of the lake (2768445 E±2760 m, 6271932 N± 1390 m) (model 1, Fig. 8), whereas 65% of the 1996–1999 uplift can be explained by a pressure source located beneath the eastern part of the lake in the area of the Horomatangi Reefs (ΔP=0.1±0.6 MPa yr^{-1} 2768366 E±3650 m, 6259257 N±201 m, 1±0.4 km depth) (model 4, Fig. 8). For the 1982–1983 period, the lack of data to well constrain the pressure source may explain its larger dimension.

The two periods of lake tilting to the west (December 1999–June 2001 and December 2004–September 2007) can be explained by inflating pressure sources close to each other located at a deeper level compared to the previous ones. The best fitting model (92% data explained) for the December 1999–June 2001 period is obtained with a pressure source (ΔP=5±1.8 MPa yr^{-1}) located at 11±3 km depth (coordinates: 2773988 E±1330 m, 6268871 N±1110 m) (model 5, Fig. 8). For the December 2004–September 2007 period, 90% of the data are explained by a pressure source (ΔP=3.5±1.2 MPa yr^{-1}) located close to the previous one (coordinates: 2776527 E±1730 m, 6267293 N±1370 m) at 13±4 km depth (model 8, Fig. 8).

5.2.2.2. Deep deflating pressure source. The large scale and long-term global subsidence recorded in the northern part of the lake between January 1984 and March 1996 can be explained by a deflating source (ΔP=−1±0.5 MPa yr^{-1}), located just north of the lake (2765946 E±2750 m, 6280561 N±3280 m) at around 15±5 km depth (model 3, Fig. 8) which fits 85% of the observed data. This under-pressurized source is in general agreement with the Mogi point source found by Smith et al. (2007) for the same period (similar location and depth within the uncertainties : 2763900 E±960 m, 6275500 N±1250 m, depth: 7.7±1.1 km).

5.2.2.3. Fault motions. The decoupling of the north-eastern part and the north-western part of the lake occurring over short time periods can be explained by motion on the Kaiapo fault. The best model that explains 69% of the data recorded at the northern sites between June 1983 and January 1984 is a westward-dipping normal fault motion or an eastward-dipping reverse fault motion corresponding to the Kaiapo fault. The tectonic setting of the Kaiapo fault is characterized by a dip toward the west (Villamor and Berryman, 2001). Accordingly, we favour the hypothesis of a westward-dipping fault (88±9°W, 5480±1200 m deep, normal stress along the fault dip ΔS=5±2 MPa yr^{-1}, mean slip motion=0.38 m yr^{-1} over 7 months) (model 2, Fig. 8). The modelled surface fault offset of 0.08 m is in agreement with field observations (0.05 m; Grindley and Hull, 1984). In the same way, the disturbed vertical deformation recorded at the northern sites in 2001–2002 and 2002–2003 can be explained by Kaiapo fault motion. 0.12 m yr^{-1} of normal slip along the Kaiapo fault over one year is required to fit 67% of the vertical displacements recorded north of the lake between June 2001 and June 2002 (87±9°W, 1000±450 m deep, normal stress along the fault dip ΔS=1.6±0.9 MPa yr^{-1}) (model 6, Fig. 8). Whereas the reverse of the signal on the northern sites in 2002–2003 can be explained at 75% (93% of the northern data) by a reversed motion of the fault (85±6°W, 1200±480 m deep, with reverse stress along the fault dip ΔS=6±2.5 MPa yr^{-1}) (model 7, Fig. 8).

The different depths found for these three periods reveal that different sections of the fault were involved in the motion (Fig. 8B).

5.3. Limits

Our investigations are limited by several parameters which can not be constrained by lake levelling data like the deformation distribution outside of the lake, the orientation and intensity of the horizontal displacements, and the motion of the reference site, RP. As already suggested by Otway et al. (2002), the reference site, RP, is very likely to be affected also by deformation induced by regional stresses, and possibly by geothermal exploitation. The Wairakei geothermal field, located 10 km north of the RP site, is subsiding due to fluid extraction. But the Mogi source located at 0.55 km depth, modelled by Darby et al. (2000) to explain this subsidence, generates a negligible effect on the closest lake levelling sites.

Concerning the exclusive use of vertical displacement data to constrain the shape and the location of the pressure source, finite element models made by Dieterich and Decker (1975) showed that the inversion of vertical displacements only may provide results that are not unique and that the exact shape of the source can not be well determined without consideration of vertical and horizontal displacements. But except for a few GPS data recorded between 2005 and 2007, no horizontal displacement information was available to better constrain our models.

Another limitation which can explain part of the discrepancies between modelled and measured ground displacements is the simplifying assumptions made in the models. In the inversion modelling, the medium is considered to be elastic and homogeneous. Consequently, the assumption of elastic response to the overpressures could yield a possible underestimate of the volume changes involved in the pressure sources.

6. Discussion: Origin of the evolution in vertical deformation

During the 30 years of lake levelling monitoring at Lake Taupo, several distinct vertical deformation patterns have been highlighted involving different structures and thus different processes.

6.1. Long term subsidence

The best-defined feature is a long term global subsidence of the northern part of the lake (highest rate around 7 mm yr^{-1}). Even if this global subsidence is particularly well defined during the quiet seismic period of 1984–1996 (Fig. 4), it has occurred since (and presumably before) the beginning of the lake monitoring in 1979. Indeed, except for the disturbed periods of uplift linked with seismic activities and fault motions, the subsidence rate relative to RP recorded at the northern sites (TK, KH, TA, WO, OO, KA, WI, KO) has been relatively constant since 1979, revealing a global and constant long-term subsidence for at least 30 years. Precise levelling measurements recorded in the TVZ zone reveal that the subsiding area recorded by lake levelling represents the southern end of a larger subsiding zone extending along the TVZ axis (Blick and Otway, 1995). In the absence of underlying uplift, this subsidence would be linked with the sagging of the TVZ in response to the regional crustal extension. Our models reveal that the greatest subsidence rate recorded at the northern sites can be partly explained by the abrupt extension rate changes (Villamor and Berryman, 2006) and to a lesser extent by the presence of the caldera to the north (Fig. 7C). But a deep pressure source in deflation (around 10 km depth) also needs to be involved to match all the observed data (Fig. 7C). As already suggested by Otway et al. (2002), Smith et al. (2007) but also by Dzurisin et al. (1994), Wicks et al. (1998) and Wicks et al. (2006) for the Yellowstone subsidence, several origins can be advanced (1) depressurization and fluid loss from a deep hydrothermal system or (2) contraction and cooling of deep magma. In addition to these effects, Smith et al. (2007) reviewed other hypotheses to explain ground subsidence involving a deep magma source: isostatic relaxation following uplift resulting from a magma injection (before 1979), subsidence of a magma body, release of water from a magma body diffusing away into the crust and resulting in a volumetric loss at its source and a transfer of heat from its source to the overlying crust, shrinking of a magma body as a result of a combination of loss of volatiles and thermal contraction after heat loss, and/or flow of the magma away laterally. In the case of pure contraction of a magma body, numerical modelling suggests a volume change of 4.4×10^{6} m^{3} to cater for the observed deformation. About two-thirds of the subsidence of the northern part of the lake over at least the last 30 years would be thus attributed to various combinations of these two processes (hydrothermal circulation and cooling of magma), while one-third would be due to the crustal stretching (Fig. 7C).

6.2. Short term perturbation

Superimposed on the long-term subsidence, local perturbations occurred in 1983 and since 1996. Modelled pressure sources fitting these uplifts were roughly located north-east of the lake or around the Horomatangi Reefs (Fig. 8A). The Horomatangi Reefs corresponds to

Please cite this article as: Peltier, A., et al., Structures involved in the vertical deformation at Lake Taupo (New Zealand) between 1979 and 2007: New insights from numerical modelling, Journal of Volcanology and Geothermal Research (2009), doi:10.1016/j.jvolgeores.2009.01.017

an active geothermal system directly associated with the main source vent of the 1.8 ka Taupo eruption (de Ronde et al., 2002). The pressure sources below this zone and below the north-eastern part of the lake highlight periodic reactivations of the geothermal fields at different depths with fluid circulations. The 1982–1983 and 1996–1999 pressure sources are shallower (around 1–4 km depth) than the 1999–2001 and 2004–2007 ones (around 11–13 km depth). The deepest sources are located at depths where a magnetotelluric profile to the north of Taupo showed high conductivity interpreted as bodies of partial melt with the shallowest lying at a depth of 10–15 km (Ogawa et al., 1999). Heise et al. (2007) interpreted the rapid increase in conductivity at a depth of 10 km beneath the TVZ as marking the presence of an interconnected melt fraction (<4%) within the lower crust. These magma bodies could extend to the south of the TVZ below the lake where old volcanic activity has been recorded. The deep pressure sources involved in 1999–2001 and 2004–2007 could be thus linked with magma body emplacements and/or magma dewatering at around 10 km depth below the lake.

The uplift generated by the shallowest sources are followed (1982–1983) or accompanied (1996–1999) by seismic swarms near the Horomatangi Reefs (Fig. 2C), revealing a close correlation in space and in time between these two phenomena. Webb et al. (1986) suggested that the 1983 swarms could not have been caused by a localized magma intrusion into the crust due to the lack of low-frequency volcanic earthquakes. Pressurization of the shallow hydrothermal system by fluid release or change in the fluid pressure is thus favoured to explain the uplifts and the seismic swarms (Fig. 2C). At Yellowstone, Waite and Smith (2002) attributed the seismic swarms associated with short-term ground deformation to rapid migration of hydrothermal fluids within the caldera after rupture of an impermeable envelope around the magma body. Uplift preceding the seismic swarms gave rise to tensional stresses in the upper crust. When these stresses exceeded some critical value, failure of faults occurred in response to an increase in fluid pressure, resulting in seismic swarms. The abundant past volcanic activity near the thermally active Horomatangi Reefs area suggests that dewatering of a deeper crystallizing magma body into the crust could be the most likely cause of the fluid release in the upper crust.

The 1982–1983 and 1999–2001 uplifts were followed by strongly disturbed vertical deformation north of the lake (Fig. 4). Without any associated seismic activity, this short-term deformation can be attributed to the effect of aseismic slow slip motion along the Kaiapo fault which decoupled a rising area from a falling one. As already suggested by Smith et al. (2007), the increase in pore fluid pressure in the faults at the north-eastern part of the lake can produce aseismic fault slip. The motion of the southern end of the Kaiapo fault in 2001–2002 and 2002–2003 occurred just after the seismic swarm along the northern end of this fault. This temporal relation reveals a link between these two events with a propagation of the stress release toward the south: a seismic swarm to the north followed by an aseismic slow slip motion to the south due to the presence of a free surface and pore fluid pressure associated with the nearby geothermal field. At the same time, the reversal of the tilt to the east recorded by the western sites could reveal a deflation of the preceding over-pressurized source. The strong deformation linked with the Kaiapo fault motion hides the overall global process to the north and prevents us modelling the deflation source by numerical modelling. The deflation of the preceding over-pressurized source near the Horomatangi Reefs could explain the reversal of the fault motion in 2002–2003.

7. Conclusions

The changes in lake levels around Lake Taupo over the last 30 years have highlighted the role of both local (hydrothermal and/or magma system activation, fault creep motion) and regional (tectonic extension) effects in the deformation processes. The best-defined feature is a long term global subsidence of about 3 to 7 mm yr^{-1} of the northern part of the lake due to the role of the crustal stretching and a deep deflation source. This long term subsidence is occasionally disturbed by strong and short-term uplifts near the geothermal fields. Episodes of uplift are attributed to various combinations of the following two processes taking place beneath the geothermal fields: (1) movement or formation of rhyolitic magma (deeper sources) and/or (2) pressurization of a hydrothermal fluid reservoir that traps volatiles exsolved from a crystallizing rhyolitic magma (shallower sources). The pressurization of the shallow hydrothermal system gives rise to tensional stresses in the upper crust, resulting in seismic swarms and aseismic fault creep motion. Periodic creep motion of the Kaiapo fault temporarily decouples on a short-term scale the ground deformation on both sides of the fault. The knowledge of the present-day deformation derived from modelling of lake levelling data, separating the deformation due to regional setting, hydrothermal circulations and seismic activity, reveal that each seismic swarm is preceded by an inflation period (1–3 years) below the lake. This systematic behaviour may allow us in the future to better predict seismic swarm below the lake.

Acknowledgements

Part of this work was supported by grants from the Earthquake Commission of New Zealand (EQC) and the European Commission, 6th Framework Project-'VOLUME', Contract No. 08471. We thank John Beavan, Susan Ellis, Steve Sherburn for helpful advices and comments, and Nicolas Fournier, Maurizio Battaglia for their constructive reviews. This is ~~GNS contribution number XXXX and~~ IPGP contribution number ~~XXXX~~. Q1-2

References

Abaqus, 2004. Abaqus/Standard User Manual Vol. 1 and 2, Version 6.4. Abaqus Inc., Pawtucket, RI, USA.
Blick, G.H., Otway, P.M., 1995. Regional vertical deformation from repeated precise levelling in the Taupo Volcanic Zone. Institute of Geological and Nuclear Sciences Ldt Science Report, 95/23.
Bryan, C.J., Sherburn, S., Bibby, H.M., Bannister, S.C., Hurst, A.W., 1999. Shallow seismicity of the central Taupo Volcanic Zone, New Zealand: its distribution and nature. New Zealand Journal of Geology and Geophysics 42, 533–542.
Caldwell, T.G., Bibby, H., 1992. Geothermal implications of resistivity mapping on Lake Taupo. Proc. 14th N.Z. Geotherm. Workshop 1992. University of Auckland, pp. 207–212.
Cayol, V., Cornet, F.H., 1997. 3D mixed boundary elements for elastostatic deformation field analysis. International Journal of Rock Mechanics and Mining Sciences 34 (2), 275–287.
Darby, D.J., Hodgkinson, K.M., Blick, G.H., 2000. Geodetic measurement of deformation in the Taupo Volcanic Zone, New Zealand: the North Taupo network revisited. New Zealand Journal of Geology and Geophysics 43, 157–170.
Davy, B.W., Caldwell, T.G., 1998. Gravity, magnetic and seismic survey of the caldera complex, Lake Taupo, North Island, New Zealand. Journal of Volcanology and Geothermal Research 81, 69–89.
de Ronde, C.E.J., et al., 2002. Discovery of active hydrothermal venting in Lake Taupo, New Zealand. Journal of Volcanology and Geothermal Research 115 (3–4), 257–275.
Dieterich, J.H., Decker, R.W., 1975. Finite element modeling of surface deformation associated with volcanism. Journal of Geophysical Research 80 (29), 4094–4102.
Dzurisin, D., Yamashita, K.M., Kleinman, W., 1994. Mechanisms of crustal uplift and subsidence at the Yellowstone caldera, Wyoming. Bulletin of Volcanology 56, 261–270.
Ellis, S.M., et al., 2007. A future magma inflation event under the rhyolitic Taupo volcano, New Zealand: numerical models based on constraints from geochemical, geological, and geophysical data. Journal of Volcanology and Geothermal Research 168 (1–4), 1–27.
Fukushima, Y., Cayol, V., Durand, P., 2005. Finding realistic dike models from interferometric synthetic aperture radar data: the February 2000 eruption at Piton de La Fournaise. Journal of Geophysical Research 110, B03206. doi:10.1029/2004JB003268.
Grindley, G.W., Hull, A.G., 1984. Historical Taupo earthquakes and Earth deformation. Bulletin of Royal Society of New Zealand 24, 173–186.
Gudmundsson, A., Brenner, S.L., 2004. How mechanical layering affects local stresses unrests, and eruptions of volcanoes. Geophysical Research Letters 31, L16606. doi:10.1029/2004GL020083.
Hamilton, W.L., 1987. Water level records used to evaluate deformation within the Yellowstone caldera, Yellowstone National Park. Journal of Volcanology and Geothermal Research 31 (3–4), 205–215.
Heise, W., Bibby, H.M., Caldwell, T.G., Bannister, S.C., Ogawa, Y., Takakura, S., Uchida, T., 2007. Melt distribution beneath a young continental rift: the Taupo Volcanic Zone, New Zealand. Geophysical Research Letters 34, L14313. doi:10.1029/2007GL029629.
Hole, J.K., Bromley, C.J., Stevens, N.F., Wadge, G., 2007. Subsidence in the geothermal fields of the Taupo Volcanic Zone, New Zealand from 1996 to 2005 measured by InSAR. Journal of Volcanology and Geothermal Research 166, 125–146.

Please cite this article as: Peltier, A., et al., Structures involved in the vertical deformation at Lake Taupo (New Zealand) between 1979 and 2007: New insights from numerical modelling, Journal of Volcanology and Geothermal Research (2009), doi:10.1016/j.jvolgeores.2009.01.017

Hudnut, K.W., Beavan, J., 1989. Vertical deformation (1952–1987) in the Salton Trough, California, from water level recordings. Journal of Geophysical Research 94 (B7), 9463–9476.

Letourneur, L., Peltier, A., Staudacher, T., Gudmundsson, A., 2008. The effects of rock heterogeneities on dyke paths and asymmetric ground deformation: the example of Piton de la Fournaise (Réunion Island). Journal of Volcanology and Geothermal Research 173 (3–4), 289–302.

Manville, V., Wilson, C.J.N., 2003. Interactions between volcanism, rifting and subsidence: implications of intracaldera palaeoshorelines at Taupo volcano, New Zealand. Journal of the Geological Society, London 160, 3–6.

Ogawa, Y., et al., 1999. Wide-band magnetotelluric measurements across the Taupo volcanic zone: preliminary results. Geophysical Research Letters 26, 3673–3676.

Otway, P.M., 1986. Vertical deformation associated with the Taupo earthquake swarm, June 1983. Royal Society of New Zealand Bulletin 24, 187–200.

Otway, P.M., 1987. Taupo Volcanic Centre deformation surveys. New Zealand Volcanological Record 15, 68–70.

Otway, P.M., 1989. Vertical deformation monitoring by periodic water level observations, Lake Taupo, New Zealand. In: hazards, V. (Ed.), Proceedings in Volcanology. Springer-Verlag, pp. 561–574.

Otway, P.M., Sherburn, S., 1994. Vertical deformation and shallow seismicity around Lake Taupo, New Zealand, 1985–90. New Zealand Journal of Geology and Geophysics 37, 195–200.

Otway, P.M., Blick, G.H., Scott, B.J., 2002. Vertical deformation at Lake Taupo, New Zealand, from lake levelling surveys, 1979–99. New Zealand Journal of Geology and Geophysics 45, 121–132.

Peltier, A., Staudacher, T., Bachèlery, P., 2007. Constraints on magma transfers and structures involved in the 2003 activity at Piton de La Fournaise from displacement data. Journal of Geophysical Research 112, B03207. doi:10.1029/2006JB004379.

Sambridge, M., 1999. Geophysical inversion with a neighbourhood algorithm — i. Searching a parameter space. Geophysical Journal International 138, 479–494.

Sherburn, S., 1992. Seismicity of the Lake Taupo region, New Zealand, 1985–90. New Zealand Journal of Geology and Geophysics 35, 331–335.

Smith, E.G.C., Williams, T.D., Darby, D.J., 2007. Principal component analysis and modeling of the subsidence of the shoreline of Lake Taupo, New Zealand, 1983–1999: evidence for dewatering of a magmatic intrusion? Journal of Geophysical Research 112, B08406. doi:10.1029/2006JB004652.

Sutton, A.N., Blake, S., Wilson, C.J.N., Charlier, B.L.A., 2000. An outline geochemistry of rhyolite eruptives from Taupo volcanic centre, New Zealand. Journal of the Geological Society, London 157, 537–552.

Villamor, P., Berryman, K.R., 2001. A Late Quaternary extension rate in the Taupo Volcanic Zone, New-Zealand, derived from fault slip data. New Zealand Journal of Geology and Geophysics 44 (2), 243–269.

Villamor, P., Berryman, K.R., 2006. Evolution of the southern termination of the Taupo Rift, New Zealand. New Zealand Journal of Geology and Geophysics 49, 23–37.

Waite, G.R., Smith, R.B., 2002. Seismic evidence for fluid migration accompanying subsidence of the Yellowstone Caldera. Journal of Geophysical Research 107, B9 2177. doi:10.1029/2001JB000586.

Wallace, L., Beavan, J., McCaffrey, R., Darby, D.J., 2004. Subduction zone coupling and tectonic block rotations in the North Island, New Zealand. Journal of Geophysical Research 109, BI12406. doi:10.1029/2004JB003241.

Webb, T.H., Ferris, B.G., Harris, J.S., 1986. The Lake Taupo, New Zealand, earthquake swarms of 1983. New Zealand Journal of Geology and Geophysics 29, 377–389.

Whiteford, P.C., Caldwell, T.G., Bibby, H., 1994. Examination of heat flow and resistivity values at the boundaries of the geothermal systems beneath Lake Taupo, North Island, New Zealand. Proc. 16th Geotherm. Workshop. University of Auckland, pp. 157–162.

Wicks, C., Thatcher, W., Dzurisin, D., 1998. Migration of fluids beneath Yellowstone caldera inferred from satellite radar interferometry. Science 282, 458–462.

Wicks, C., Thatcher, W., Dzurisin, D., Svarc, J., 2006. Uplift thermal unrest and magma intrusion at Yellowstone caldera. Nature 440, 72–75. doi:10.1038/nature04507.

Wilson, C.J.N., 2001. The 26.5 ka Oruanui eruption, New Zealand: an introduction and overview. Journal of Volcanology and Geothermal Research 112, 133–174.

Wilson, M.E., Wood, S.H., 1980. Tectonic tilt rates derived from lake-level measurements, Salton Sea, California. Science 207, 183–186.

Wilson, C.J.N., et al., 1984. Caldera volcanoes of the Taupo Volcanic Zone, New Zealand. Journal of Geophysical Research 89, 8463–8484.

Wilson, C.J.N., et al., 1995. Volcanic and structural evolution of Taupo Volcanic Zone, New Zealand: a review. Journal of Volcanology and Geothermal Research 68, 1–28.

Journal of Volcanology and Geothermal Research xxx (2009) xxx–xxx

Contents lists available at ScienceDirect

Journal of Volcanology and Geothermal Research

journal homepage: www.elsevier.com/locate/jvolgeores

Ground deformation patterns at White Island volcano (New Zealand) between 1967 and 2008 deduced from levelling data

Aline Peltier[a,*], Bradley Scott[b], Tony Hurst[a]

[a] ~~GNS Science, Lower Hutt, New Zealand~~
[b] ~~GNS Science, Taupo, New Zealand~~

ARTICLE INFO

Article history:
Received 7 August 2008
Accepted 9 January 2009
Available online xxxx

Keywords:
White Island
levelling measurement
numerical modelling
vertical deformation
magma injection
hydrothermal circulation

ABSTRACT

Since 1967, levelling measurements have been conducted in the main crater of White Island volcano. Interpretation of these data using numerical modelling reveals that shallow pressure sources (200–600 m deep) extending up to the subsurface dominated the long-term deformation pattern consisting of inflation/deflation cycles. The time sequence of height changes, magnetic changes, and fumarole temperature and chemistry reveal that surface changes were caused by increasing temperature below the main crater, reflecting the presence of magma at shallow depth. The uplift and subsidence are interpreted in terms of increase or decrease in fluid pore pressure in response to changes of the heat and gas flux. The subsidence during and following eruptions could be also linked with removal of material at depth to feed the eruptions.

1. Introduction

For several decades, ground deformation studies in volcanic area have provided useful information to enable eruption forecasts and to constrain the shape and the evolution of volcano plumbing systems with time (Dvorak and Dzurisin, 1997; Dzurisin, 2003). At White Island (New-Zealand), the monitoring of vertical deformation has been conducted since 1967 by periodic levelling surveys of the Main Crater floor. Changes in the levels of the crater floor and their relation to the eruptive activity have been previously described for the 1967–1982 period by Clark (1973, 1982) and Clark and Otway (1989) but the origin of the ground deformation is poorly known. The active role of hydrothermal systems in the dynamics of ground deformation has been recently highlighted in several volcanoes worldwide, such as Campi Flegrei (Gottsmann et al., 2006) and Yellowstone (Dzurisin et al., 1994; Wicks et al., 1998). White Island is characterized both by strong hydrothermal and magmatic activity, and ground deformation induced by these two activities must be distinguished in order to better forecast eruptions in the future. Compilation of a large database over 40 years allows us to make a precise analysis of the long-term ground deformation pattern. The aim of this paper is to constrain the sources of ground deformation at White Island between 1967 and 2008 through numerical modelling inversions in order to understand the relationship between ground deformation, eruptive activity and hydrothermal circulation.

2. Geological setting

White Island is an offshore andesitic composite volcano located about 50 km from the Bay of Plenty coast (North Island of New Zealand, Fig. 1). It lies at the north-eastern end of the Taupo Volcanic Zone, a zone of crustal thinning and extension located above the oblique subduction of the Pacific plate beneath the Australian plate. A main crater divided into three sub-craters (eastern, central and western sub-craters) occupies the eastern end of the Island (Figs. 1 and 2). Historic activity is concentrated in the western half of this crater (Fig. 1) and is characterized by continuous sulphur and fumarolic gas emissions and intermittent minor phreatic, phreato-magmatic and magmatic eruptions (Clark, 1973; Cole and Nairn, 1975). During the last 40 years, a variety of eruptions have occurred. Most eruptions are dominantly phreatic and phreatomagmatic and emitted very small volumes of eruptive products, around 10^6–10^7 m^3. The large eruptive sequences of 1976–1982 and 1986–1994 led progressively to the formation of a collapse crater complex in the western sub-crater (Fig. 2B), which has been partly filled by an acid lake since February 2003. Previous studies suggest that magma feeding these eruptions probably originated from reservoirs located at shallow depths of around 500 m below sea level (Houghton and Nairn, 1989; Cole et al., 2000). Two other deeper reservoirs, located at depths of between 1–2 and 2–7 km, respectively, have been

* Corresponding author. Present address: Institut de Physique du Globe de Paris, CNRS, UMR 7154-Géologie des Systèmes Volcaniques, 4 place jussieu, Paris, France. Tel.: +33 1 44 27 25 06; fax: +33 1 44 27 73 85.
E-mail addresses: peltier@ipgp.jussieu.fr (A. Peltier), b.scott@gns.cri.nz (B. Scott), t.hurst@gns.cri.nz (T. Hurst).

0377-0273/$ – see front matter © 2009 Elsevier B.V. All rights reserved.
doi:10.1016/j.jvolgeores.2009.01.020

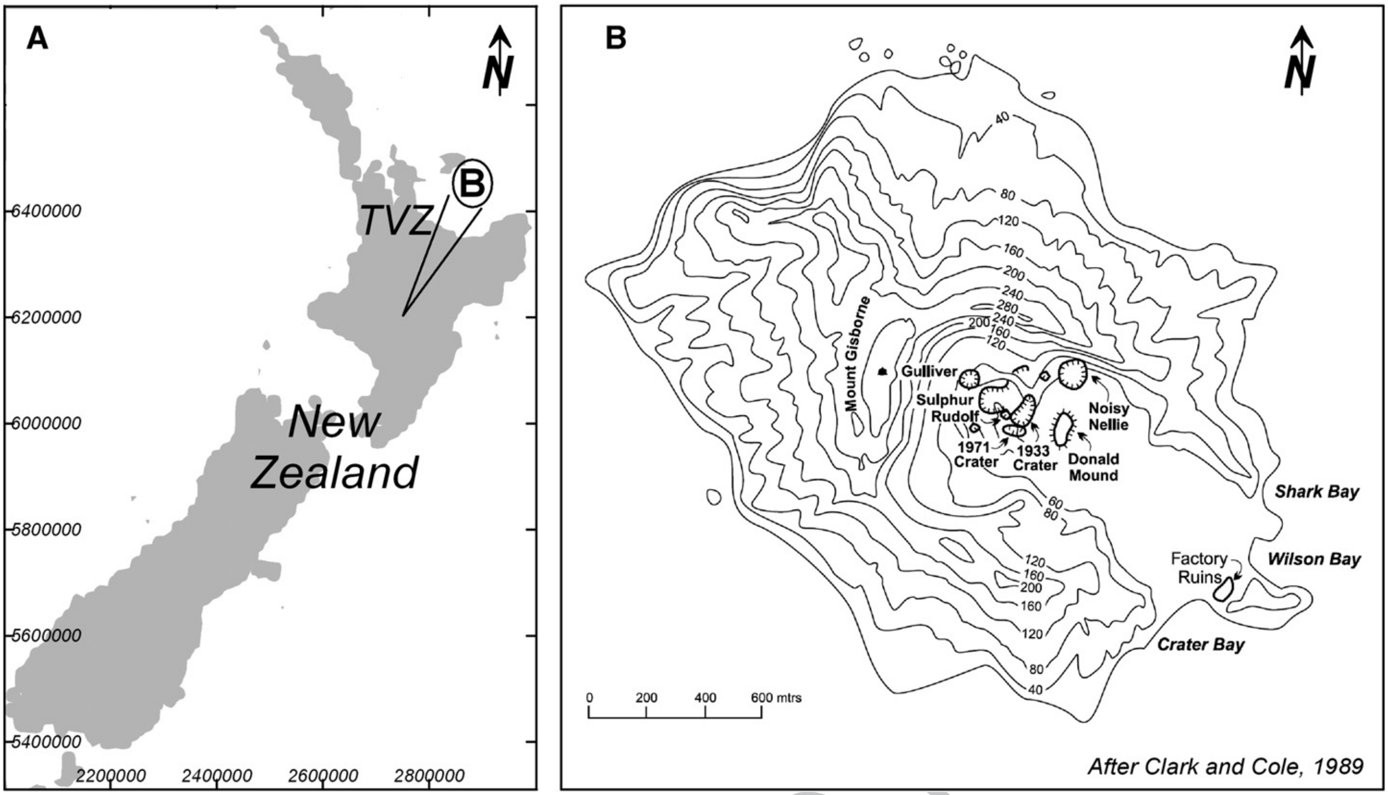

Fig. 1. (A) Location of the Taupo Volcanic Zone (TVZ) and White Island (circle). (B) Topography of White Island and location of the main structures (after Clark and Cole, 1989). Coordinates are in New Zealand Map Grid Projection (metres).

highlighted by geochemical studies (Houghton and Nairn, 1989; Cole et al., 2000). An active hydrothermal system, expressed at the surface by areas of steaming ground, hot springs and fumaroles, lies below the main crater (Giggenbach et al., 1989). Volcano-tectonic earthquakes mainly originate in the hydrothermal area at very shallow depths (<1 km) beneath the central and eastern sub-craters of the main crater (Nishi et al., 1996b). Nishi et al. (1996b) interpreted the shallow earthquakes to result from rapid changes in pore fluid pressure.

3. Levelling data

3.1. Survey method

Since 1967, periodic (3–4 times per year) levelling surveys have been conducted across accessible portions of the main crater floor to monitor relative vertical displacements (Fig. 2A, B). Currently these vertical displacements are measured at 22 sites located on the main crater floor (Fig. 2B). The site numbering system was changed in 1993.

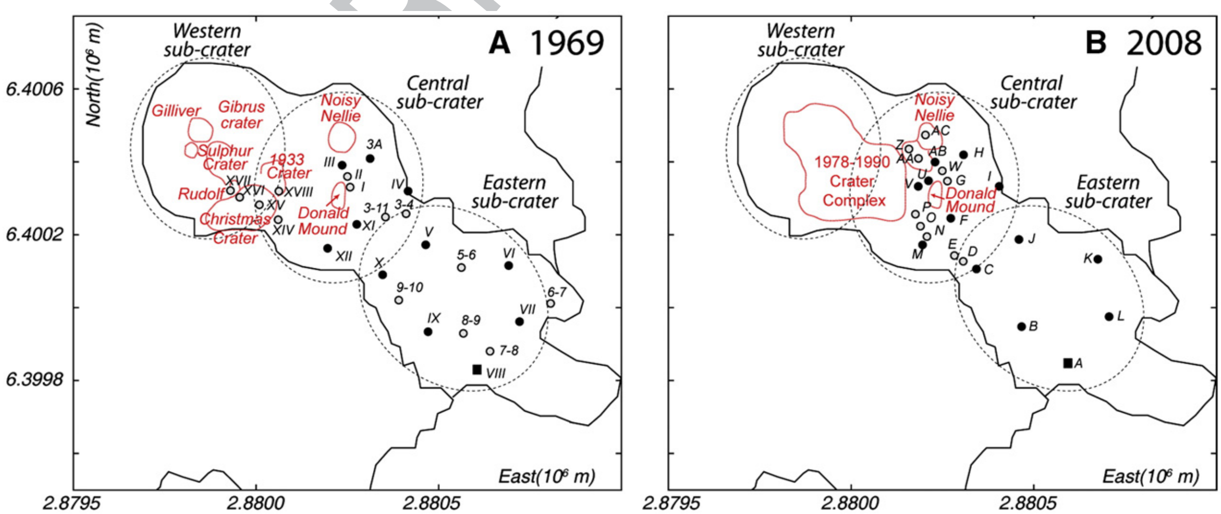

Fig. 2. Location of levelling sites inside the White Island main crater in (A) 1969 and in (B) 2008. Squares represent the origin (VIII and A), filled and open circles represent the sites common and not common for the two periods, respectively. Dashed circles and bold red contour underlined the sub-craters and the crater boundaries, respectively. Note that in 1993 peg identification changed. (For interpretation of the references to color in this figure legend, the reader is referred to the web version of this article.)

Please cite this article as: Peltier, A., et al., Ground deformation patterns at White Island volcano (New Zealand) between 1967 and 2008 deduced from levelling data, Journal of Volcanology and Geothermal Research (2009), doi:10.1016/j.jvolgeores.2009.01.020

Over the 40 years of level monitoring, significant topographical changes have occurred within the main crater due to eruptive activity and formation of collapse craters (Fig. 2A, B) and these sometimes led to the destruction of pegs, disrupting the continuity of measurements at many sites (Figs. 2 and 3). In particular, the pegs located in the western part of the network (XV, XVI, XVII) were destroyed and engulfed into Christmas Crater in early 1977.

The estimated standard deviation for a typical survey ranges from 2–5 mm and is directly proportional to the distance of each site from the origin, peg A, which is located in the south-eastern part of the

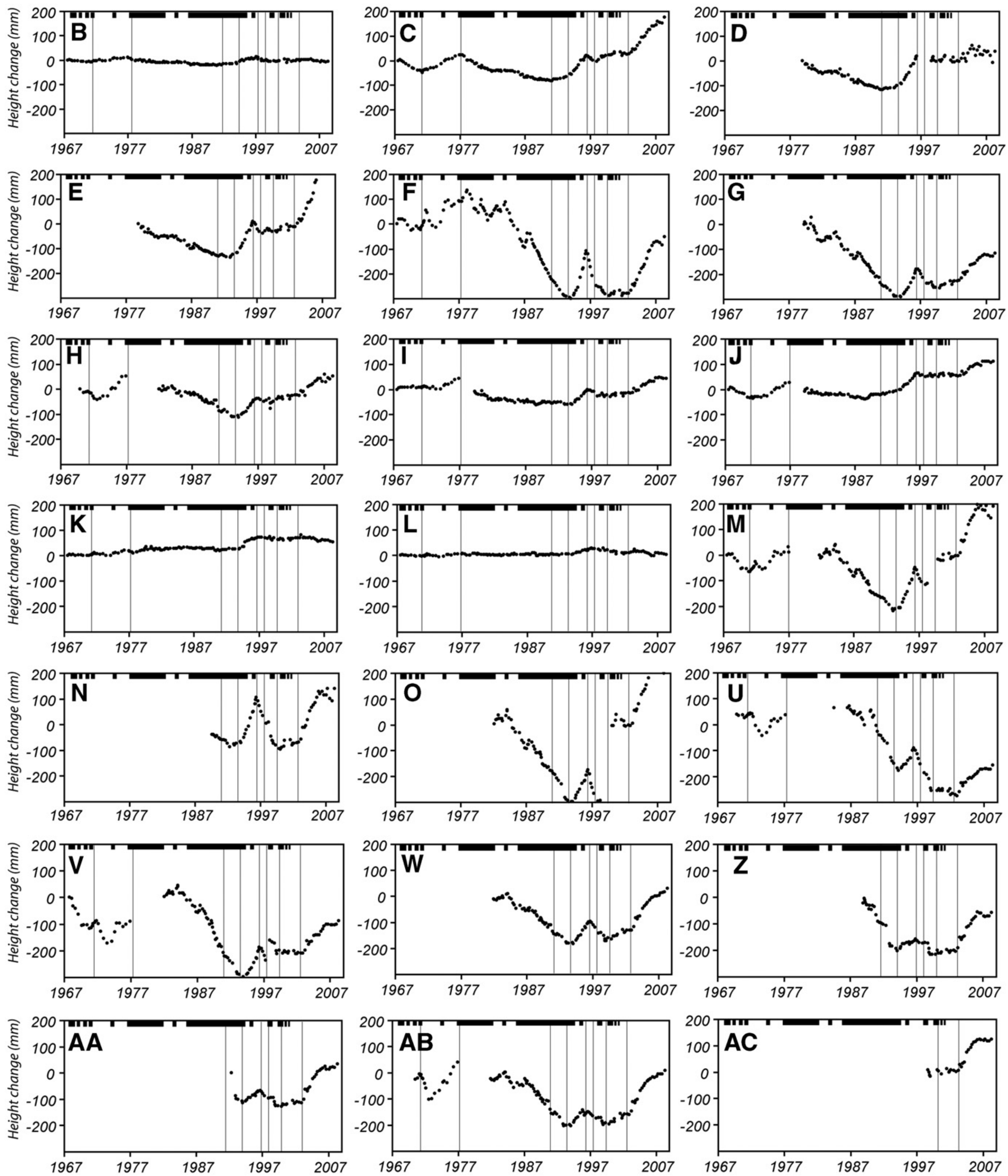

Fig. 3. Height changes relative to the origin, peg A, (mm) recorded between July 1967 and April 2008 at White Island. The lines highlight changes in the global deformation trend. Eruptive periods are highlighted by black lines at the top of each chart.

Please cite this article as: Peltier, A., et al., Ground deformation patterns at White Island volcano (New Zealand) between 1967 and 2008 deduced from levelling data, Journal of Volcanology and Geothermal Research (2009), doi:10.1016/j.jvolgeores.2009.01.020

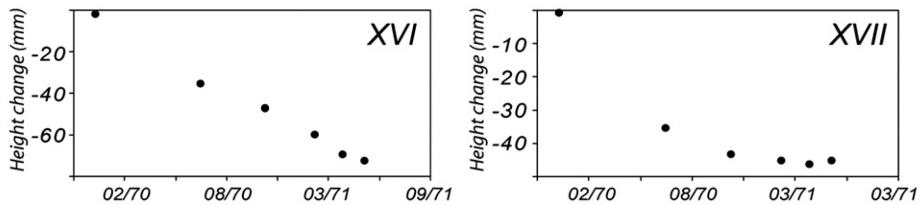

Fig. 4. Height changes (mm) relative to the origin recorded on pegs XV and XVI located inside the 1933 crater between 1969 and 1971. The measurements between 1971 and 1976 are discontinuous and not reported in this figure.

network (see Fig. 2B for location; Scott, 1992). Because of financial constraints, no measurements of horizontal deformation by GPS have been made on White Island.

3.2. Vertical deformation evolution between 1967 and 2008

The levelling data from the pegs not destroyed by the 1976–1982 and 1986–1994 eruptive sequences are plotted in Figs. 3 and 4 in the form of apparent height changes relative to the origin, peg A. Short-term disturbances are visible at many sites, however we recognise eight long-term episodes of deformation between 1967 and 2008: (1) July 1967–April 1971, (2) April 1971–December 1976, (3) December 1976–November 1990, (4) November 1990–January 1994, (5) January 1994–May 1996, (6) May 1996–December 1997, (7) December 1997–February 2000 and (8) November 2002–May 2008. Between 2000 and 2002, vertical deformation was weak and no clear trend can be highlighted (Fig. 3). To visualize the pattern and the distribution of vertical deformation, the average rate of vertical displacement relative to the origin, peg A, is shown for the eight selected periods in Fig. 5.

3.2.1. July 1967–April 1971

Between July 1967 and April 1971, the major ground deformation signal was a subsidence centred to the west of the network (maximum rates of 0.03–0.04 m yr^{-1}) (Figs. 3 and 5). The installation of pegs inside the 1933 crater in December 1969 revealed that the greatest subsidence occurred inside the 1933 Crater (0.05 m yr^{-1}) (Figs. 4 and 5). Note that a short-term broad asymmetric uplift was recorded at the first re-level, in November 1967, with a maximum rate of 0.07 m yr^{-1} near Donald Mound (F on Fig. 3). This uplift preceded an episode of eruptive activity inside the Rudolf vent (Clark, 1970). During this period, Rudolf fumarole (on the back wall of the 1933 crater) developed into an active vent with the occurrence of intermittent ash eruptions: January 27th 1968–February 1969, August–September 1969 and June 1970. The main phase of ash eruption inside the Rudolf vent was in February 1968 (Clark, 1970).

3.2.2. April 1971–December 1976

In April 1971, the signal reversed at all sites highlighting an uplift of the central sub-crater relative to the origin (Figs. 3 and 5). The highest uplift was recorded around Donald Mound, with a mean rate of 0.03–0.04 m yr^{-1}. Three eruptions occurred during this period and disturbed the long-term pattern: April 1971 (Noisy Nellie Crater), 19–20 July 1971 (South of Rudolf crater) and September 1974 (south-east of Donald Mound). After each of these eruptions a slight short-term subsidence of the crater floor was recorded on pegs F, H, V, M, U, AB before uplift centred below Donald Mound started again (Fig. 3).

3.2.3. December 1976–November 1990

From December 1976 to November 1990, the most significant deformation signal was a subsidence of the central sub-crater floor. The largest deformation rates of 0.02 m yr^{-1} were measured at pegs F and G (Figs. 3 and 5). Over this period, the long-term subsidence was centred near eruptive vents that developed west of the monitored network. Superimposed on the long-term subsidence, short-term episodes of uplift and subsidence were recorded on sites F, G and H with peaks visible in March 1978, May 1980, November 1982, February 1984 and June 1987 (Fig. 3).

This more or less continuous subsidence corresponds to a period of quasi continuous eruptive activity marking the largest historic eruptions. During this period many collapse craters, including Christmas, Gibrus and 1978 craters, were formed during cyclic eruptive sequences (Houghton and Nairn, 1989). Localized inflation centred near the Donald Mound preceded or accompanied the resurgences of eruptive activity during this period. For instance, the rising signal at sites F, G and H in 1987 occurred before the first explosive eruption of a renewed cycle of activity at that time.

3.2.4. November 1990–January 1994

The crater subsidence recorded between 1976 and 1990 was interrupted after November 1990. Two signals became apparent within the monitored area; both uplift and subsidence were recorded until January 1994. Sites located in the middle of the network (B, C, D, J) recorded an uplift relative to the origin (maximum rate of 0.008 m yr^{-1} on site C), whereas the sites located to the west (E, F, G, H, I, M) recorded a subsidence (0.01 to 0.03 m yr^{-1}) (Figs. 3 and 5). The eruptive sequence which began in 1986 continued during this period, with notably the formation of a new crater collapse in 1990 (enlargement of the 1978–1990 Crater Complex).

3.2.5. January 1994–May 1996

After January 1994 the deformation signal reversed at sites located to the west and increased on the sites to the east revealing a crater wide uplift relative to the origin, with a maximum rise recorded on sites F and M (0.08 m yr^{-1} and 0.07 m yr^{-1}, respectively, Figs. 3 and 5). This period corresponds to the end of the eruptive sequence of 1976–1994 (in July). Minor eruptions occurred on 28–29 June, 1995 but did not disturb the deformation behaviour and the global inflation of the central sub-crater continued until May 1996.

3.2.6. May 1996–December 1997

In May 1996, a reversal of the previous trend occurred with a drop recorded at all sites (Figs. 3 and 5). The maximum subsidence rate of 0.09 m yr^{-1} was recorded on peg F. No eruptive activity occurred over this period.

3.2.7. December 1997–February 2000

Between December 1997 and February 2000, the sites located at the west of the network continued to record a strong subsidence (maximum rate of 0.04 m yr^{-1} on peg N) whereas at the same time an inflation centred on site C was recorded (Figs. 3 and 5).

During this period minor explosive eruptions, ash emissions and crater formation continued from 1978/1990 Crater Complex. The largest magmatic eruption of the 1976–2000 period occurred in July 2000, marking the end of the eruptive episode.

Please cite this article as: Peltier, A., et al., Ground deformation patterns at White Island volcano (New Zealand) between 1967 and 2008 deduced from levelling data, Journal of Volcanology and Geothermal Research (2009), doi:10.1016/j.jvolgeores.2009.01.020

3.2.8. November 2002–May 2008

After November 2002, a deformation signal characterized by a strong uplift at the western sites became established and continued until at least April 2008. The main uplift was centred in the western crater around sites F, M, N and O (rates of 0.04–0.05 m yr^{-1}, Figs. 3 and 5) with two other small signals near pegs C and AA–AB. By contrast levelling points furthest to the east were characterized by no significant changes or a slight subsidence relative to peg A. No eruptive activity was noted over this period but the greatest uplift occurred at the same time as a crater lake became established inside the 1978/1990 Crater Complex in

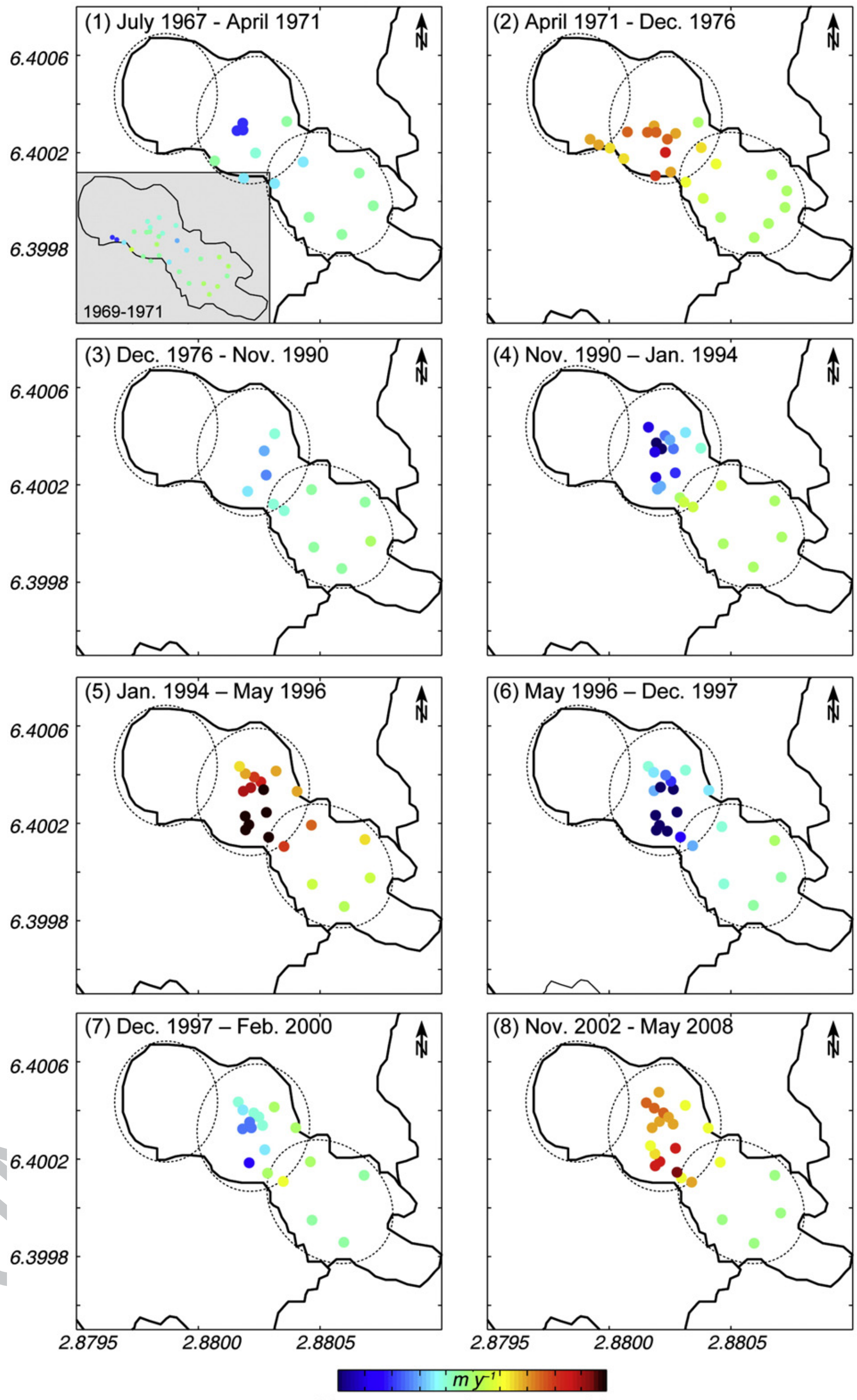

Fig. 5. Average vertical deformation rates relative to the origin, peg A, (in m yr^{-1}) for the eight separate periods: (1) July 1967–April 1971, (2) April 1971–December 1976, (3) December 1976–November 1990, (4) November 1990–January 1994, (5) January 1994–May 1996, (6) May 1996–December 1997, (7) December 1997–February 2000 and (8) November 2002–May 2008. The contours plots are every 0.005 m yr^{-1}. Coordinates are in New Zealand Map Grid Projection (10^6 m).

Please cite this article as: Peltier, A., et al., Ground deformation patterns at White Island volcano (New Zealand) between 1967 and 2008 deduced from levelling data, Journal of Volcanology and Geothermal Research (2009), doi:10.1016/j.jvolgeores.2009.01.020

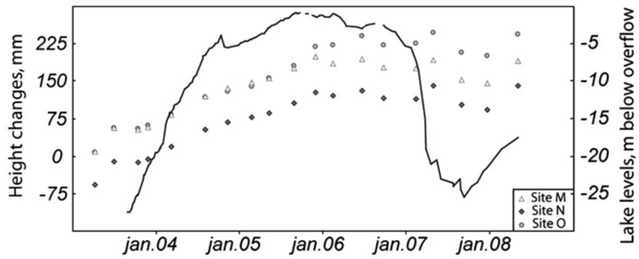

Fig. 6. Comparison between the height changes recorded on sites M, N, O and the Crater Lake levels (solid line) between 2003 and 2008.

February 2003 (Fig. 6; Scott et al., 2004). Fumarole activity also increased in the area of pegs C, D and E.

4. Comparison of levelling data with magnetic changes, fumarole temperature and fumarole chemistry

4.1. Magnetic changes

Christoffel (1989), Hurst and Christoffel (1973) and Hurst et al. (2004) noted an anti-correlation between the short-term height levels and the magnetic changes. These authors observed changes of several hundred nanoTesla over periods of months to years at points on the crater floor with drops in the magnetic field strength corresponding to ground level rises and vice-versa. This inverse correlation is expected when both height level and magnetic changes are due to temperature fluctuations. A rise of temperature at depth would affect the magnetic field if rock temperatures were in the range of 350–600 °C and thus approaching or reaching the Curie point temperature which produces total thermal demagnetisation (Hurst et al., 2004). The long-term level subsidence recorded in 1990–1994, do not seem to be correlated with magnetic changes (Hurst et al., 2004). Hurst et al. (2004) suggested that this might reflect the sensitivity of the level monitoring to slow processes such a loss of fluid from the hydrothermal system or sagging of ground into the large collapse craters, which do not directly affect the magnetic measurements.

4.2. Fumarole temperature

A good temporal correlation is observed between peaks of fumarole maximum temperature at Donald Mound and uplift of the nearby sites (Fig. 7A). During the eruptive sequences of 1976–1982 and 1986–1994, the short term inflation linked with resurgence of surface activity was immediately followed by strong deflation, with declining temperatures and surface activity (Fig. 7A).

4.3. Fumarole chemistry

Fig. 7B, C, D, E compares the concentration of HCl, S, CO_2 and N_2 in the fumaroles of the Donald Mound area with the height change at site F over the 1971–1997 period. At low temperatures, hydrochloric acid (HCl) and sulphur gases react with the rocks and a smaller proportion of these gases reach the surface. CO_2 and N_2 are less reactive gases, so their concentrations in fumaroles are more closely related to the amount of these gases released from magma. A good correlation between HCl and S concentrations and the height changes is observed until 1978. After 1978, HCl and S concentrations and the height changes were anti-correlated (peak of S corresponding to low height level). During the energetic eruptive sequence of 1976–1982, the underground hydrothermal system was disturbed by the formation of collapse craters west of Donald Mound. After these changes, HCl and S were in much lower concentrations than during the 1971–1980 period. During the 1971–1976 period, peaks of HCl and S were preceded a few months earlier by peaks of CO_2 and N_2 which reacted less with the rocks, whereas during the 1976–1984 period the peaks of S, HCl, CO_2 and N_2 were coincident, indicating gas flux via the open eruptive vents.

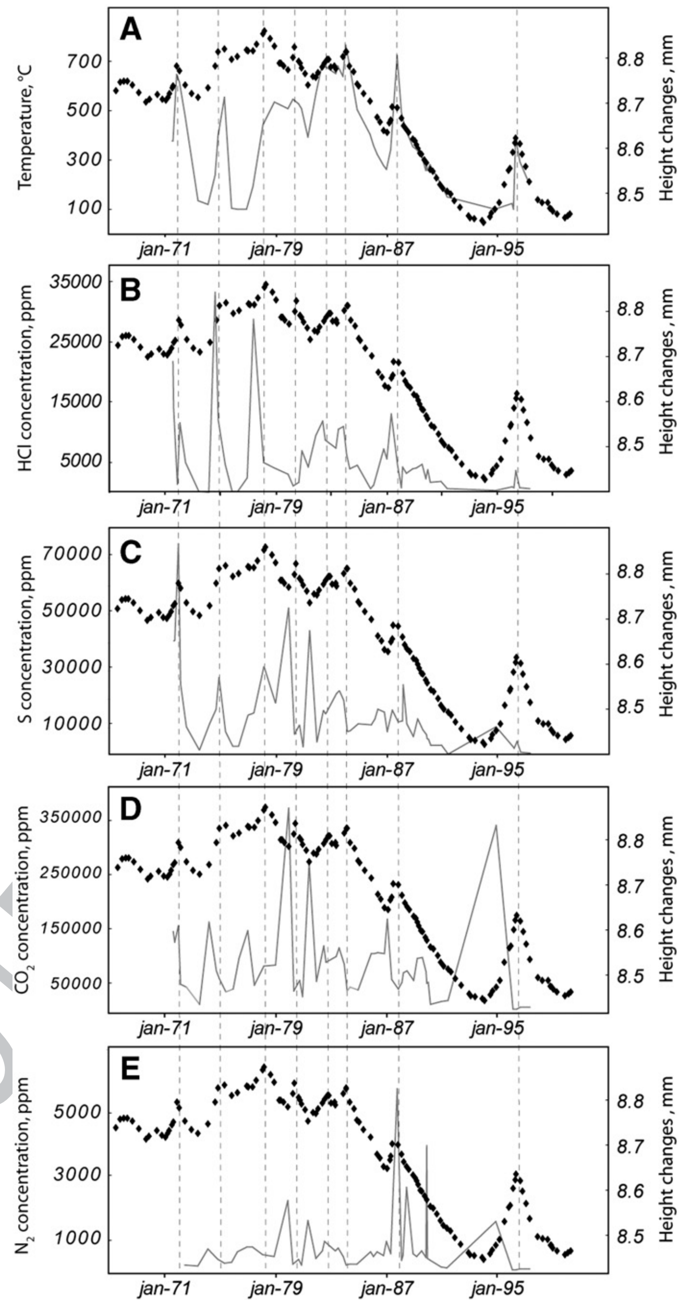

Fig. 7. Comparison between the height changes recorded on site F (black) relative to the origin and (A) the temperature at Donald Mound, (B) HCl, (C) S, (D) CO_2 and (E) N_2 gas concentrations in Donald Mound fumaroles (grey). HCl, S, CO_2 and N_2 data are from (Giggenbach and Sheppard, 1989) and Bruce Christenson (personal communication). Dashed lines represent the peaks of uplift on site F.

Fig. 8. Location and geometry of the pressure sources modelled for the eight periods: (1, blue) July 1967–April 1971, (2, green) April 1971–December 1976, (3, red) December 1976–November 1990, (4, black) November 1990–January 1994, (5, orange) January 1994–May 1996, (6; grey) May 1996–December 1997, (7, purple) December 1997–February 2000 and (8, brown) November 2002–May 2008. (For interpretation of the references to color in this figure legend, the reader is referred to the web version of this article.)

Please cite this article as: Peltier, A., et al., Ground deformation patterns at White Island volcano (New Zealand) between 1967 and 2008 deduced from levelling data, Journal of Volcanology and Geothermal Research (2009), doi:10.1016/j.jvolgeores.2009.01.020

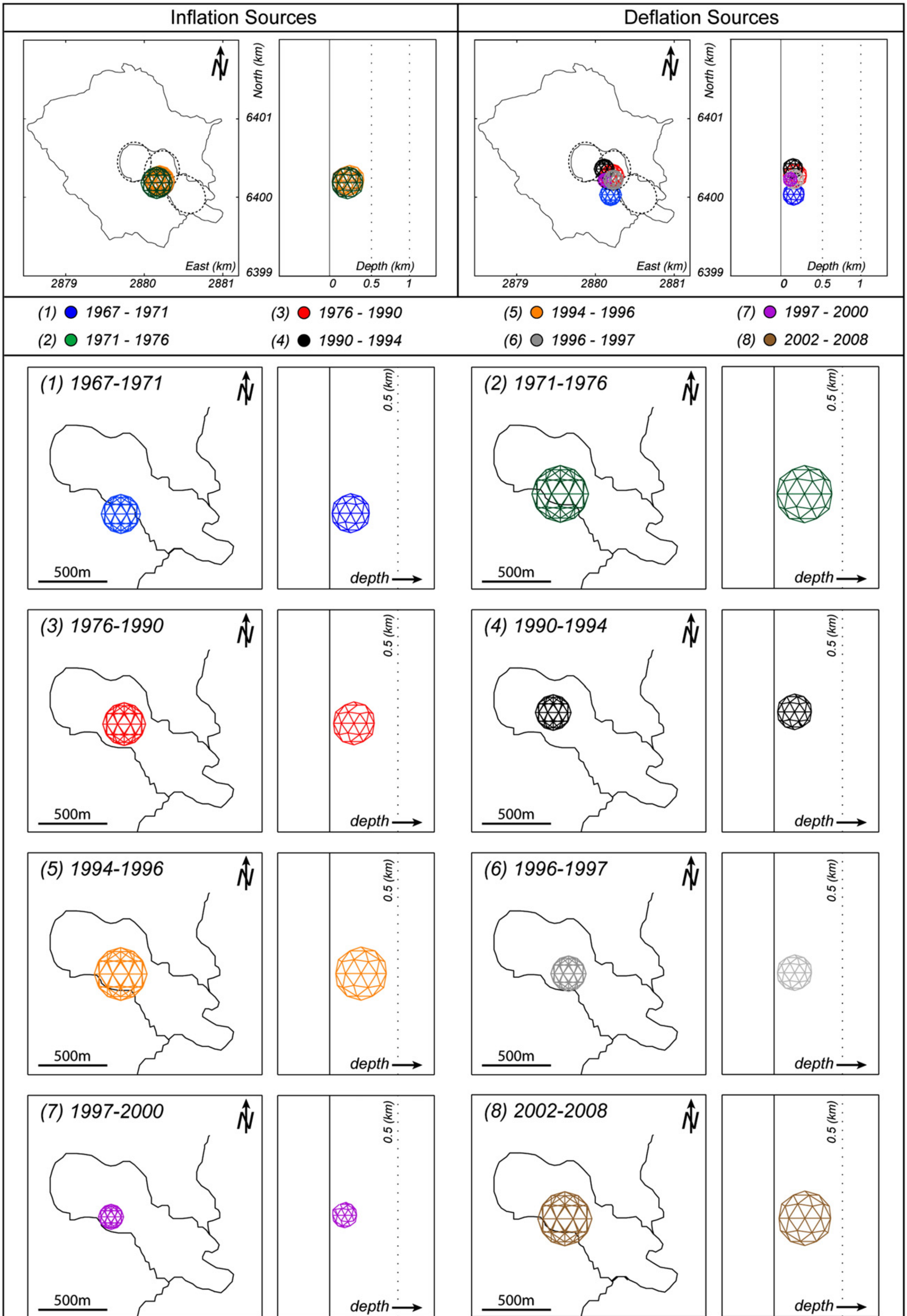
Inflation Sources
Deflation Sources
North (km)
6401
6400
6399
East (km)
2879
2880
2881
Depth (km)
0
0.5
1
(1) 1967 - 1971
(2) 1971 - 1976
(3) 1976 - 1990
(4) 1990 - 1994
(5) 1994 - 1996
(6) 1996 - 1997
(7) 1997 - 2000
(8) 2002 - 2008
(1) 1967-1971
(2) 1971-1976
(3) 1976-1990
(4) 1990-1994
(5) 1994-1996
(6) 1996-1997
(7) 1997-2000
(8) 2002-2008
500m
0.5 (km)
depth

5. Numerical modelling

5.1. Inversion and method

Levelling data was inverted using numerical modelling to constrain source locations that could account for the deformation patterns observed during the successive long-term periods of crater floor inflation and deflation. We used the vertical displacements of the pegs obtained by subtracting the initial displacement from the final one during each defined time periods. Vertical displacements are used as data input in a 3D elastic model, Mc3f, based on a mixed boundary element method (Cayol, 1996; Cayol and Cornet, 1997). The model is combined with Sambridge's Monte Carlo inversion method (Sambridge, 1999) to minimize the misfit function (Fukushima et al., 2005), i.e. the normalized root mean square error between calculated and observed displacements. For the calculation, the medium is assumed to be elastic, homogeneous and isotropic (Cayol, 1996; Cayol and Cornet, 1997), with a Young's modulus of 30 GPa, and a Poisson's ratio of 0.25. The structures

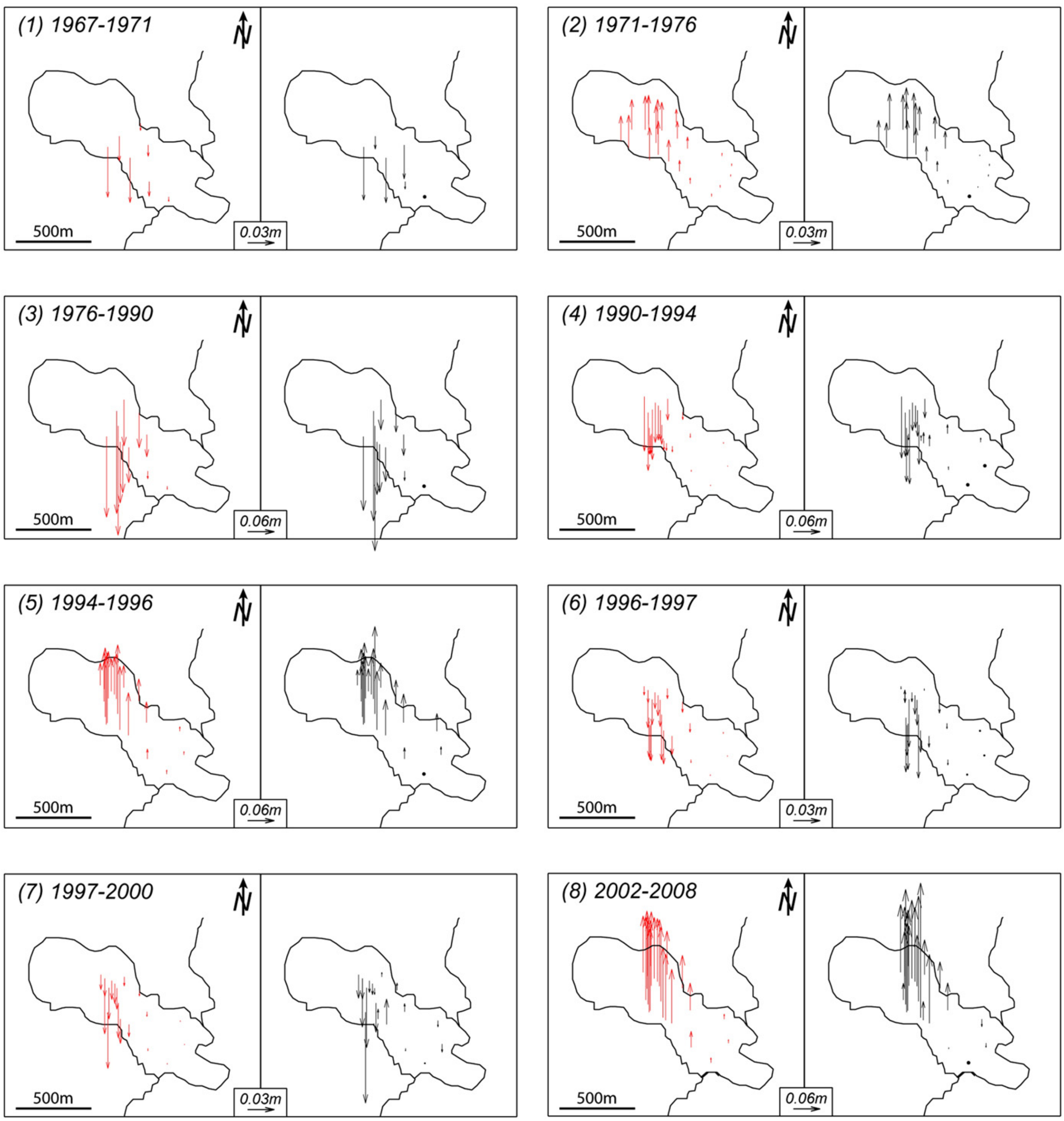

Fig. 9. Comparison between calculated (red) and observed (black) height changes relative to the origin represented as vectors for the eight periods: (1) July 1967–April 1971, (2) April 1971–December 1976, (3) December 1976–November 1990, (4) November 1990–January 1994, (5) January 1994–May 1996, (6) May 1996–December 1997, (7) December 1997–February 2000 and (8) November 2002–May 2008. (For interpretation of the references to color in this figure legend, the reader is referred to the web version of this article.)

Please cite this article as: Peltier, A., et al., Ground deformation patterns at White Island volcano (New Zealand) between 1967 and 2008 deduced from levelling data, Journal of Volcanology and Geothermal Research (2009), doi:10.1016/j.jvolgeores.2009.01.020

Table 1
Summary of the modelled pressure source parameters

Periods	ΔP (MPa)	+−	Radius (m)	+−	X (m)	+−	Y (m)	+−	Depth (m)	+−	ΔV (m^3)	Consistency (%)
1967–1971	−2.3	1.2	157	40	2,880,200	75	6,400,067	113	−278	216	-1×10^4	87
1971–1976	1.5	1.3	211	14	2,880,142	68	6,400,262	127	−364	181	1.7×10^4	94
1976–1990	−4.6	1.3	184	40	2,880,190	61	6,400,270	89	−241	146	-3×10^4	97
1990–1994	−5.7	2.1	100	36	2,880,224	82	6,400,326	90	−157	169	-0.6×10^4	64
1994–1996	4.8	1.3	158	40	2,880,208	70	6,400,222	75	−234	174	2.3×10^4	97
1996–1997	−3	1	150	37	2,880,223	60	6,400,209	80	−221	176	-1.2×10^4	81
1997–2000	−4.7	1.4	108	37	2,880,136	62	6,400,221	87	−186	201	-0.7×10^4	65
2002–2008	3.1	1.5	220	35	2,880,222	77	6,400,241	108	−322	158	4×10^4	84

(topography and pressure sources) are modelled using a mesh with triangular elements. Sources of deformation are modelled by pressure changes (ΔP being the change in pressure) in spherical volumes below the crater. We chose to model the pressure sources as spheres and not as sills because the lack of horizontal data do not allow us to well constrain the exact shape of the source (Dieterich and Decker, 1975). Spheres are defined by five parameters: the 3D coordinates of its centre, the dimension of its half axis and ΔP (Peltier et al., 2007).

5.2. Results

The location of the pressure sources that best explain the vertical deformation of the main crater associated with the eight periods previously defined is shown in Fig. 8. The consistency of the modelling is shown in Fig. 9 and Table 1. We are not able to model many of the short-term localized inflations/deflations recorded at less than 3 sites as there is not enough data to constrain the associated sources, so we modelled only the global trend of each period defined in Section 3.2. Between 64% and 97% of the levelling data of the eight periods can be explained by shallow pressure sources, located in a well constrained area below the central sub-crater and extending from a depth of 200–600 m up to the subsurface (Figs. 8–10, Table 1). The location of the inflation sources is very similar from one period to the others, whereas the location of the deflation sources differs slightly (Fig. 8). We plotted on Fig. 10 the parameters of each source with error bars. Even if the depth of pressure sources appears to be within the size of the error bars, their radius and thus their vertical elongation differ (Figs. 8 and 10). The radius of the pressure sources ranged from 100 ± 36 m to 220 ± 36 m, thus the inflation pressure source of the 1971–1976 period reached nearly 600 m depth whereas the deflation pressure source of 1990–1994 the period reached only about 250 m depth. We distinguished thus three main pressure source depths, as already suggested by Clark and Otway (1989) for the 1976–1982 period: 1) Deep inflation sources extending down to a depth of ~600 m with a radius of ~200 m apparently centred near Donald Mound: 1971–1976, 1994–1996 and 2002–2008 inflation sources (models 2, 5, 8; Figs. 8–10); 2) Shallow deflation sources (180–400 m deep and a radius of 100–150 m) (models 1, 3, 4, 6, 7; Figs. 8–10) located below the central sub-crater; and 3) Very shallow inflation sources generating the short-term cycles of uplift and subsidence recorded only at a few sites between 1979 and 1990.

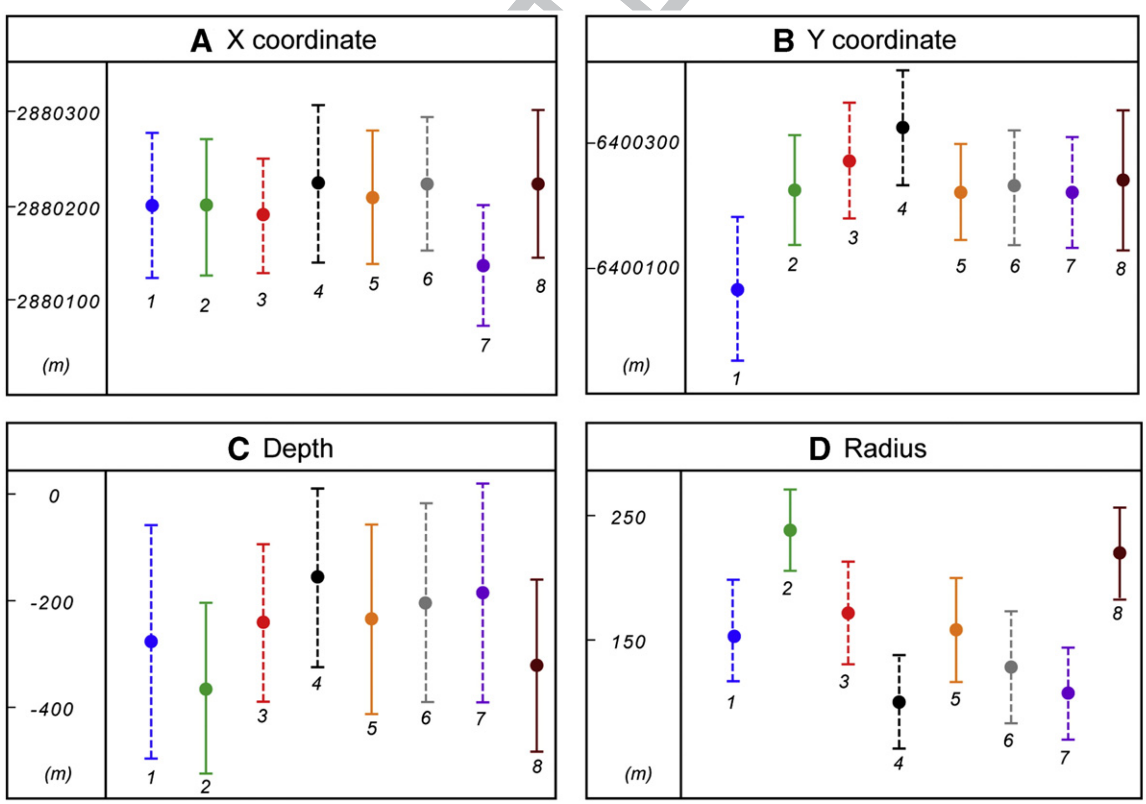

Fig. 10. Parameters of the pressure sources, (A) X coordinate, (B) Y coordinate, (C) depth of the center, (D) radius, within the error bars modelled for the eight periods: (1) July 1967–April 1971, (2) April 1971–December 1976, (3) December 1976–November 1990, (4) November 1990–January 1994, (5) January 1994–May 1996, (6) May 1996–December 1997, (7) December 1997–February 2000 and (8) November 2002–May 2008. Dotted and continuous lines represent deflation and inflation sources, respectively.

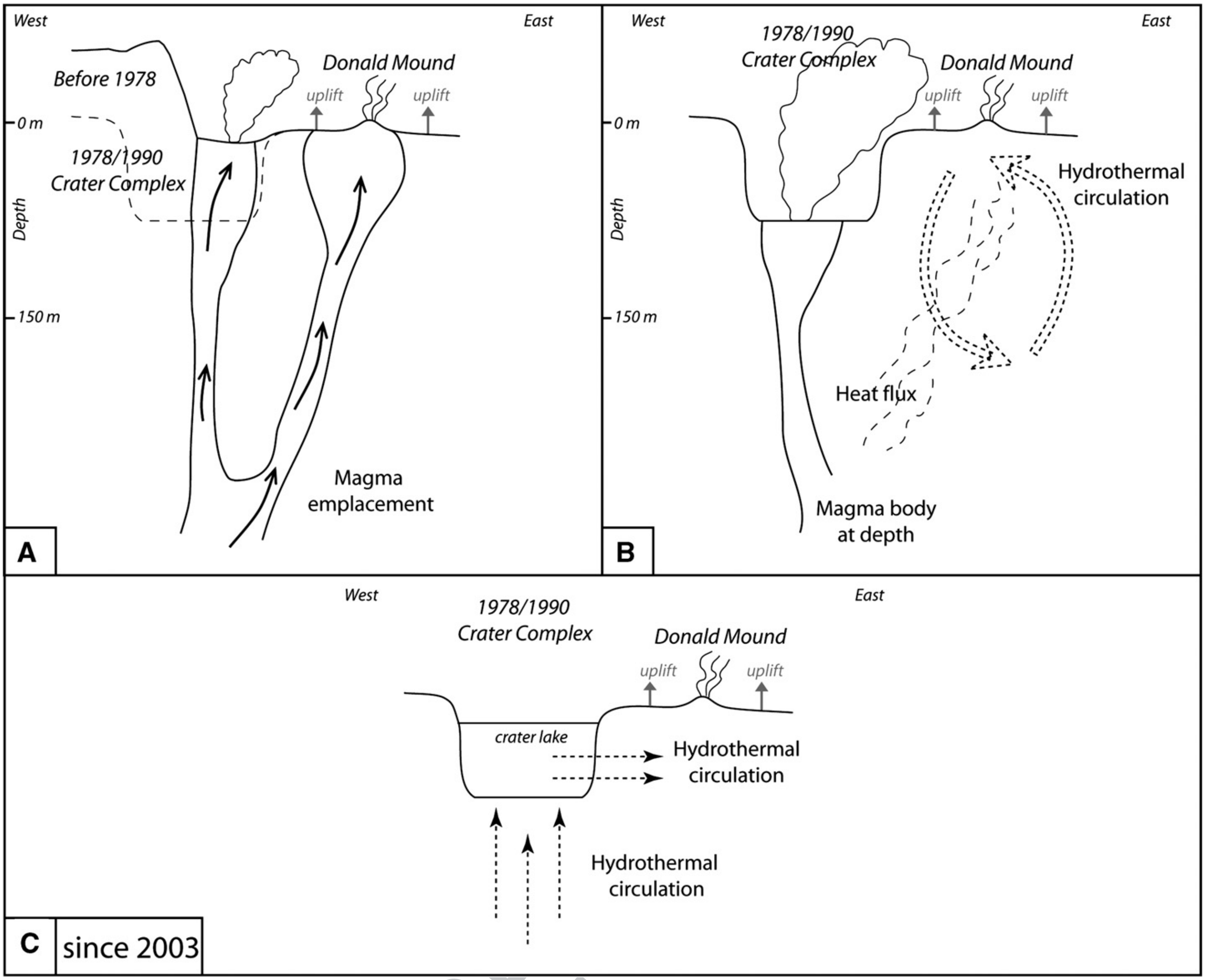

Fig. 11. Schematic sections through the White Island crater representing the three hypotheses advanced to explain uplift episodes: (A) magma emplacement at very shallow depth, (B) hydrothermal circulations, (C) and since 2003, drainage of the lake. The shape of the plumbing system is drawn after Houghton and Nairn (1991) and Nishi et al. (1996a,b).

5.3. Limits

Our investigations are limited by the lack of data in the western sub-crater due to the formation of successive collapse craters in this area. So, not enough data is available to constrain with precision the source extension toward the west and its depth. The monitored area, restricted to the crater, gives us only a minimum depth of the pressure sources but the largest changes recorded within the measured area and the lack of deformation in the eastern part of the crater gives some assurance that pressure sources are shallow (Fig. 5).

Another limitation of our models is the lack of horizontal displacement to constrain the shape of the pressure sources. Finite element models made by Dietrick and Decker (1975) showed that the inversion of only vertical displacement data may provide results that are not unique and that the exact shape of the source cannot be well determined without consideration of vertical and horizontal displacements.

6. Discussion

During the 40 years of levelling monitoring at White Island, successive uplift and subsidence of the main crater floor has been highlighted. Two main causes can be proposed to explain the inflation and deflation cycles: (1) hydrothermal source (fluid circulations, pressurization/de-pressurization/convection of a sealed hydrothermal fluid reservoir); and (2) magma source (magma intrusions, pressurization/de-pressurization/convection of a shallow magma reservoir) (Fig. 11a, b).

6.1. Origin of the crater uplift episodes

The periods of main crater uplift preceded the resurgences of eruptive activity. These more or less long periods of pre-eruptive uplift signals can be interpreted as due to new input of magma at shallow depth in the volcano somewhere beneath Donald Mound (Fig. 8) as already suggested by Clark and Otway (1989) for the 1971–1976 period. As no relationship exists between the location of the pre-eruptive inflation sources and the 1976–1982 active vents, Clark and Otway (1989) suggested that the inflation was most probably generated by increase of fluid pore pressure in response to heat flux and thermal expansion rather than directly by magma intrusion to shallow depth. Self-potential (SP) surveys carried out in 1993 and 1996 reveal the presence of a well developed volcano-hydrothermal system (Nishi et al., 1996a, 1995). Positive SP anomalies were present over the fumarole areas both in the main crater floor and in the outer slope boarding the main crater. These anomalies, which correlated well with the thermal

Please cite this article as: Peltier, A., et al., Ground deformation patterns at White Island volcano (New Zealand) between 1967 and 2008 deduced from levelling data, Journal of Volcanology and Geothermal Research (2009), doi:10.1016/j.jvolgeores.2009.01.020

anomalies derived from airborne thermal infrared mapping (Mongillo and Wood, 1995), have been interpreted as upflows along the edge of the sub-craters. The inflation sources can be thus explained by the rise of hot fluids from a deeper magma source to shallower levels beneath Donald Mound where they convect through the host rocks to cause thermal expansion. Note that the 1994–1996 crater uplift was not followed by a major eruption as expected by the size of the deformation signal. Accumulated magma at depth during this period might have fed, a few years later, the eruptive period of December 1998–July 2000 which was not preceded by any significant crater uplift (Fig. 3).

The evolution of height changes, magnetic changes, fumarole temperatures and chemistry, previously described (Fig. ~~1~~7), can all be explained if we suppose that exsolved gases from a magma body were diffused into the hydrothermal system and released to the surface. In consequence we can suppose that the ground uplift that was correlated with high temperatures and peaks in gas concentration was due to a hydrothermal response with an increase of fluid pore pressure in response to heat flow and thermal expansion rather than directly by magma emplacement itself (Fig. 7B). Nishi et al. (1996b) interpreted the shallow earthquakes, mainly originating in the shallow hydrothermal area located beneath the central and eastern sub-craters of the main crater, as resulting from rapid changes in pore fluid pressure.

For the most recent period (2002–2008), another hypothesis involving the drainage of the Crater Lake toward the hydrothermal system (Fig. 11C) can be advanced to explain the uplift centred in the southern part of the central sub-crater (Fig. 5). Just after the formation of the lake in February 2003, the increase of the crater uplift rate was accompanied by an increase in fumarole activity (around peg C, D and E) and by a 26 m rise of the Crater Lake until 2007 (Fig. 6), suggesting that a significant amount of the volcanic H_2O vapour was condensing into the liquid phase. By contrast, in 2007 a short-term subsidence of the crater floor was accompanied by a drop of the Crater Lake level (Fig. 6). According to Werner et al. (2008) the inflation source could be related to a build up of volatiles in the shallow subsurface due to changes in the permeability structure of the crater following lake filling, and that very little of the magma providing the volatiles was emplaced to permanently reside at shallow depth. A Self Potential (SP) survey in December 2003 revealed a change in the SP anomaly relative to the 1996 survey (Hashimoto et al., 2004; Nishi et al., 1996a). In 1996, a negative SP patch in the middle of the crater floor had been identified by Nishi et al. (1996a) whereas in 2003 a positive zone in the middle-south area had been highlighted by Hashimoto et al. (2004). The change in the SP anomaly distribution between 1996 and 2003 could be attributed to a change in the direction of the ground water supply from/toward the crater lake due to the rise of the lake water level; we can thus suggest a flow from the coast side (east) towards the lake in 1996 and a flow from the lake towards the east in 2003 (Hashimoto et al., 2004). Fluid drainage is favoured along pre-existing fractures, explaining also why the most active fumarole and the peak of uplift are located along the rims delimiting the eastern and the middle sub-craters.

6.2. Origin of the crater subsidence episodes

Crater wide subsidences were recorded during periods of relatively intense eruptive activity (1967–1971, 1979–1990 and 1990–1994 periods, Fig. 8). The ground subsidence can be thus attributed to the continuing removal of magma from depth to feed eruptions at the surface which generate a decrease of pressure and/or volume in depth. The volume variations of the pressure sources found by numerical modelling are in agreement with the low volumes of eruptive materials emitted during the eruptions associated with these deflation periods. The volume variations of the pressure sources during deflation periods were estimated at −0.6 to −3 × 10^4 m^3 (Table 1), while the volume of emitted products were between 10^4 and 10^5 m^3 for the 1967–1971, 1990–1994, 1996–1997 and 1997–2000 eruptive periods, and was estimated to be 10^7 m^3 for the 1976–1990 period (Houghton and Nairn, 1989; Scott, 1992; Scott et al., 2004). The different locations of the eruptive vents probably explain the slight differences in the location of the modelled deflation source from one period to the other. Superimposed on this behaviour a decompression of the hydrothermal system could also occur. The occasional brief localized inflationary/deflationary episodes during some eruptive sequences (March 1978, May 1980, November 1982, February 1984 and June 1987, Fig. 3) would be linked to changes in very shallow heat flows and superficial activity which generated thermal expansion/contraction of the ground in localized areas (commonly the active vent and Donald Mound areas) (see Fig. 2 for location).

Note that following the crater collapse in 1990, subsidence persisted to the west due to continuous material removal associated with the eruption whereas weak uplift was recorded to the east (Fig. 5). Change in the plumbing system just after the crater collapse could have released fluids or magma from a reservoir or subterranean collapse generating uplift in the eastern part of the crater (Otway, 1995, Internal Report GNS).

7. Conclusion

The analysis of 40 years of levelling monitoring at White Island allows us to highlight successive episodes of uplift and subsidence of the main crater. The periods of central sub-crater uplift preceded eruptions or resurgence of eruptive activity, whereas the periods of subsidence accompanied or followed eruptions, indicating a close correlation between ground deformation and eruptive activity. The subsidence during and following eruptions could be linked with removal of material at depth and changes to the hydrothermal system. But as no relationship exists between the locations of the pre-eruptive inflation source and the active vents, we suggested that inflation episodes were most probably generated by the thermal response of the relatively shallow volcano-hydrothermal system to magmatic intrusion, with an increase in fluid pore pressure in response to change of heat and gas flux rather than directly by magma intrusion to shallow depth.

Acknowledgements

Part of this work was supported by grants from the Earthquake Commission of New Zealand (EQC) and the European Commission, 6th Framework Project-'VOLUME', Contract No. 08471. We thank Hugh Bibby, Susan Ellis, Craig Miller and two anonymous reviewers for helpful advices and comments. We also thank Art and Gill Jolly for useful discussions. This is ~~GNS contribution no. XXXX and~~ IPGP contribution no. ~~XXXX~~.

References

Cayol, V., 1996. Analyse élastostatique tridimensionnelle du champ de déformations des édifices volcaniques par éléments frontières mixtes. ~~doctoral~~ Thesis, Université de Paris VII.

Cayol, V., Cornet, F.H., 1997. 3D mixed boundary elements for elastostatic deformation field analysis. International Journal of Rock Mechanics and Mining Sciences 34 (2), 275–287.

Christoffel, D.A., 1989. Variations in magnetic field Intensity at White Island Volcano related to the 1976–82 eruption sequence. New Zealand Geological Survey Bulletin 103, 109–118.

Clark, R.H., 1970. Volcanic activity on White Island, Bay of Plenty, 1966–69. Part 1. Chronology and crater floor level changes. New Zealand Journal of Geology and Geophysics 13 (3), 565–574.

Clark, R.H., 1973. Surveillance of White Island volcano, 1968–1972. Part 1—volcanic events and deformation of the crater floor. New Zealand Journal of Geology and Geophysics 16, 949–957.

Clark, R.H., 1982. Surveillance of White Island volcano 1972–77: volcanic events and deformation of the crater floor. New Zealand Journal of Geology and Geophysics 25, 317–324.

Clark, R.H., Cole, J.W., 1989. Volcanic monitoring and surveillance at White Island before the 1972–82 eruption sequence. New Zealand Geological Survey Bulletin 103, 9–11.

Clark, R.H., Otway, P.M., 1989. Deformation monitoring associated with the 1976–82 White Island eruption sequence. New Zealand Geological Survey Bulletin 103, 69–84.

Cole, J.W., Nairn, I.A., 1975. Catalogue of the active volcanoes of the world including solfatara fields—Part 22 New Zealand. International Association of Volcanology and Chemistry of the Earth's Interior. 156 pp.

Cole, J.W., Thordarson, T., Burt, R.M., 2000. Magma origin and evolution of White Island (Whakaari) volcano, Bay of Plenty, New Zealand. Journal of Petrology 41 (6), 867–895.

Dieterich, J.H., Decker, R.W., 1975. Finite element modeling of surface deformation associated with volcanism. Journal of Geophysical Research 80 (29), 4094–4102.

Dvorak, J.J., Dzurisin, D., 1997. Volcano geodesy: the search for magma reservoirs and the formation of eruptive vents. Reviews of Geophysics 35 (3). doi:10.1029/97RG00070.

Dzurisin, D., 2003. A comprehensive approach to monitoring volcano deformation as a window on the eruption cycle. Reviews of Geophysics 41 (1). doi:10.1029/2001RG000107.

Dzurisin, D., Yamashita, K.M., Kleinman, W., 1994. Mechanisms of crustal uplift and subsidence at the Yellowstone caldera, Wyoming. Bulletin of Volcanology 56 (261–270).

Fukushima, Y., Cayol, V., Durand, P., 2005. Finding realistic dike models from interferometric synthetic aperture radar data: the February 2000 eruption at Piton de La Fournaise. Journal of Geophysical Research 110 (B03206). doi:10.1029/2004JB003268.

Giggenbach, W.F., Sheppard, D.S., 1989. Variations in the temperature and chemistry of White Island fumarole discharges 1972–1985. New Zealand Geological Survey Bulletin 103, 119–126.

Giggenbach, W.F., Hedenquist, J.W., Houghton, B.F., Otway, P.M., Allis, R.G., 1989. Research drilling into the volcanic hydrothermal system on White Island, New Zealand. EOS 70 (7), 98–102.

Gottsmann, J., Rymer, H., Berrino, G., 2006. Unrest at the Campi Flegrei caldera (Italy): a critical evaluation of source parameters from geodetic data inversion. Journal of Geophysical Research 150 (1–3), 132–145.

Hashimoto, T., et al., 2004. Self-potential studies in Volcanic Areas (5)—Rishiri, Kusatsu-Shirane, and White Island. Journal of the Faculty of Science, Hokkaido University. Series 7, Geophysics 12 (2), 97–113.

Houghton, B.F., Nairn, I.A., 1989. A model for the 1976–82 phreatomagmatic and Strombolian eruption sequence at White Island volcano, New Zealand. New Zealand Geological Survey Bulletin 103, 127–136.

Hurst, A.W., Christoffel, D.A., 1973. Surveillance of White Island volcano, 1968–1972. Part 3—thermo-magnetic effects due to volcanic activity. New Zealand Journal of Geology and Geophysics 16 (4), 965–972.

Hurst, A.W., Rickerby, P.C., Scott, B.J., Hashimoto, T., 2004. Magnetic field changes on White Island, New Zealand, and the value of magnetic changes for eruption forecasting. Journal of Volcanology and Geothermal Research 136, 53–70.

Mongillo, M.A., Wood, C.P., 1995. Thermal infrared mapping of White Island volcano, New Zealand. Journal of Volcanology and Geothermal Research 69, 59–71.

Nishi, Y., Tosha, T., Scott, B.J., Sherburn, S., 1995. Self-potential survey of White Island, Volcano and geothermal observations 1993. Institute of Geological and Nuclear Sciences Report 95/11. Institute of Geological and Nuclear Sciences, Lower Hutt, New Zealand. 34 p.

Nishi, Y., et al., 1996a. Self-potential and audio-magnetotelluric survey in White Island volcano. In: Simmons, S.F., Rahman, M.M., Watson, A. (Eds.), Proceedings of the 18th New Zealand Geothermal workshop, Auckland: University of Auckland, pp. 237–242.

Nishi, Y., Sherburn, S., Scott, B.J., Sugihara, M., 1996b. High-frequency earthquakes at White Island volcano, New Zealand: insights into the shallow structure of a volcano-hydrothermal system. Journal of Volcanology and Geothermal Research 72, 183–197.

Peltier, A., Staudacher, T., Bachèlery, P., 2007. Constraints on magma transfers and structures involved in the 2003 activity at Piton de La Fournaise from displacement data. Journal of Geophysical Research 112, B03207. doi:10.1029/2006JB004379.

Sambridge, M., 1999. Geophysical inversion with a neighbourhood algorithm-I. searching a parameter space. Geophysical Journal International 138, 479–494.

Scott, B.J., 1992. White Island Volcano: eruption observations, seismicity and crater geomorphology, 1991. Institute of Geological and Nuclear Sciences Report 1991. Institute of Geological and Nuclear Sciences, Lower Hutt, New Zealand, pp. 17–23.

Scott, B.J., Manville, V.R., Hancox, G.T., Smith, W.D., Hoverd, J.L., 2004. Assessment of the hazard posed by the Crater Lake, White Island. Institute of Geological and Nuclear Sciences Report 2004/28. Institute of Geological and Nuclear Sciences, Lower Hutt, New Zealand. 34 p.

Werner, C., et al., 2008. Variability of passive gas emissions, seismicity, and deformation during crater lake growth at White Island Volcano, New Zealand, 2002–2006. Journal of Geophysical Research 113 (B01204). doi:10.1029/2007JB005094.

Wicks, C., Thatcher, W., Dzurisin, D., 1998. Migration of fluids beneath Yellowstone caldera inferred from satellite radar interferometry. Science 282, 458–462.

APPENDIX 4 IAVCEI CONFERENCE POSTER (REYKJAVIK, ICELAND, AUGUST 2008)

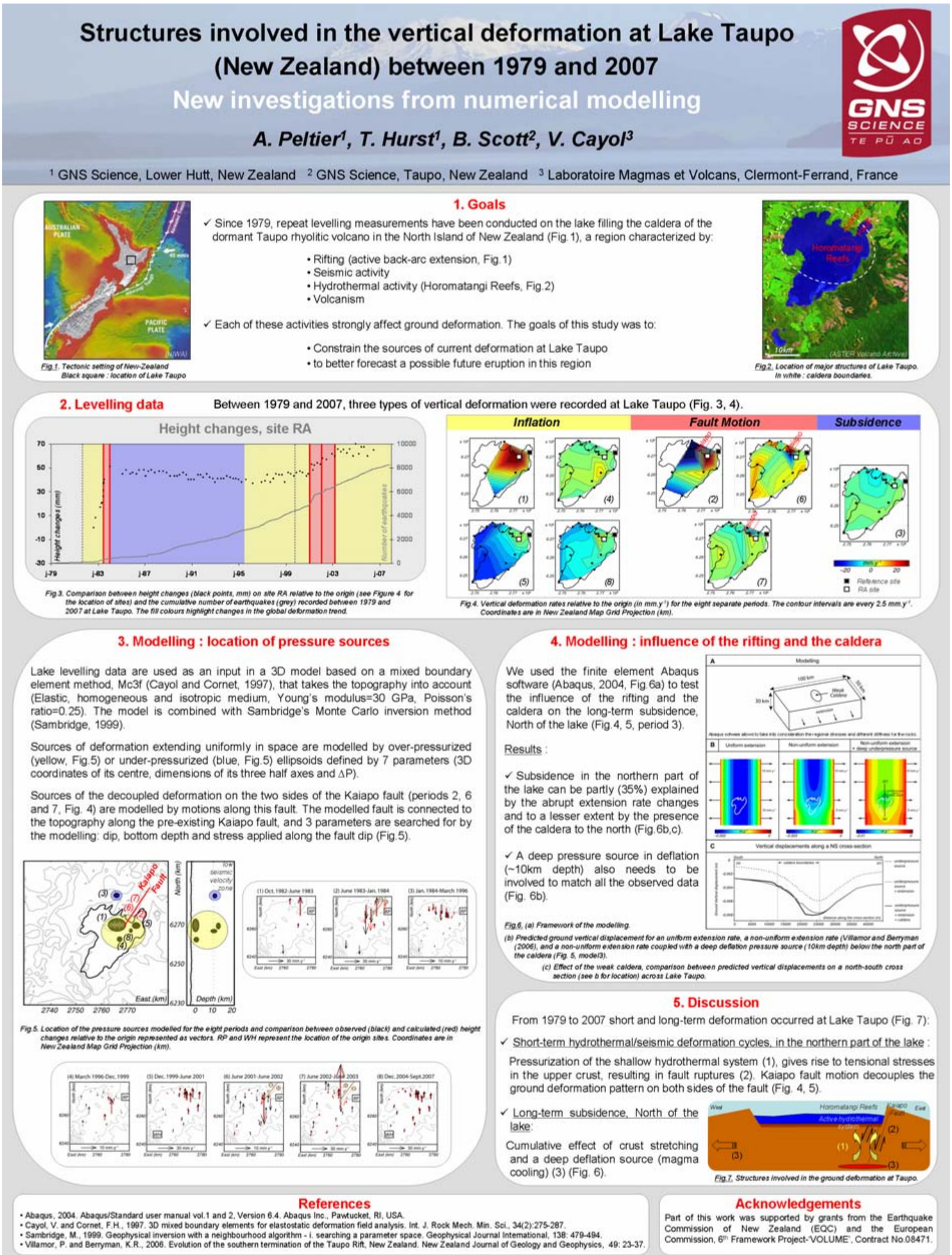

Structures involved in the vertical deformation at Lake Taupo (New Zealand) between 1979 and 2007

New investigations from numerical modelling

A. Peltier[1], T. Hurst[1], B. Scott[2], V. Cayol[3]

[1] GNS Science, Lower Hutt, New Zealand [2] GNS Science, Taupo, New Zealand [3] Laboratoire Magmas et Volcans, Clermont-Ferrand, France

1. Goals

✓ Since 1979, repeat levelling measurements have been conducted on the lake filling the caldera of the dormant Taupo rhyolitic volcano in the North Island of New Zealand (Fig. 1), a region characterized by:

- Rifting (active back-arc extension, Fig. 1)
- Seismic activity
- Hydrothermal activity (Horomatangi Reefs, Fig. 2)
- Volcanism

✓ Each of these activities strongly affect ground deformation. The goals of this study was to:

- Constrain the sources of current deformation at Lake Taupo
- to better forecast a possible future eruption in this region

Fig.1. Tectonic setting of New-Zealand Black square : location of Lake Taupo

Fig.2. Location of major structures of Lake Taupo. In white : caldera boundaries.

2. Levelling data

Between 1979 and 2007, three types of vertical deformation were recorded at Lake Taupo (Fig. 3, 4).

Height changes, site RA

Inflation | Fault Motion | Subsidence

Fig.3. Comparison between height changes (black points, mm) on site RA relative to the origin (see Figure 4 for the location of sites) and the cumulative number of earthquakes (grey) recorded between 1979 and 2007 at Lake Taupo. The fill colours highlight changes in the global deformation trend.

Fig.4. Vertical deformation rates relative to the origin (in mm.y^{-1}) for the eight separate periods. The contour intervals are every 2.5 mm.y^{-1}. Coordinates are in New Zealand Map Grid Projection (km).

3. Modelling : location of pressure sources

Lake levelling data are used as an input in a 3D model based on a mixed boundary element method, Mc3f (Cayol and Cornet, 1997), that takes the topography into account (Elastic, homogeneous and isotropic medium, Young's modulus=30 GPa, Poisson's ratio=0.25). The model is combined with Sambridge's Monte Carlo inversion method (Sambridge, 1999).

Sources of deformation extending uniformly in space are modelled by over-pressurized (yellow, Fig.5) or under-pressurized (blue, Fig.5) ellipsoids defined by 7 parameters (3D coordinates of its centre, dimensions of its three half axes and ΔP).

Sources of the decoupled deformation on the two sides of the Kaiapo fault (periods 2, 6 and 7, Fig. 4) are modelled by motions along this fault. The modelled fault is connected to the topography along the pre-existing Kaiapo fault, and 3 parameters are searched for by the modelling: dip, bottom depth and stress applied along the fault dip (Fig.5).

Fig.5. Location of the pressure sources modelled for the eight periods and comparison between observed (black) and calculated (red) height changes relative to the origin represented as vectors. RP and WH represent the location of the origin sites. Coordinates are in New Zealand Map Grid Projection (km).

4. Modelling : influence of the rifting and the caldera

We used the finite element Abaqus software (Abaqus, 2004, Fig.6a) to test the influence of the rifting and the caldera on the long-term subsidence, North of the lake (Fig.4, 5, period 3).

Results :

✓ Subsidence in the northern part of the lake can be partly (35%) explained by the abrupt extension rate changes and to a lesser extent by the presence of the caldera to the north (Fig.6b,c).

✓ A deep pressure source in deflation (~10km depth) also needs to be involved to match all the observed data (Fig. 6b).

Fig.6. (a) Framework of the modelling.
(b) Predicted ground vertical displacement for an uniform extension rate, a non-uniform extension rate (Villamor and Berryman (2006), and a non-uniform extension rate coupled with a deep deflation pressure source (10km depth) below the north part of the caldera (Fig. 5, model3).
(c) Effect of the weak caldera, comparison between predicted vertical displacements on a north-south cross section (see b for location) across Lake Taupo.

5. Discussion

From 1979 to 2007 short and long-term deformation occurred at Lake Taupo (Fig. 7):

✓ Short-term hydrothermal/seismic deformation cycles, in the northern part of the lake :

Pressurization of the shallow hydrothermal system (1), gives rise to tensional stresses in the upper crust, resulting in fault ruptures (2). Kaiapo fault motion decouples the ground deformation pattern on both sides of the fault (Fig. 4, 5).

✓ Long-term subsidence, North of the lake:

Cumulative effect of crust stretching and a deep deflation source (magma cooling) (3) (Fig. 6).

Fig.7. Structures involved in the ground deformation at Taupo.

References

- Abaqus, 2004. Abaqus/Standard user manual vol.1 and 2, Version 6.4. Abaqus Inc., Pawtucket, RI, USA.
- Cayol, V. and Cornet, F.H., 1997. 3D mixed boundary elements for elastostatic deformation field analysis. Int. J. Rock Mech. Min. Sci., 34(2):275-287.
- Sambridge, M., 1999. Geophysical inversion with a neighbourhood algorithm - i. searching a parameter space. Geophysical Journal International, 138: 479-494.
- Villamor, P. and Berryman, K.R., 2006. Evolution of the southern termination of the Taupo Rift, New Zealand. New Zealand Journal of Geology and Geophysics, 49: 23-37.

Acknowledgements

Part of this work was supported by grants from the Earthquake Commission of New Zealand (EQC) and the European Commission, 6th Framework Project-'VOLUME', Contract No.08471.

www.gns.cri.nz

Principal Location

1 Fairway Drive
Avalon
PO Box 30368
Lower Hutt
New Zealand
T +64-4-570 1444
F +64-4-570 4600

Other Locations

Dunedin Research Centre
764 Cumberland Street
Private Bag 1930
Dunedin
New Zealand
T +64-3-477 4050
F +64-3-477 5232

Wairakei Research Centre
114 Karetoto Road
Wairakei
Private Bag 2000, Taupo
New Zealand
T +64-7-374 8211
F +64-7-374 8199

National Isotope Centre
30 Gracefield Road
PO Box 31312
Lower Hutt
New Zealand
T +64-4-570 1444
F +64-4-570 4657